
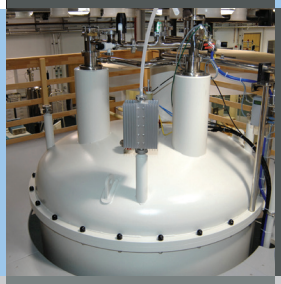
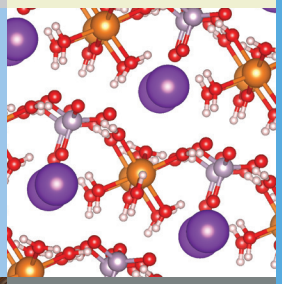


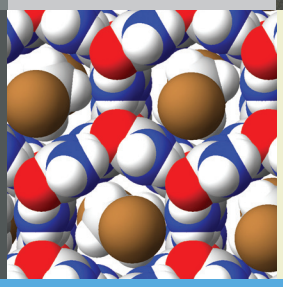

The UK 850 MHz Solid-State NMR Facility

Annual Report 2013

The UK 850 MHz Solid-State NMR Facility

In the first **4** years of operation:

1248 days have been allocated to

44 PIs from **22** different UK institutions

with **1835** days being requested.

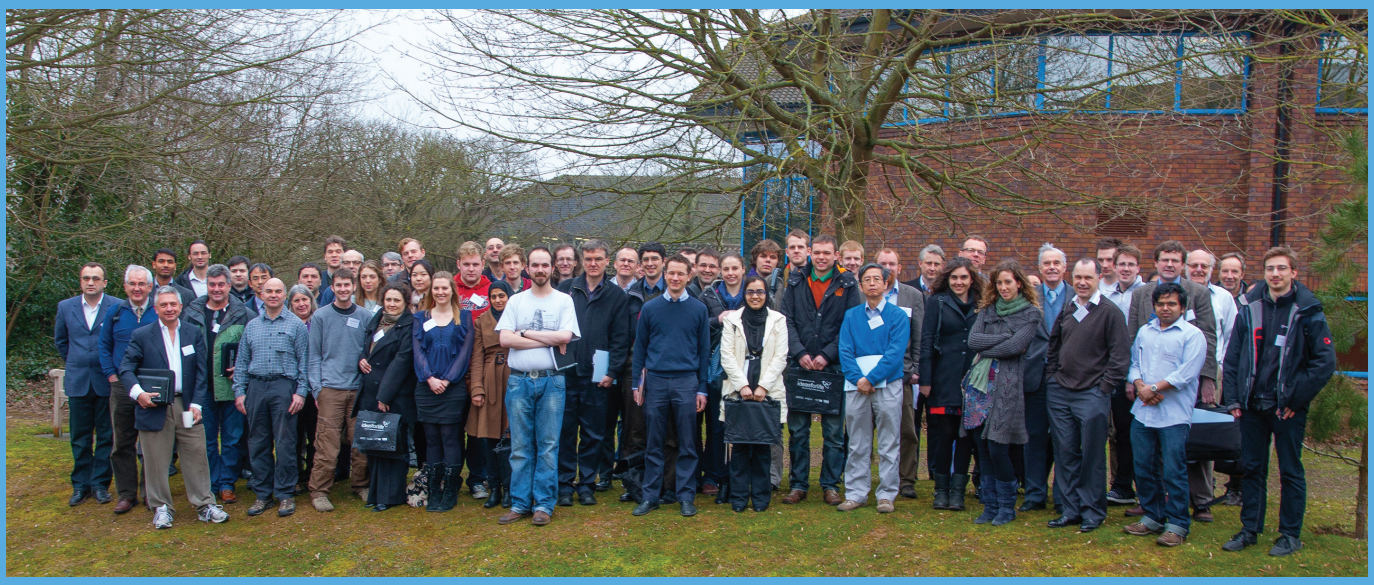

Attendees at the 2013 Annual Symposium that took place at the University of Warwick on Thursday 11th April.

Contents

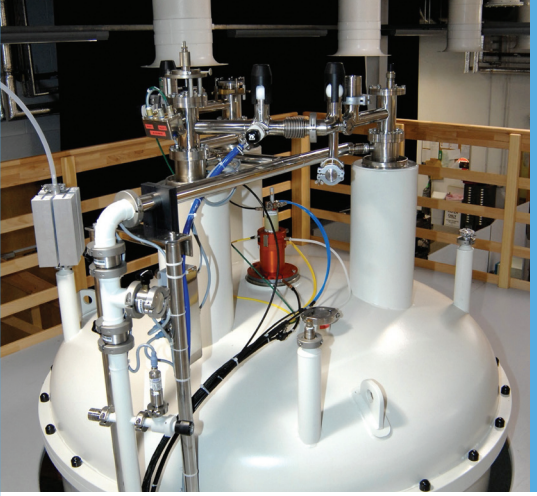

Introduction

We are pleased to present our fourth annual report showcasing the breadth of high-quality scientific research that has been performed at the UK 850 MHz Solid-State NMR Facility in the last year. The Facility was originally funded for five years, starting in January 2009, by a grant from EPSRC (with a 10% contribution from BBSRC) to a consortium of UK solid-state NMR spectroscopists who form the National Management Committee of the Facility, with additional financial contributions from the University of Warwick (in part through the Birmingham Science City Advanced Materials Projects 1 and 2, supported by Advantage West Midlands) and the European Regional Development Fund.

We were delighted when, earlier this year, EPSRC announced an extension of the original grant by a further 12 months, meaning that the Facility is now fully funded till January 2015 and bringing the total value of the grant to nearly £4M. Having welcomed the first visiting scientists in February 2010, the Facility has demonstrated itself to be an extremely valuable shared resource for the UK scientific community, with researchers from more than 20 different institutions carrying out experiments in a range of disciplines including chemistry, materials science, Earth sciences, biology and physics.

The use of high magnetic fields in NMR spectroscopy brings increases in both resolution and sensitivity, and so the 850 MHz Facility enables experiments to be performed that are simply impossible at lower fields. High magnetic fields are particularly important for quadrupolar nuclei (such as ^{17}O, ^{25}Mg, ^{33}S and ^{71}Ga), with an additional gain in resolution owing to the reduction in quadrupolar line broadening. This report presents descriptions of the research carried out at the Facility in its fourth year of operation. Examples of this work have been published this year in leading international journals, including Chem. Sci., J. Phys. Chem., Phys. Chem. Chem. Phys. and Acc. Chem. Res. Particular highlights in this report include a ^{71}Ga NMR study of gallophosphates, high-resolution two-dimensional NMR spectroscopy of ^{33}S at natural abundance (0.76%), ^{93}Nb fast-MAS NMR of ion conductors, the measurement of ^{1}H chemical shift anisotropies under fast-MAS conditions, studies of zinc phosphates by ^{67}Zn NMR, ^{13}C NMR studies of whole plant stems, and a study of the binding of water molecules to an immobilised enzyme biocatalyst by ^{17}O multiple-quantum filtration NMR.

The third Annual Symposium of the Facility was held in April 2013, and attracted 67 registered attendees, with talks by graduate students, postdoctoral researchers and PIs from 8 different institutions, as well as a presentation by a member of the International Advisory Board. This meeting presents an excellent opportunity for researchers around the country to discuss new scientific advances, and provides graduate students in particular with the opportunity to meet each other and to present their work. The Facility is looking forward to welcoming both experienced and new users during the upcoming year, with the Facility Manager available to advise those less familiar with the technique, before, during and after a visit.

In conclusion, we hope you enjoy reading about the exciting science carried out at the UK 850 MHz Solid-State NMR Facility, and we look forward to another successful and productive year.

Further details of the Facility can be found on our website: **http://go.warwick.ac.uk/850mhz/**

The National Management Committee

Sharon E Ashbrook
(St Andrews)

Steven P Brown
(Chair, Warwick)

Melinda J Duer
(Cambridge)

Ray Dupree
(Warwick)

Robin K Harris
(Durham)

Mark E Smith
(Lancaster)

Jeremy J Titman
(Nottingham)

Stephen Wimperis
(Glasgow)

Organization and Management of the Facility

The UK 850 MHz solid-state NMR Facility was established with the aid of several linked research grants from EPSRC. The eight investigators on the grant comprise the National Management Committee (NMC) which determines the strategic objectives for the Facility and the procedures by that these are to be achieved. The NMC meets twice a year, communicating informally more frequently as the need arises. The operation of the Facility is the responsibility of the Local Management Team (LMT) comprising the Facility Manager (FM) who is an ex-officio member of the NMC and the Warwick-based NMC chair. The duties of the Facility Manager include maintaining the instrumentation and assisting visitors to the Facility with their experiments. The management of the Facility is overseen by the International Advisory Board (IAB) which is made up of three eminent solid-state NMR spectroscopists from overseas: Chris Jaroniec (Ohio), Arno Kentgens (Nijmegen, until April 2013), Dominique Massiot (Orléans, from May 2013), Roderick Wasylishen (Alberta). The terms of reference of the NMC and IAB, the remit of the LMT and the duties of the FM are available on the Facility website.

Time Allocation Process

All UK academics who are eligible to apply for Research Council funding, as well as UK researchers of similar standing in industry, may apply for an allocation of spectrometer time at the Facility. Users are expected to run their own experiments with the assistance of the Facility Manager, so personnel with previous solid-state NMR experience should be identified to visit the Facility and carry out the research (inexperienced users should contact the Facility Manager in advance, to agree a collaborative arrangement with the Facility Manager relating to the Facility Manager's role in carrying out the experiments). A minimum of 80% of the available time is allocated by an independent Time Allocation Panel (TAP) that comprises three UK scientists, including one member of the NMC, as well as the Facility Manager in an *ex-officio* capacity. The balance is allocated by the NMC and is reserved for fast-track applications, measurements referred from the EPSRC solid-state NMR service, the Facility Manager's designated research time, to compensate users who were unable to take up their allocated time because of instrument downtime, and a small number of maintenance days. Members of the TAP normally serve for a two-year term.

There are two allocation rounds each year for time, each covering a six-month period, starting in either February or August, corresponding to deadlines of November 30th and May 31st. Previous users of the Facility are notified of upcoming deadlines by email. Previous time allocations and instructions for applicants are given on the Facility website. The main criterion for allocating time is overall scientific merit, as well as the quality of the case made for high-field solid-state NMR. Where appropriate, the TAP will consider additional factors, such as the quality of publications arising from previous allocations of time and whether the research is supported by peer-reviewed grants or involves students funded by EPSRC or BBSRC. The TAP is charged with ensuring that the balance of the allocated time broadly reflects the research objectives of the original grant and with providing feedback for unsuccessful applicants. During the TAP meeting, the Facility Manager gives advice on the feasibility of the proposed experiments and the spectrometer time required.

The maximum time that can be requested by an individual applicant during any allocation round is 28 days, but this can be split between several applications. It is a condition that the Facility is mentioned in any publication arising wholly or partly from an allocation of time. Furthermore, a user report must be produced by the original applicant no later than the 7th of the month following the end of the specific six-month time-allocation period, i.e., 7th February or 7th August. Applications are not accepted from users who have outstanding reports from previous allocations of time. The code for all NMR pulse sequences implemented by users on the Facility's spectrometer must be deposited in a shared database. If the experiment is a new one, the code will only be made available to other users after the pulse sequence has been published. Reasonable travel costs associated with the use of the facility will be paid to academic users. The Facility rents accommodation on the University of Warwick campus for use by Facility visitors.

TAP membership (2013): Chair: Sharon Ashbrook, St Andrews; non-NMC members: Kenneth Harris, Cardiff (up to the February 2013 round), Paul Hodgkinson, Durham (for the August 2013 round onwards) & Phil Williamson, Southampton.

What is the Facility?

UK 850 MHz Solid-State NMR Facility Probes

No	Probe
1	1.3 mm probe HXY (+19F) conventional insert design H13863
2	2.5 mm HXY DBB (double-broadband) H13856
3	2.5 mm HX (+19F) H13889
4	2.5 mm HFX H13894
5	3.2 mm HXY DBB (double-broadband) H13857
6	3.2 mm HXY low E field for biosolids LLC H13900
7	3.2 mm HXY conventional insert design H13888
8	4 mm HXY conventional insert design (+19F) H13694
9	4 mm HX (low gamma) H13892
10	7 mm X (low gamma) H13895
11	Static
12	1 mm HX (produced by Jeol)
13	DOR probe (produced by Samoson group, Tallinn, Estonia)

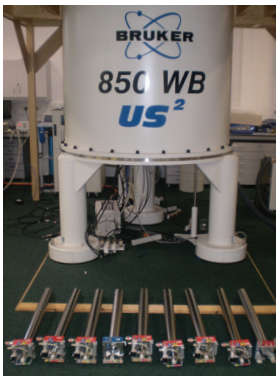

850 MHz spectrometer and probes. Probes 1 to 11 were supplied by Bruker. Maximum MAS frequencies: 4 mm probes 15 kHz; 3.2 mm probes 24 kHz, 2.5 mm probes 35 kHz; 1.3 mm probe 65 kHz. All 3.2 mm and 4 mm MAS probes are equipped with DVT stators and can operate between –140 °C and + 150 °C.

Probe usage 2010 and 2013

Year 1 to Year 4 (Round 1 to Round 8)

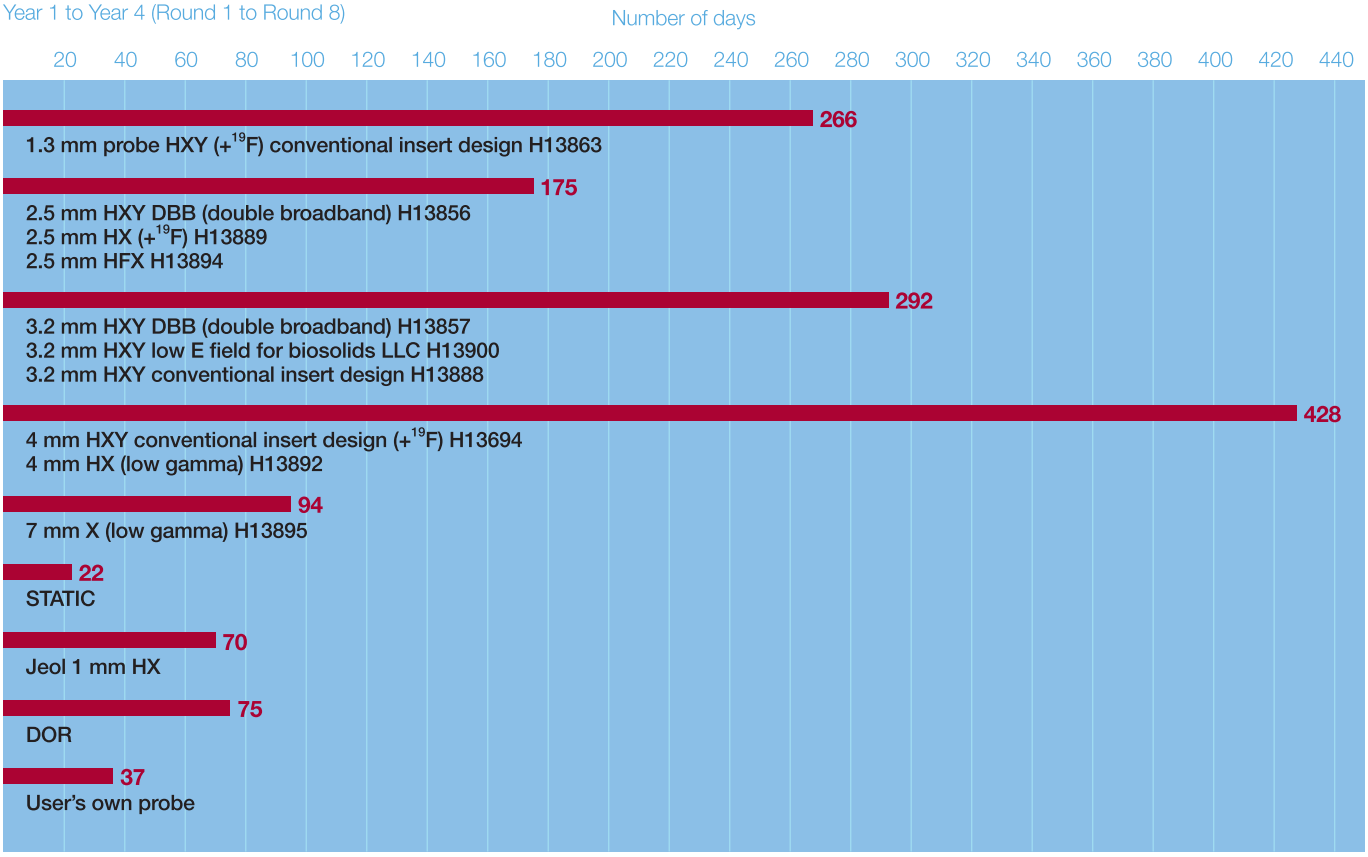

Nuclei tested in Double Resonance Mode

Probe in double Resonance mode	Mode	X-Nucleus: ^{31}P	^{7}Li	^{119}Sn	^{87}Rb	^{11}B	^{71}Ga	^{65}Cu	^{23}Na	^{27}Al	^{13}C	^{79}Br	^{93}Nb	^{45}Sc	^{69}Ga	^{29}Si	^{2}H	^{6}Li	^{17}O	^{135}Ba	^{15}N	^{35}Cl	^{33}S	^{14}N	^{91}Zr	^{43}Ca	^{67}Zn	^{25}Mg	^{89}Y	^{39}K	^{87}Sr	^{183}W	^{73}Ge
1.3 mm HXY (+^{19}F) conventional insert design	DR ^{1}H-X DR ^{19}F-X ●	■	✸	✸	✸	✸	■	✸	✸	✸ ■	■	■	■	■	■	✸	✸	✸	■	✸	■	✸	✸	■									
2.5 mm HX (+^{19}F) 2.5 mm HFX 2.5mm HXY DBB	DR ^{1}H-X DR ^{19}F-X ●	■	✸	✸	■	✸	■	✸	✸	■ ■	■ ■	■	✸	■	■	✸	■	✸	■	✸	■	✸	✸	■	✸	✸	✸	■					
3.2 mm HXY low E field for biosolids LLC	DR ^{1}H-X				✸	✸	✸	✸	✸	✸	■	■	✸	✸	✸	✸	✸	✸	✸	✸	■	✸	✸	✸									
3.2 mm HXY conventional insert design 3.2mm HXY DBB	DR ^{1}H-X				■	■	■	✸	■	■	■	■	✸	✸	✸	✸	✸	✸	■	✸	■	■	✸	■									
4 mm HXY conventional insert design (+^{19}F)	DR ^{1}H-X DR ^{19}F-X ●	■	✸	■	✸	✸	✸	✸	■	■	■ ■	■	✸	✸	✸	■	✸	✸	✸	✸	■ ■	✸	✸	✸									
4 mm HX (low gamma)	DR ^{1}H-X										■	■	■	✸	■	✸	■	■	■	✸	■	✸	■	■	■	■	■	■	■	■	■	✸	✸
7 mm X (low gamma)	X																		✸	■	✸	■	✸	■	✸	■	✸	✸	■	■	■	■	■
Static	X	■	✸	✸	✸	✸	■	■	✸	✸	■	✸	■	✸	■	✸	■	✸	✸	✸	✸	■	✸	■	✸	✸	✸	✸	✸	■	✸	✸	✸
DOR	X				■	■	■	✸	■	■	✸	✸	✸	✸	✸	✸	✸	✸	■	✸	✸	✸	✸	✸	✸	■	✸	✸					
Jeol 1 mm HX	DR ^{1}H-X		■	✸	■	✸	■	✸	■	✸	■	✸	■	✸	✸	✸	✸	✸	✸	✸	✸	✸	✸	■									

■ *Experiments performed at the facility to date*

✸ *Bench tests indicate should be possible*

● *Other ^{19}F-X DR combinations have not yet been investigated*

For triple-resonance capabilities, refer to the facility website

Time Allocation

469 days requested by 28 PIs from 13 different institutions (Barts and The London School of Medicine and Dentistry, Cambridge, Cardiff, Glasgow, ISIS, Lancaster, Liverpool, Nottingham, Sheffield, Southampton, St Andrews, Strathclyde and Warwick). 319 days allocated by the Time Allocation Panel.

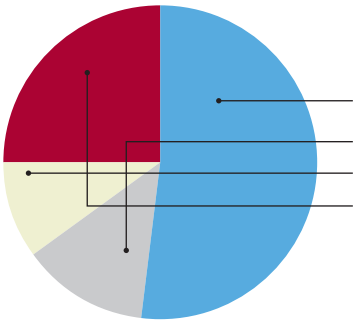

Requested time

Outside Warwick and non-NMC **52%**
NMC outside Warwick **13%**
Warwick NMC **10%**
Warwick non-NMC **25%**

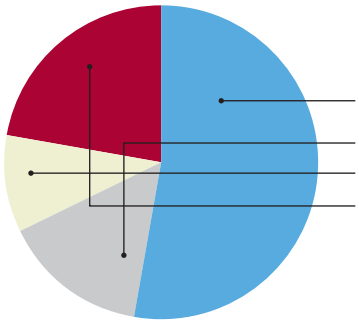

Allocated time

Outside Warwick and non-NMC **53%**
NMC outside Warwick **15%**
Warwick NMC **10%**
Warwick non-NMC **22%**

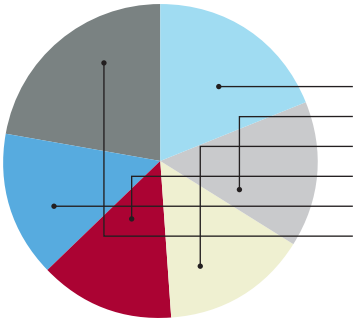

Requested time

Advanced materials **19%**
Bio-materials **15%**
Energy materials **15%**
Methods development **14%**
Proteins **15%**
Pharmaceuticals and self assembly **22%**

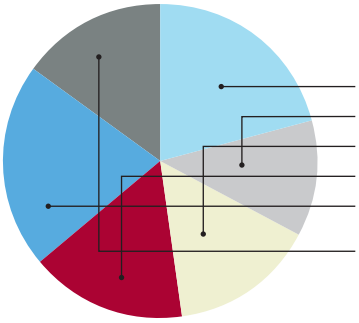

Allocated time

Advanced materials **21%**
Bio-materials **12%**
Energy materials **15%**
Methods development **16%**
Proteins **21%**
Pharmaceuticals and self assembly **15%**

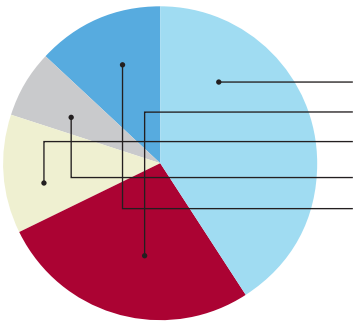

Requested time

EPSRC **41%**
BBSRC **27%**
Other agencies **12%**
Industrial **7%**
No external funding **13%**

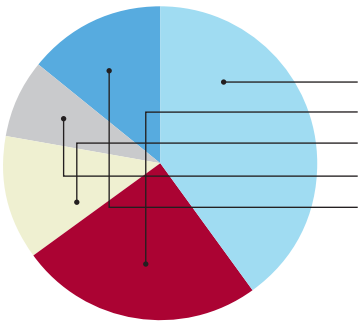

Allocated time

EPSRC **40%**
BBSRC **25%**
Other agencies **13%**
Industrial **8%**
No external funding **14%**

Projects with more than one funding source were counted only once. Other agencies that are funding facility users are: STFC, Leverhulme Trust, Royal Society, Wellcome Trust, EU, agencies from Chile, France, Greece, Iraq, Sweden and the USA as well as industry (AWE, Bruker, Dupont, GSK, Nissan and NDA).

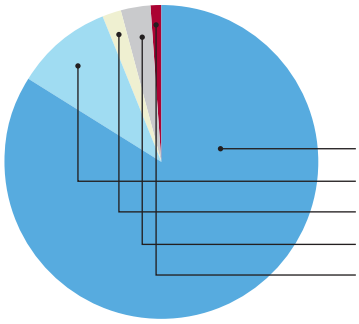

Spectrometer time

Feb 1 2013 – Jan 31 2014 (the facility operates 24 hours a day, 7 days a week)

TAP allocated days **84%**
Facility manager research **10%**
Maintenance **2%**
Fast track **3%**
Compensation **1%**

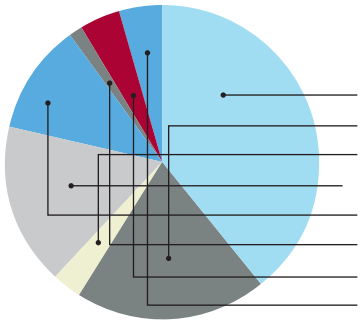

Facility users

Feb 1 2013 – Jan 31 2014

PIs **28**
EPSRC PhD students* **14**
BBSRC PhD students **2**
Other PhD students** **12**
PDRAs*** **8**
UG student **1**
Research staff **3**
Overseas collaborators **3**

* *One student partially funded by industry*
** *5 overseas (Chile, France, Iraq, Italy), 3 UK university funding, 2 industrial, 2 self-funded*
*** *3 BBSRC, 1 ESPRC, 1 Leverhulme Trust, 3 EU Funding*

Results from User Questionnaire Feb 2013 – Jan 2014

Facility users are asked to complete feedback questionnaires which contain a series of questions and provide the opportunity for visitors to make comments and suggestions. The responses are graded from 1 (least satisfied) to 5 (most satisfied). The average scores are based on the responses from 12 PIs and 24 visitors for visits over the period February 2013 to January 2014.

Section 1 to be completed by the PI

Application for time

1 Ease of application process
2 Transparency of application process
3 Feedback on any unsuccessful time request

Scheduling of time awarded

4 Scheduling of your time by the facility

Overall impact

5 Quality of results obtained

Section 2 to be completed by the visitor

Accommodation

6 Ease of arranging accommodation
7 Quality of accommodation
8 Location of accommodation

At the 850 MHz Facility

9 Support from the Facility Manager upon arrival
10 Support from the Facility Manager throughout your visit
11 Quality of the NMR facilities
12 Quality of the sample preparation area and storage facilities
13 Ease of access to the facility out of hours
14 Your overall time at the facility

Post visit experience

15 Arrangements for accessing data
16 Arrangements for returning any samples
17 Reimbursement of expenses

Average scores from feedback questionnaires over period Feb 2013 – Jan 2014

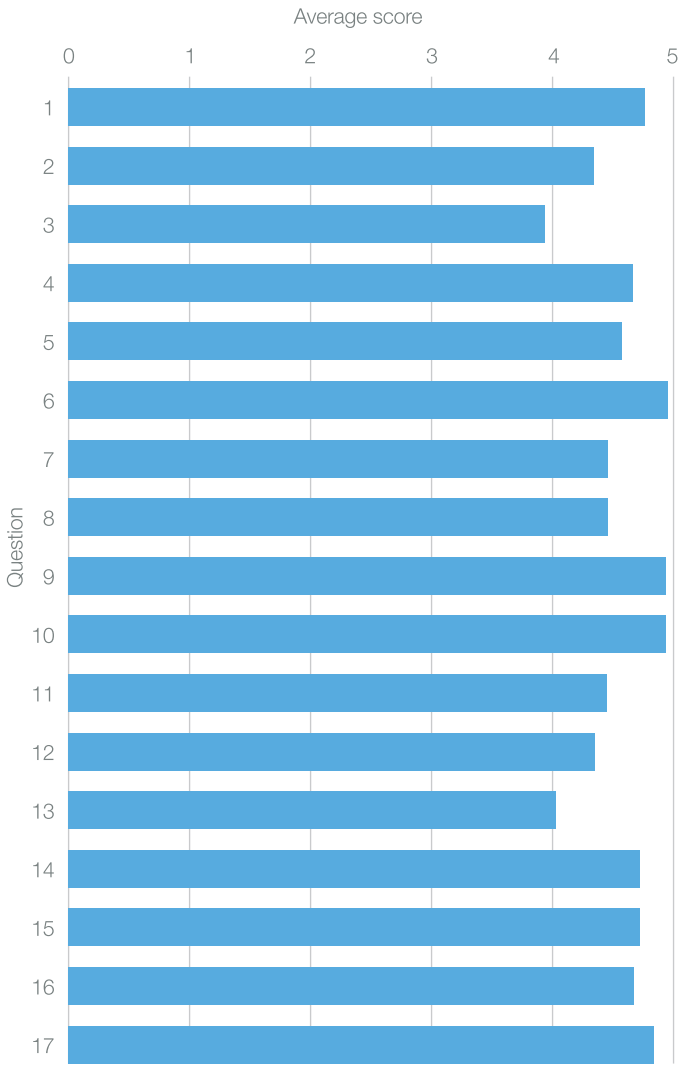

UK 850 MHz Solid-State NMR Facility
3rd Annual Symposium

Thursday 11 April 2013
Millburn House, University of Warwick
Symposium Organiser: Ray Dupree

List of talks

1 ***'Fast Magic Angle Spinning at High Fields: Advancements in ^{1}H detection and Protein Dynamics'***
Józef Lewandowski *(University of Warwick)*

2 ***'NMR of Enzymes Immobilised on Silica Surfaces'***
Nicole Fauré *(University of Glasgow)*

3 ***'Discovering New Aspects of Crystallization Processes by In-Situ NMR Studies'***
Colan Hughes *(Cardiff University)*

4 ***'Solid-State NMR Investigation of GaPO-34'***
Daniel Dawson *(University of St. Andrews)*

5 ***'Understanding Heteronuclear Decoupling at High Magnetic Fields and MAS rates'***
Paul Hodgkinson *(Durham University)*

6 ***'Measuring Proton Shift Anisotropies with Ultrafast MAS'***
Habeeba Miah *(The University of Nottingham)*

7 ***'High Field Solid-State NMR studies of Proton-Conducting Ceramics'***
Luke Sperrin *(University of Cambridge)*

8 ***'Pinpointing Ligand Binding Sites within Amyloid Fibrils Using Solid-State NMR'***
David Middleton *(University of Liverpool)*

9 ***'Exploring the Structure of Alzheimer's Amyloid Aggregates Using High Field Solid-State NMR'***
Robert Kelly *(University of Warwick)*

10 ***'Hunting for Hydrogen in Wadsleyite: Multinuclear Solid-State NMR and First-Principles Calculations'***
Sharon Ashbrook *(University of St Andrews)*

11 ***'Solid-State NMR Structural Studies of Proteins Using Paramagnetic Probes'***
Christopher Jaroniec *(Ohio State University)*

Publications

'Exploiting the Synergy of Powder X-ray Diffraction and Solid-State NMR Spectroscopy in Structure Determination of Organic Molecular Solids'

D.V. Dudenko, P.A. Williams, C.E. Hughes, O.N. Antzutkin, S.P. Velaga, S.P. Brown, K.D.M. Harris

J. Phys. Chem. C, 117, 12258-12265 (2013)

'Measuring Proton Shift Tensors with Ultrafast MAS NMR'

H.K. Miah, D.A. Bennett, D. Iuga, J.J. Titman

J. Magn. Reson. 235, 1-5 (2013)

'A Multinuclear Solid State NMR, Density Functional Theory and X-Ray Diffraction Study of Hydrogen Bonding in Group I Hydrogen Dibenzoates'

G.J. Rees, S.P. Day, A. Lari, A.P. Howes, D. Iuga, M.B. Pitak, S.J. Coles, T.L. Threlfall, M.E. Light, M.E. Smith, D. Quigley, J. D. Wallis, J.V. Hanna

CrystEngComm, 15, 8823-8839 (2013)

'Whewellite, $CaC_2O_4.H_2O$: Structural Study by a Combined NMR, Crystallography and Modelling Approach'

H. Colas, L. Bonhomme-Coury, C. Coelho Diogo, F. Tielens, F. Babonneau, C. Gervais, D. Bazin, D. Laurencin, M.E. Smith, J.V. Hanna, M. Daudon, C. Bonhomme

CrystEngComm, 15, 8840-8847 (2013)

'Structural Study of Calcium Phosphonates: a Combined Synchrotron Powder Diffraction, Solid-State NMR and First-Principle Calculations Approach'

S. Sene, B. Bouchevreau, C. Martineau, C. Gervais, C. Bonhomme, P. Gaveau, F. Mauri, S. Bégu, P.H. Mutin, M.E. Smith, D. Laurencin

CrystEngComm, 15, 8763-8775 (2013)

'Application of NMR Crystallography to the Determination of the Mechanism of Charge-Balancing in Organocation-Templated AlPO STA-2'

V.R. Seymour, E.C.V. Eschenroeder, M. Castro, P.A. Wright, S.E. Ashbrook

CrystEngComm, 15, 8668-8679 (2013)

'Advances in Solid-State Relaxation Methodology for Probing Site-Specific Protein Dynamics'

J.R. Lewandowski

Acc. Chem. Res., 46, 2018-2027 (2013)

'Water in the Earth's Mantle: a Solid-State NMR Study of Hydrous Wadsleyite'

J.M. Griffin, A.J. Berry, D.J. Frost, S.Wimperis, S.E. Ashbrook

Chem. Sci., 4, 1523-1538 (2013)

'High-Resolution Solid-State NMR of Lipid Membranes'

B.B Bonev

Advances in Planar Lipid Bilayers and Liposomes, 17, 299-329 (2013)

'Expanding the Solid-State Landscape of L-Phenylalanine: Discovery of Polymorphism and New Hydrate Phases, with Rationalization of Hydration/Dehydration Processes'

P.A. Williams, C.E. Hughes, A.B.M. Buanz, S. Gaisford, K.D.M. Harris

J. Phys. Chem. C, 117, 12136-12145 (2013)

'Spectral Assignments and NMR Parameter–Structure Relationships in Borates Using High-Resolution ^{11}B NMR and Density Functional Theory'

O.L.G. Alderman, D. Iuga, A.P. Howes, K.J. Pike, D. Holland, R. Dupree

Phys. Chem. Chem. Phys., 15, 8208-8221 (2013)

'Probing Hydrogen Bonding in Cocrystals and Amorphous Dispersions Using ^{14}N–^{1}H HMQC Solid-State NMR'

A.S. Tatton, T.N. Pham, F.G. Vogt, D. Iuga, A.J. Edwards, S.P. Brown

Mol. Pharm., 10, 999-1007 (2013)

'High-Resolution Solid-State ^{13}C NMR Spectroscopy of the Paramagnetic Metal–Organic Frameworks, STAM-1 and HKUST-1'

D.M. Dawson , L.E. Jamieson , M.H. Mohideen, A.C. McKinlay, I.A. Smellie, R. Cadou, N.S. Keddie, R.E. Morris, S.E. Ashbrook

Phys. Chem. Chem. Phys., 15, 919-929 (2013)

In addition, users reported 28 talks and 18 posters at conferences and seminars in 2013, where results obtained at the UK 850 MHz Solid-State NMR Facility were presented.

PhD Theses

Student	Department	University	Supervisor	Title	Date
Martin Mitchell	Chemistry	St Andrews	Sharon E Ashbrook	*'Investigation of Structure and Disorder in Inorganic Solids Using Solid-State NMR'*	Jan 2013
Valerie R. Seymour	Chemistry	St Andrews	Sharon E Ashbrook	*'Multinuclear Solid-State NMR for the Characterisation of Inorganic Materials'*	Jan 2013
David Bennett	Chemistry	Nottingham	Jeremy Titman	*'Structural Methods in Solid-state NMR'*	Mar 2013
Hannah Davies	Biology	Liverpool	David Middleton	*'Expression and Characterisation of Cardiovascular Amyloid Proteins'*	May 2013
Oliver Alderman	Physics	Warwick	Diane Holland	*'The Structure of Vitreous Binary Oxides: Silicate, Germanate and Plumbite Networks'*	Sep 2013
Andrew Grigg	Physics	Warwick	Diane Holland	*'The Structure of Divalent and Trivalent Cation Substituted Beta-Tricalcium Phosphate'*	Oct 2013

The UK 850 MHz Solid-State NMR Facility PhD Travel Fund

Chamonix Mont-Blanc, France, setting for the 8th Alpine Conference on Solid-State NMR in September 2013. Photo: Simo Räsänen

Supported by Bruker

The UK 850 MHz Solid-State NMR Facility PhD travel fund supported by Bruker provides funding for: (a) attendance at an internationally recognised, high-profile conference where a PhD student presents results he/she obtained at the 850 MHz Facility, or (b) a "start-up" visit to another lab to learn new methods to be implemented at the 850 MHz Facility. For further details see: **http://go.warwick.ac.uk/850mhz/travel_fund/**

2013 Awards

- **Nicole Fauré** (University of Glasgow) awarded £1000 to attend the 8th Alpine Conference on Solid-State NMR in Chamonix Mont-Blanc, France, (September 2013) and present a poster entitled *Improved Understanding of Immobilised Enzymes Using Solid-State NMR*.
- **Robert Kelly** (University of Warwick) awarded £900 to attend the 8th Alpine Conference on Solid-State NMR in Chamonix Mont-Blanc, France (September 2013) and present a poster entitled *Exploring the Structure of Alzheimer's Amyloid Aggregates with Copper Using Solid-State NMR*.
- **Jonathan Lamley** (University of Warwick) awarded £1000 to attend the 8th Alpine Conference on Solid-State NMR in Chamonix Mont-Blanc, France, (September 2013) and present a poster entitled *Site-Specific ^{13}C $R_{1\rho}$ Relaxation Measurements in Proteins in the Solid State*.
- **Scott Sneddon** (University of St Andrews) awarded £1000 to attend the 8th Alpine Conference on Solid-State NMR in Chamonix Mont-Blanc, France (September 2013) and present a poster entitled *Exploiting the ^{31}P Chemical Shift Anisotropy of Aluminophosphates*.

Conference Publicity Support

In order to facilitate the publicising of the capabilities of solid-state NMR to new users, the UK 850 MHz Solid-State NMR Facility offers support for PIs or PDRAs to present results at UK conferences. For further details see: **http://go.warwick.ac.uk/850mhz/conference-publicity-funding/**

2013 Awards

- **Steven Brown** (University of Warwick) awarded £500 to attend the 21st International Conference on the Chemistry of the Organic Solid State (ICCOSS) in Oxford (August 2013) and present a talk entitled *Solid-State NMR Spectroscopy of Organic Solids: Probing Structure-Directing Interactions*.

The UK 850 MHz Solid-State NMR Facility User Reports

Investigating the Efficiency of "FAM-N" Pulses in MQMAS Experiments at High MAS Rate

Henri Colaux, Daniel M. Dawson and Sharon E. Ashbrook

School of Chemistry and EaStCHEM, University of St Andrews

Overview

Quadrupolar nuclei comprise 75% of all NMR-active nuclei, yet their study is more challenging than spin I = 1/2 nuclei, owing to the presence of second-order quadrupolar broadening, which cannot be removed completely under magic-angle spinning (MAS). The introduction of the multiple-quantum (MQ) MAS technique[1] provided a convenient and efficient way to investigate quadrupolar nuclei through the separation of each component of the signal according to their respective quadrupolar coupling constants and isotropic chemical shifts. However, this method often suffers from inherently poor sensitivity, decreasing significantly as the MAS rate increases.[2] As shown in Figure 1, a MQMAS experiment consists of at least two pulses: one to excite multiple-quantum coherences and the other to convert these to observable single-quantum coherences. It has been established that this second conversion using a single pulse, as proposed in the original MQMAS experiment, has poor efficiency and numerous alternative conversion pulses have been proposed in the literature, including the SPAM,[3] FAM-I,[4] FAM-II,[4] and DFS[5] pulses shown in Figure 1b. We have recently developed an alternative approach, using computationally pre-optimised composite pulses, termed FAM-N, consisting of a succession of N subsequent and oppositely phased pulses, optimised independently using a program built on MATLAB and SIMPSON. This method results in significant signal enhancements over a single conversion pulse at MAS rates between 6 and 20 kHz. In this work we investigate the performance of a number of MQMAS conversion pulses at high MAS rate.

MQMAS experiments at fast MAS rate

In order to assess the performance of FAM-N (and other conversion pulses) under fast MAS conditions, MQMAS spectra have been recorded for $RbNO_3$ at a MAS rate of 75 kHz using the 1 mm JEOL MAS probe. The isotropic spectra (showing three distinct Rb sites) are shown in Figure 1c. The signal observed using FAM-N (where N = 15) is ~2.2 times that obtained using a single pulse, and also has better sensitivity than the other approaches. The signal improvements found are comparable to those observed at lower MAS rates.

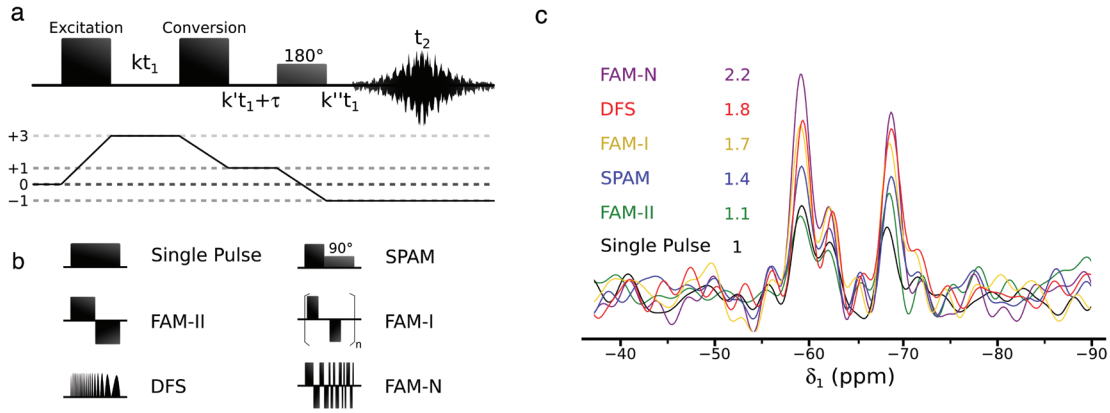

Figure 1. (a) Typical MQMAS (split-t_1 shifted echo) pulse sequence, (b) pulses for the conversion of triple- to single-quantum coherences and (c) isotropic ^{87}Rb (20.0 T, 75 kHz MAS) MQMAS spectra of $RbNO_3$, recorded using the sequence in (a), with the pulses shown in (b).

References

1. Frydman, L.; Harwood, L. *J. Am. Chem. Soc.* **1995**, *117*, 5367.
2. Amoureux, J. P.; Fernandez, C.; Frydman, L. *Chem. Phys. Lett.* **1996**, *259*, 347.
3. Gan, Z.; Kwak, H.-T. *J. Magn. Reson*. **2004**, 168, 346.
4. Madhu, P. K.; Goldbourt, A.; Frydman, L.; Vega, S. *Chem. Phys. Lett*. **1999**, *307*, 41.
5. Kentgens, A. P. M; Verhagen, R. *Chem. Phys. Lett*. **1999**, 300, 41.

High-Field ^{17}O Solid-State NMR Investigation of $Y_2Sn_{2-x}Zr_x{}^{17}O_7$

Scott Sneddon,[1] Frédéric Blanc[2] and Sharon E. Ashbrook[1]

[1]*School of Chemistry and EaStCHEM, University of St Andrews*

[2]*Department of Chemistry, University of Liverpool*

Overview

Pyrochlore materials, with the general formula $A_2B_2O_7$, have important applications as components of SYNROC, a ceramic wasteform used to safely encapsulate the radioactive actinides and lanthanides present in nuclear waste.[1] The stability of the pyrochlore phase depends upon the ratio of the radii of the A and B cations, r_A/r_B. When r_A/r_B is between 1.46 and 1.78, the pyrochlore structure is favoured. However, when $r_A/r_B < 1.46$, a defect fluorite phase is formed with both cation and anion disorder. For $Y_2Sn_{2-x}Zr_xO_7$, a transformation between ordered pyrochlore and disordered defect fluorite phases is expected, and a detailed understanding of the phase(s) formed for each composition and the extent of the anion and cation disorder is crucial. Recent work on $Y_2Sn_xTi_{2-x}O_7$ has showed that the ^{89}Y isotropic and anisotropic chemical shift can provide detailed information about the next-nearest neighbour environment.[2] In principle, ^{17}O NMR should be ideal for probing both cation and anion disorder as the shielding and quadrupolar parameters are sensitive to the nature of the neighbouring cations. In order to ease acquisition of ^{17}O NMR spectra, our $Y_2Sn_{2-x}Zr_xO_7$ materials have been post-synthetically enriched (to ~8-12%), by heating to ~1000 °C in a sealed capsule in the presence of 35% $^{17}O_2$.

^{17}O Solid-State NMR of $Y_2Sn_{2-x}Zr_x{}^{17}O_7$

The ^{17}O MAS NMR spectrum of $Y_2Sn_2{}^{17}O_7$ in Figure 1a shows two peaks (at 173.0 and 383.9 ppm), corresponding to the OY_2Sn_2 and OY_4 environments expected in the pyrochlore phase, with quadrupolar coupling constants (C_Q) of 3.1 and 0.05 MHz, respectively. The ^{17}O MAS NMR spectrum of $Y_2Zr_2{}^{17}O_7$, shows a broad resonance between 375 and 335 ppm. An ^{17}O MQMAS spectrum (Figure 1c) reveals that this signal results from a distribution of chemical shifts and not quadrupolar broadening. This is consistent with the defect fluorite phase, where disorder of cations and anions is expected. A number of changes in the ^{17}O spectra are observed as x increases: (i) a broadening of all peaks; (ii) pyrochlore peaks gradually decrease in intensity, whilst broad peaks from the disordered phase grow; (iii) an intermediate peak appears, and then decreases in intensity. The ^{17}O MAS NMR spectrum of $Y_2Sn_{1.8}Zr_{0.2}{}^{17}O_7$ in Figure 1b contains additional resonances at 382.9 and 260.3 ppm, corresponding to OY_2Zr_2 and OY_2SnZr environments, respectively. Notably, the peak at ~383 ppm is split, demonstrating the sensitivity of ^{17}O NMR to more distant cation substitution. Full analysis of all spectra should enable the relative amounts of each phase and ordering of cations and anions to be investigated.

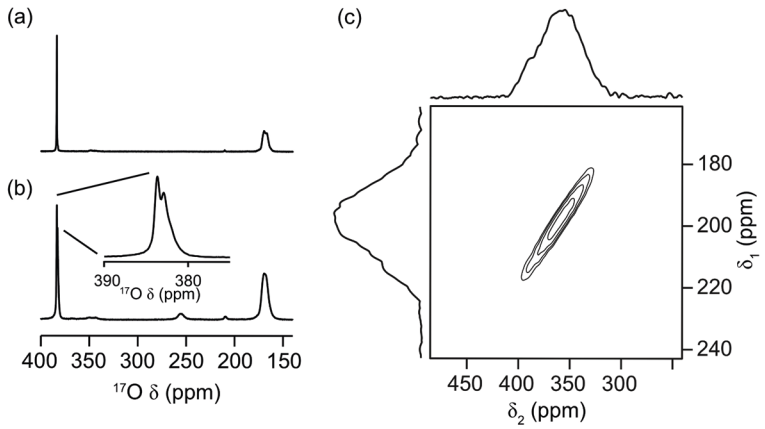

Figure 1. ^{17}O (20.0 T, 20 kHz MAS) NMR spectra of (a) $Y_2Sn_2{}^{17}O_7$ and (b) $Y_2Sn_{1.8}Zr_{0.2}{}^{17}O_7$ and (c) MQMAS NMR spectrum of $Y_2Zr_2{}^{17}O_7$ (shown after a shearing transformation has been applied).

References

1. Ringwood, A. E., Safe Disposal of High Level Nuclear Reactor Wastes: A New Strategy, *Australian National University Press*, **1978.**
2. Mitchell, M. R., PhD. thesis, University of St Andrews, **2012.**

2D ^{1}H Detected NMR of A$\beta_{1\text{-}40}$/Cu Aggregates at 95 kHz MAS

Robert T. Kelly,[1] Jonathan M. Lamley,[2] Dinu Iuga,[1] Andreas Oss,[3] Steven P. Brown,[1] Anders Olofsson,[4] Ago Samoson,[3] Józef R. Lewandowski[2] and Oleg N. Antzutkin[1,5]

[1]*Department of Physics, University of Warwick*

[2]*Department of Chemistry, University of Warwick*

[3]*Tallinn University of Technology, Tallinn, Estonia*

[4]*Department of Pharmacology and Clinical Neuroscience, Umeå University, Umeå, Sweden*

[5]*Chemistry of Interfaces, Luleå University of Technology, Luleå, Sweden*

Overview

Achieving spectral resolution and sensitivity required for detailed structural studies is one of the main challenges for working with biomolecular aggregates. In contrast to highly successful liquid-state multi-dimensional NMR methodology for small-size molecules, which relies upon a high resolution in the ^{1}H dimension, a residual ^{1}H-^{1}H dipole-dipole broadening is a large obstacle for using these highly sensitive nuclei for structure determination of macromolecules and aggregates of a size > 50 kDa in solution or/and in the solid state. Here we demonstrate that by combining 95 kHz magic-angle-spinning and fast recycling of experiments enabled by a paramagnetic relaxation enhancing agent (Cu^{2+} ions bound to amyloid aggregates) and by employing ^{1}H-detected experiments one can obtain high quality 2D and 3D ^{1}H-^{13}C and ^{1}H-^{15}N correlation spectra in a few hours on < 1 mg of fully-protonated Alzheimer's [U-^{13}C,^{15}N]-A$\beta_{1\text{-}40}$ aggregates formed from aqueous solutions with $CuCl_2$, thus enabling their detailed structural studies.

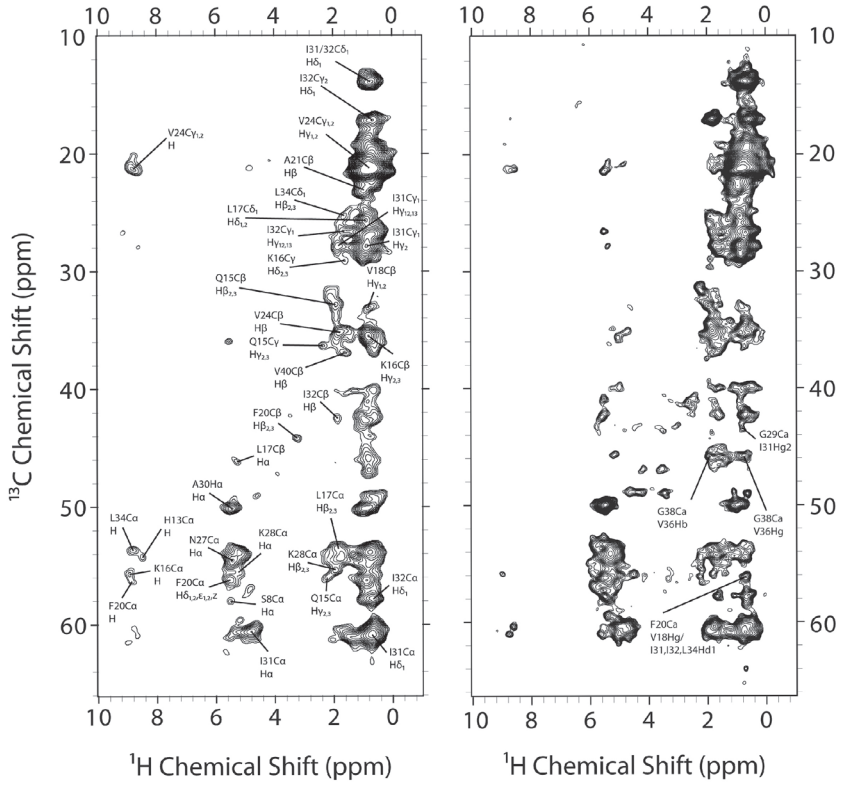

Figure 1. ^{1}H-detected ^{1}H-^{13}C 2D correlation spectra of <1.0 mg of fully-protonated [U-^{13}C,^{15}N]-A$\beta_{1\text{-}40}$ /Cu aggregates obtained at 95 kHz MAS and 850.2 MHz ^{1}H Larmor frequency. Shortening of ^{1}H T_1 due to the presence of paramagnetic copper allowed the use of a recycle delay of 0.3 s, resulting in a total experimental time of only ~50 minutes. Assignments (left panel) and ^{13}C-^{1}H long-range contacts (right panel) are indicated in the spectra. (The second CP ^{13}C-^{1}H contact time / ^{1}H-^{1}H mixing time) were (0.2/2.0 ms) and (1.2/1.0 ms) for the left and the right panels, respectively.

^{1}H-Detected Spectroscopy at ~100 kHz MAS Frequency

Fast magic-angle-spinning (95 kHz) achieved with 0.8 mm MAS instrumentation developed in Samoson's laboratory provides a substantial averaging of the ^{1}H-^{1}H dipole-dipole interaction and, therefore, a significant narrowing of ^{1}H resonance lines. In addition, sensitivity in multi-dimensional experiments is further boosted using ^{1}H-signal detection methodology: high quality spectra were obtained on a range of sub-milligram samples of fully protonated Alzheimer's amyloid peptide aggregates and toxic oligomers in a matter of minutes to hours. Figure 1 shows two selected 2D ^{1}H-^{13}C correlation spectra of < 1 mg hydrated [U-^{13}C,^{15}N]-A$\beta_{1\text{-}40}$ aggregates formed in the presence of copper ions. In these experiments, after the standard ^{1}H-^{13}C CP and ^{13}C-frequency evolution, the second ^{13}C-^{1}H CP was followed by a ^{1}H-^{1}H mixing period. Interestingly, apart from cross peaks from carbons to several nearby protons (left panel) even a number of long-range ^{13}C-^{1}H contacts were detected (right panel). The latter contacts may provide very useful structural constraints for modelling of the supramolecular structure of these aggregates. The combination of the sensitivity enhancement using ^{1}H-signal detection and a fast recycling (300 ms) due to the presence of paramagnetic copper ions in the sample resulted in high-quality 2D spectra obtained in less than an hour each. Therefore, good quality 3D correlation spectra can be readily obtained using the suggested approach in only *ca.* 10-24 hours. 3D spectroscopy is often necessary for obtaining a sufficiently high spectral resolution needed for an unambiguous assignment of NMR signals and for further detailed structural studies.

Solid-State NMR of Cu-Bound Aggregated A$\beta_{1\text{-}40}$

A role of substoichiometric levels of Cu(II) in promoting aggregation kinetics and neurotoxicity of Aβ peptides has been discussed previously.[1] In our studies, the aggregates were formed and precipitated instantly by addition of $CuCl_2$(aq) at pH 7.0 to recombinant [U-^{13}C,^{15}N]-A$\beta_{1\text{-}40}$. These A$\beta_{(1\text{-}40)}$/Cu aggregates are stable in aqueous suspensions for a long time. We believe that these aggregates are a type of "kinetic trap", because they decompose completely into monomers, when a Cu(II)-chelating agent, such as EDTA, is added to the solution of A$\beta_{(1\text{-}40)}$/Cu aggregates. It is also possible that A$\beta_{(1\text{-}40)}$/Cu aggregates are β-sheet rich oligomers with an enhanced neurotoxicity. 2D ^{13}C-^{13}C DARR NMR spectra obtained on [U-^{13}C,^{15}N]-A$\beta_{1\text{-}40}$/Cu aggregates in this study were used for the ^{13}C signal assignment and analysis of the secondary ^{13}C chemical shifts, which suggest a different structure compared to previously reported supramolecular structures of A$\beta_{1\text{-}40}$ amyloid fibrils (see Figure 2). Therefore, 2D and 3D ^{1}H-detected ^{1}H-^{13}C and ^{1}H-^{15}N NMR spectroscopy is highly motivated for the full structure determination of this biologically-important system.

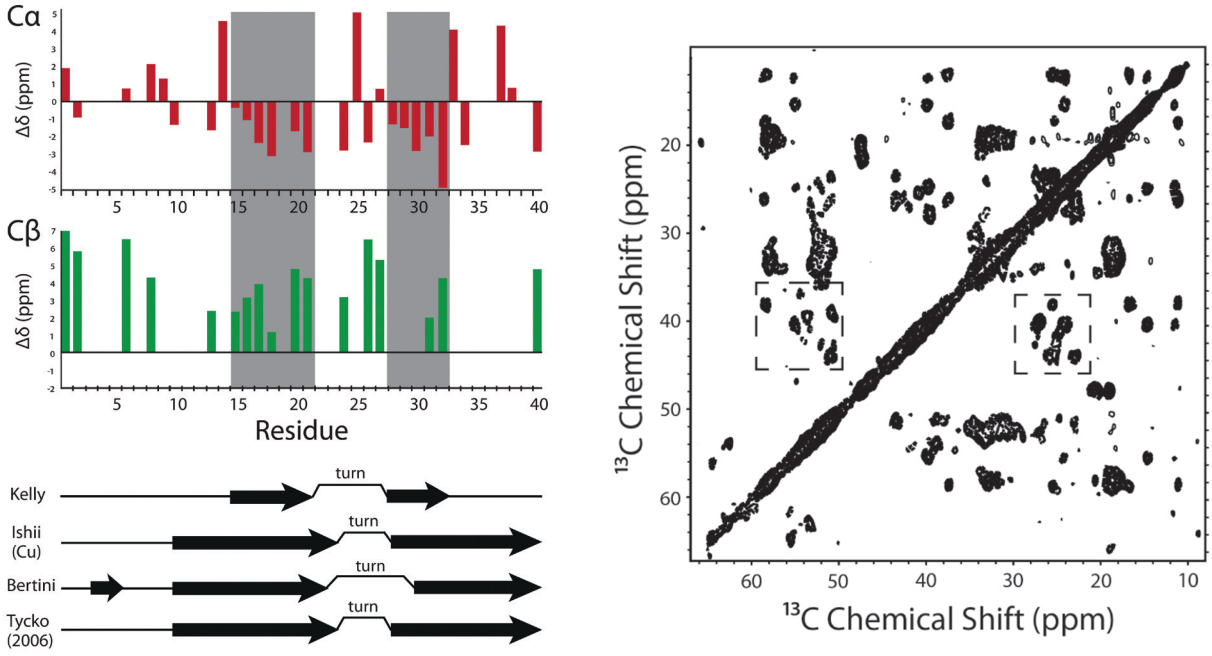

Figure 2. (top, left) Secondary ^{13}C chemical shifts obtained from 2D ^{13}C-^{13}C DARR NMR spectra (850.2 MHz, 2.5 mm MAS probe) of hydrated [U-^{13}C,^{15}N]-A$\beta_{1\text{-}40}$/Cu aggregates (right). Experimental conditions were: 20 ms DARR mixing time, 10 kHz MAS, temperature +2°C. Obviously, β-sheet structural fragments in the copper stabilised aggregates in this study (marked by grey colour) are at different positions in the peptide sequence compared to all previously reported structures of A$\beta_{1\text{-}40}$ amyloid fibrils (bottom, left).

References

1. Sarell, C. J.; Wilkinson, S. R.; Viles, J. H. *J. Biol. Chem.* **2010**, *285*, 41533.

Al Environments and Al…Al Proximities in Aluminium Tellurite Glasses

Emma R. Barney,[1] Ray Dupree,[2] Diane Holland[2] and Alex C. Hannon[3]

[1]*Department of Engineering, University of Nottingham*

[2]*Department of Physics, University of Warwick*

[3]*ISIS, STFC, Rutherford Appleton Laboratory*

Overview

A change in the dominant Te coordination in tellurite glasses has been proposed as a qualitative explanation of the variation with composition of a range of technologically-useful properties, including refractive index and non-linear optical response. However, for these properties to be exploited in optical devices, we need to have a *quantitative* understanding of the chemical interactions which drive the change in Te coordination number, n_{TeO}. We have recently developed a model which successfully predicts n_{TeO} for modifier oxide tellurites and which we are now testing on intermediate oxides that can also readily change their metal-oxygen coordination numbers. ^{27}Al MAS NMR and DQ (double-quantum) experiments at the 850 MHz Facility have (a) assisted us in the interpretation of neutron diffraction data from Al_2O_3-TeO_2 glasses and (b) shown the proximities of the various [AlO_n] species, which will help us to understand why the model in its current form fails to predict the n_{TeO} dependence on Al_2O_3 content.

Background

Until recently, the fairly extensive literature on alkali tellurite glasses has concluded that the addition of modifier oxide A_2O_z (where z is the cation valence) to TeO_2 produces a progressive change in tellurium environment from 100% [TeO_4E] pseudo-trigonal bipyramid units (E is a lone-pair), such as are found in crystalline α-TeO_2, to [TeO_3E] pseudo-tetrahedra as found in Na_2TeO_3. This coordination change, n_{TeO} decreasing from 4 to 3, is necessary so that the bonding requirements of the glass network can be accommodated.[1-3]

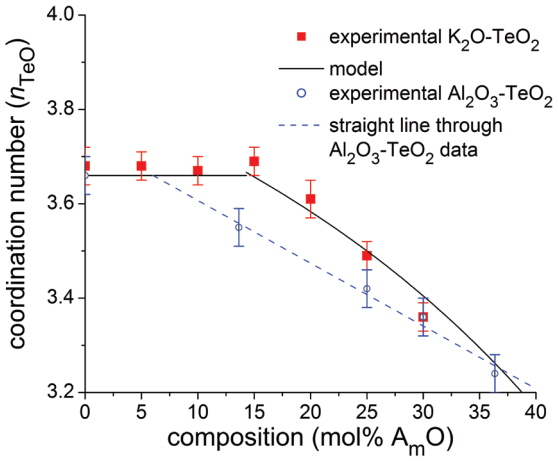

Figure 1.Comparison of the Te-O coordination numbers, n_{TeO}, for K_2O-TeO_2 [4] and Al_2O_3-TeO_2 glasses, measured using neutron diffraction, with those predicted by the model. (m = 2/z).

However, our neutron diffraction (ND) study of the potassium tellurite glass system showed that, below ~15 mol% modifier, n_{TeO} is roughly constant and *significantly less than four* (typically 3.66), even for pure amorphous a-TeO_2 (Fig. 1).[4] This contradicts previous literature, where n_{TeO} is *assumed* to be 4 initially (as in the crystal). The [TeO_3] units present in a-TeO_2 can therefore provide a significant number of non-bridging oxygens (NBO) which can contribute to the coordination of the modifier cation. Using this information, a model has been developed which accurately predicts the variation in n_{TeO} with composition (Figure 1). At low concentrations, the NBOs associated with the [TeO_3] units in amorphous TeO_2 provide surplus coordinating oxygen atoms and these, along with the 2 NBO which each added K_2O provides, can satisfy the K coordination (n_{KO} = 6) without the need to form further [TeO_3] units. However, at 14.3 mol% K_2O, the number of bonds required by K exceeds the number of bonds which this mechanism provides and the formation of further [TeO_3] becomes necessary, with a consequent reduction in n_{TeO}. This model is successful in explaining the behaviour of not just K_2O but alkali tellurites in general. We have recently extended the study to oxides which are not conventional modifiers but are intermediate in behaviour, particularly those whose coordination environments can *also* change with composition, such as Al_2O_3.

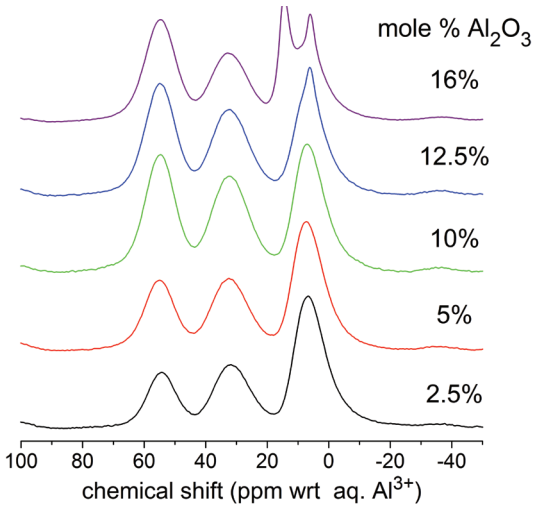

Figure 2. ^{27}Al MAS spectra for the xAl_2O_3 (100-x) TeO_2 glasses obtained at 221.5 MHz at the 850 MHz Facility using a Bruker 3.2 mm probe with an MAS frequency of 20 kHz, and a π/6 flip angle of 1 μs.

^{27}Al Solid-State NMR Experiments

Figure 2 shows the ^{27}Al MAS spectra from xAl_2O_3 (100-x)TeO_2 glasses recorded at the 850 MHz Facility. Peaks at approximately 55, 32, and 7 ppm arise from ^{27}Al in 4-, 5- and 6-fold coordination to oxygen (there is some crystallisation involving 6-coordinated Al in the high Al_2O_3 content samples). The relative amounts of each environment were obtained by integrating under the peaks and this information was used to remove the first Al-O correlation from the neutron diffraction data for the samples, where it overlaps the Te-O correlation, thus enabling the determination of the n_{TeO} values for these glass compositions. These are plotted in Figure 1 as a function of $Al_{2/3}O$ (to be comparable to K_2O) and it is obvious that they do not follow the model derived for the modifier oxides. A straight line fit through the data intercepts the n_{TeO} = 3.66 line at 6 mol% $Al_{2/3}O$ (equivalent to 2.1 mol% Al_2O_3). It is possible that this behaviour may result from phase separation or clustering such that the Al atoms are not homogeneously distributed. To address this question, a double-quantum (DQ) homonuclear correlation experiment[5] has been implemented for ^{27}Al at the 850 MHz Facility and used to probe the Al…Al proximities in these glasses.

Figure 3 shows a ^{27}Al DQ-SQ spectrum from the 12.5 Al_2O_3 87.5 TeO_2 glass sample. At this composition, approximately 1 in 5 network polyhedra are [AlO_n] and, from the combination of ^{27}Al MAS NMR and neutron diffraction data, average coordination numbers are n_{AlO} = 5.07, n_{TeO} = 3.36, n_{OAl} = 0.60, n_{OTe} = 1.38. This means that *on average* there should be no Al-O-Al through-bond connections. The 2D DQ spectrum shows through-space interactions indicating that the most significant [AlO_n]-[AlO_n] (or n-n') proximities are 6-6 and 4-4, with significantly smaller contributions from 6-4 and 6-5 and very much smaller contributions from 5-5 and 4-5. This suggests that the distribution of [AlO_n] species is not homogeneous with preferential bonding of certain species with the [TeO_4E] and [TeO_3E] units or segregation occurring. Preliminary simulations of signal build-up using SIMPSON imply that the 6-6 and 4-4 distances are 4-4.5 Å, consistent with Al-O-Te-O-Al separations. However the DQ signal is extremely sensitive to offset and further experiments will be required to confirm this.

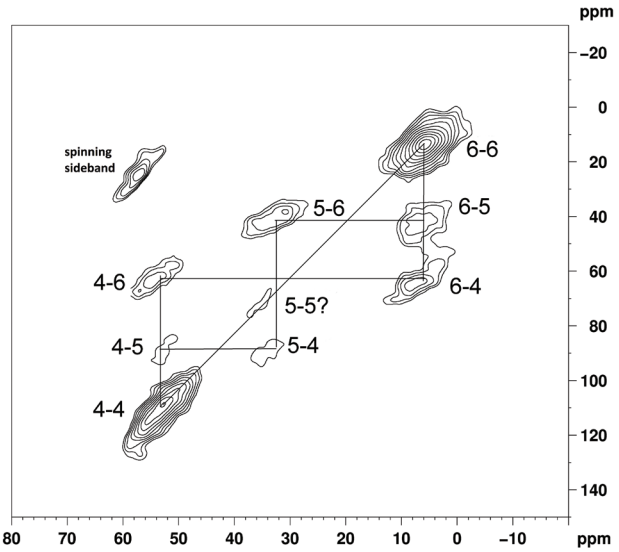

Figure 3. ^{27}Al DQ spectrum (20.0 Tesla, mixing time = 1.6 ms) of a 12.5Al_2O_3 87.5TeO_2 glass sample. 1024 transients were coadded for each of 96 t_1 slices, with a t_1 increment of 25 μs. [AlO_n]-[AlO_n] interactions are labelled as n-n'.

References

1. Himei, Y.; Osaka, A.; Nanba, T.; Miura, Y. *J. Non-Cryst. Solids* **1994**, *177*, 164.
2. McLaughlin, J. C.; Tagg, S. L.; Zwanziger, J. W. *J. Phys. Chem. B* **2001**, *105*, 67.
3. Kalampounias, A. G.; Boghosian, S. *Vib. Spectrosc.* **2012**, *59*, 18.
4. Barney, E. R.; Hannon, A. C.; Holland, D.; Umesaki, N.; Tatsumisago, M.; Orman, R. G.; Feller, S. *J. Phys. Chem. Lett.* **2013**, *4*, 2312.
5. Wang, Q.; Hu, B.; Lafon, O.; Trebosc, J.; Deng, F.; Amoureux, J. P. *J Magn. Reson.* **2009**, *200*, 251.

^{93}Nb Very Fast Magic Angle Spinning Solid-State NMR of Fergusonite Ion Conductors

Frédéric Blanc,[1] Dinu Iuga,[2] Ryan D. Bayliss[3] and Stephen J. Skinner[3]

[1]*Department of Chemistry, University of Liverpool*

[2]*Department of Physics, University of Warwick*

[3]*Department of Materials, Imperial College London*

Overview

Fergusonite materials $A^{3+}B^{5+}O_4$ have shown extremely promising fast oxide ion conduction properties for solid oxide fuel cell applications when doped with a higher valence cation $(B')^{6+}$ on the B^{5+} cation site.[1] These materials differ from others such as perovskites and fluorites as the conduction mechanism is based on interstitial oxygens (rather than oxygen vacancies), as the presence of a $(B')^{6+}$ cation at the B^{5+} cation site induces extra oxygens for charge balance. Recent work on doped perovskites showed that solid-state NMR spectroscopy yields detailed insight into the defect chemistry and ionic motion in solid electrolytes[2,3] by the identification of cations bearing oxygen vacancies (*i.e.*, a cation with a lower coordination number). In principle, doped fergusonite materials such as W doped $LaNbO_4$ (*e.g.* $LaNb_{0.92}W_{0.08}O_{4+d}$ where W^{6+} substitutes on the Nb^{5+} site) should have interstitial oxygens and therefore cations with higher coordination number. ^{93}Nb NMR at very high field and under very fast magic angle spinning (MAS) conditions should be able to provide insight into the local environments experienced by the niobium sites.[4,5]

^{93}Nb Very Fast MAS Solid-State NMR of $LaNbO_4$ and $LaNb_{0.92}W_{0.08}O_{4+d}$

A ^{93}Nb very fast MAS one dimensional solid-state NMR spectrum of $LaNbO_4$ (Figure 1a) obtained using the Jeol 1 mm probe is presented in Figure 1b, and displays a very broad pattern as anticipated for ^{93}Nb, due to its large quadrupolar broadening, even at the very high field of 20 T. The spectrum is in fair agreement with that simulated using known NMR parameters obtained from a multi magnetic field study under non spinning conditions.[5] We note that the very fast MAS rate of 78 kHz used seems still to be just not fast enough to average out the second-rank anisotropic broadening of ^{93}Nb in $LaNbO_4$, which has a static linewidth of approximately 320 kHz, and to clearly reveal the ^{93}Nb central transition. Nevertheless, the simulated spectrum does not present the experimental feature at approximately –800 ppm and this is likely due to a slightly different source of $LaNbO_4$ or method of preparation. A ^{93}Nb Triple Quantum (TQ) MAS spectrum of $LaNbO_4$, which is displayed in Figure 1b, reveals a single niobium crystallographic site at –1200 ppm with an isotropic chemical shift (δ_{iso}) of –840 ppm, in agreement with the presence of a 4 coordinated Nb site.[5] This value is very close to the reported data of –853 ppm for $LaNbO_4$[5] and demonstrates that this site corresponds to a NbO_4 environment. A ^{93}Nb very fast MAS NMR spectrum of $LaNb_{0.92}W_{0.08}O_{4+d}$ (Figure 1c) shows multiple overlapping peaks in the –600 to –900 ppm region. Notably, this spectrum presents fewer spinning sidebands than $LaNbO_4$ (Figure 1b) and may indicate faster oxygen dynamics in $LaNb_{0.92}W_{0.08}O_{4+d}$ as shown by diffusivity measurements (manuscript in preparation). The ^{93}Nb TQMAS spectrum demonstrates that in addition to the niobium site present in $LaNbO_4$ (observed at approximately –800 ppm with δ_{iso} = –853 ppm), a second additional site is present at –600 ppm with an δ_{iso} of –960 ppm and a quadrupolar coupling constant (C_Q) of ~50 MHz. Importantly, these parameters demonstrate that this corresponds to a six coordinated niobium environment (NbO_6) and therefore a niobium crystallographic site associated with interstitial oxygens (manuscript in preparation).

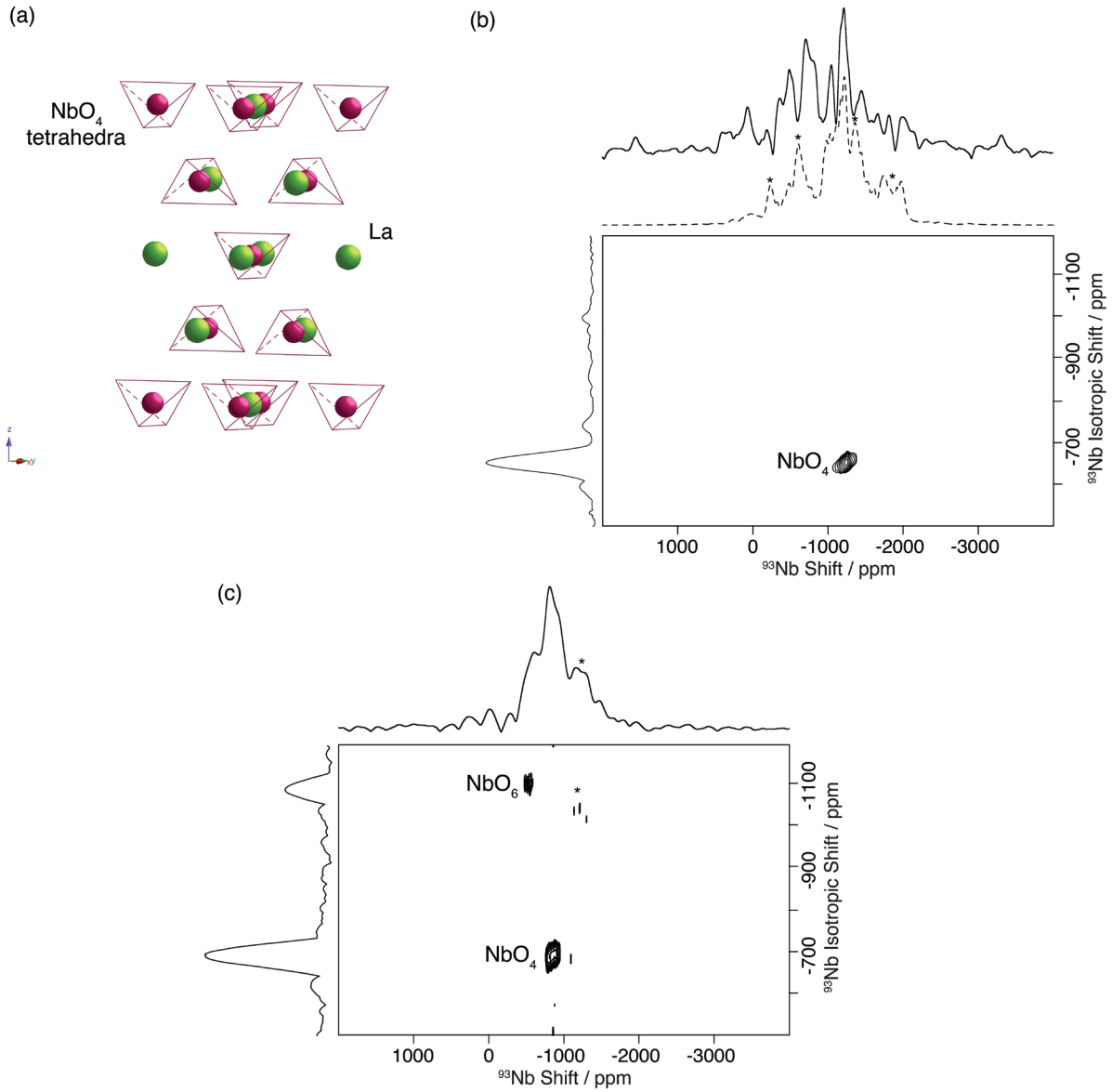

Figure 1. (a) Crystal structure of fergusonite-type $LaNbO_4$ showing NbO_4 tetrahedra. ^{93}Nb (20.0 T, 78 kHz MAS) triple-quantum MAS NMR spectra of (b) $LaNbO_4$ and (c) $LaNb_{0.92}W_{0.08}O_{4+\delta}$. Top: 1D spectrum. Left: Projection of the isotropic dimension. The dashed lines are spectra simulated using SIMPSON[6] for known parameters.[5] Asterisks (*) denote spinning sidebands.

References

1. Packer, R. J.; Skinner, S. J.; Yaremchenko, A. A.; Tsipis, E. V.; Kharton, V. V.; Patrakeev, M. V.; Bakhteeva, Y. A. *J. Mater. Chem.* **2006**, *16*, 3503.
2. Blanc, F.; Middlemiss, D. S.; Gan, Z.; Grey, C. P. *J. Am. Chem. Soc.* **2011**, *133*, 17662.
3. Buannic, L.; Blanc, F.; Middlemiss, D. S.; Grey, C. P. *J. Am. Chem. Soc.* **2012**, *134*, 14483.
4. Johnston, K. E.; Tang, C. C.; Parker, J. E.; Knight, K. S.; Lightfoot, P.; Ashbrook, S. E. *J. Am. Chem. Soc.* **2010**, *132*, 8732.
5. Hanna, J. V; Pike, K. J.; Charpentier, T.; Kemp, T. F.; Smith, M. E.; Lucier, B. E. G.; Schurko, R. W.; Cahill, L. S. *Chem. Eur. J.* **2010**, *16*, 3222.
6. Bak, M.; Rasmussen, J. T.; Nielsen, N. C. *J. Magn. Reson.* **2000**, *147*, 296.

A Solid-State NMR Study of Crystalline and Amorphous Zeolitic Imidazolate Frameworks (ZIF)

Frédéric Blanc,[1] Emma Baxter,[2] Thomas D. Bennett[2] and Anthony K. Cheetham[2]

[1]*Department of Chemistry, University of Liverpool*

[2]*Department of Materials Science and Metallurgy, University of Cambridge*

Overview

Zeolitic Imidazolate Frameworks (ZIFs) are a recently discovered class of three-dimensional Metal Organic Frameworks (MOFs) structures based on rigid MN_4 tetrahedra (M = Zn or Co) linked through bridging imidazolate (Im) $C_3H_3N_2^-$ or methyl imidazolate (mIm) $C_4H_5N_2^-$ anions, and have shown high porosity (≈ 1,800 $m^2.g^{-1}$), thermal stability (up to 550 °C) and chemical resistance.[1] Neutron and X-ray powder diffraction demonstrate that ZIF-4 ($Zn(Im)_2$) with the variscite structure (Figure 1a) undergoes a reversible crystal – amorphous phase transition on heating to 300 °C to yield an amorphous phase, *a*ZIF-4.[2,3] Further heating of *a*ZIF-4 above 400°C induces recrystallization into a dense ZIF (ZIF-zni) (Figure 1b).[2] A mechanosynthesis (ball-milling) method applied to the crystalline phases ZIF-zni or ZIF-8 ($Zn(mIm)_2$, with sodalite structure, see Figure 2a) irreversibly yields amorphous ZIF-zni (*a*ZIF-zni) or ZIF-8 (*a*ZIF-zni), respectively;[3] this is the only method of amorphization of ZIF-8, as thermal treatment up to 500 °C only yields decomposition products (i.e., ZnO). Remarkably, the pair distribution functions (PDFs), obtained from diffraction, of ZIF-4, *a*ZIF4 and ZIF-zni are virtually identical up to 6 Å, showing effectively similar local structure in these phases. We became interested in recording ^{13}C and ^{15}N solid-state NMR spectra to investigate the insight provided by NMR into these ZIFs structures.

^{13}C and ^{15}N CP MAS Spectra of Zeolitic Imidazolate Frameworks-4

^{13}C and ^{15}N CP MAS spectra of ZIF-4, *a*ZIF-4, ZIF-zni and *a*ZIF-zni are shown in Figure 1c and d. The ^{13}C and ^{15}N CP MAS spectra of ZIF4 show 11 and 7 resonances of similar intensities, and 1 resonance of twice the intensity, in agreement with the 12 different carbons and 8 nitrogens in the asymmetric unit cell as determined by X-ray crystallography.[1] These spectra exhibit very narrow lines (full width at half maximum height, FWHMH, of ~30 and ~20 Hz for ^{13}C and ^{15}N, respectively) in agreement with the very high crystallinity of ZIF-4.[1] Both ^{13}C and ^{15}N CP spectra of *a*ZIF-4 and ZIF-zni are relatively similar and reflect the $Zn(Im)_2$ stoichiometry of both materials. The peaks observed for *a*ZIF-4 are broader than those obtained for crystalline ZIF as expected for an amorphous material, although the resolution obtained in *a*ZIF-4 still suggests a very high degree of local order as suggested by the PDFs data (Figure 1b).

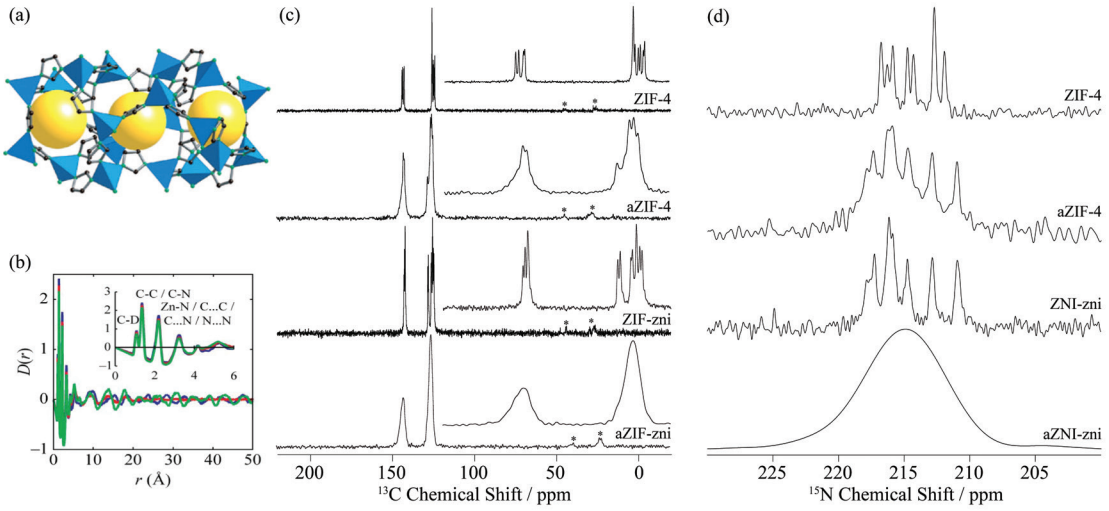

Figure 1. (a) Crystal structure of ZIF-4.[1] Blue: ZnN_4 tetrahedra, black: C, green: N. Hydrogen atoms are omitted for clarity. The yellow sphere of diameter 2.04 Å represents the largest space available in the framework. (b) Neutron diffraction differential correlation functions (PDFs) D(r), together with the corresponding interatomic correlations.[2] Blue: ZIF-4, red: aZIF-4, green: ZIF-zni. (c) ^{13}C and (d) ^{15}N (20.0 T, 21 kHz MAS) CP MAS NMR spectra of ZIF-4, aZIF-4, ZIF-zni and aZIF-zni. Inserts in (c) show a magnified view of the 120-155 ppm region. Asterisks (*) denote spinning sidebands.

^{13}C and ^{15}N CP MAS spectra of ZIF-zni (obtained from heating *a*ZIF-4 above 400 °C) also yield narrow lines (FWHMH of ~70 and ~60 Hz for ^{13}C and ^{15}N, respectively) in clear agreement with a thermal recrystallization of *a*ZIF-4 into ZIF-zni. The number of resonances observed in both ^{13}C (12 peaks) and ^{15}N (8 peaks) spectra are also in agreement with the numbers of carbons and nitrogens in the asymmetric unit cell.

^{13}C and ^{15}N CP MAS spectra of *a*ZIF-zni (obtained by mechanosynthesis of crystalline ZIF-zni) are shown in Figure 1c and d, and exhibit very broad peaks suggesting no long range order in this amorphous material. This is in sharp contrast with the thermally induced amorphization of ZIF-4, which still produces a material (*a*ZIF-4) with local order. These NMR results demonstrate that solid-state NMR provides useful information for studying ZIFs, and that there might be a memory effect upon thermal amorphization but not by mechanically induced amorphization.

^{13}C and ^{15}N CP MAS Spectra of Zeolitic Imidazolate Frameworks-8

^{13}C and ^{15}N CP MAS spectra of ZIF-8 and *a*ZIF-8 (obtained by mechanosynthesis of crystalline ZIF-8) are shown in Figure 2b and c. While both ^{13}C and ^{15}N spectra of ZIF-8 are very narrow and the three ^{13}C peaks and single ^{15}N peak match the number of carbons and nitrogen in the asymmetric unit cell,[1] the spectra of *a*ZIF-8 are very broad, indicating very little order. This is in line with the data discussed above, where mechanically induced amorphization produces poorly ordered *a*ZIF-zni material. We also note here that the mechanosynthesis method applied to ZIF-8 yields a second phase in *a*ZIF-8 (as evidence by the peaks at 147 and 117 ppm). This suggests smaller chemical resistance of ZIF-8 than ZIF-zni, although ZIF-8 shows exceptional resistance to hydrolysis and is outstanding among MOFs materials.[1]

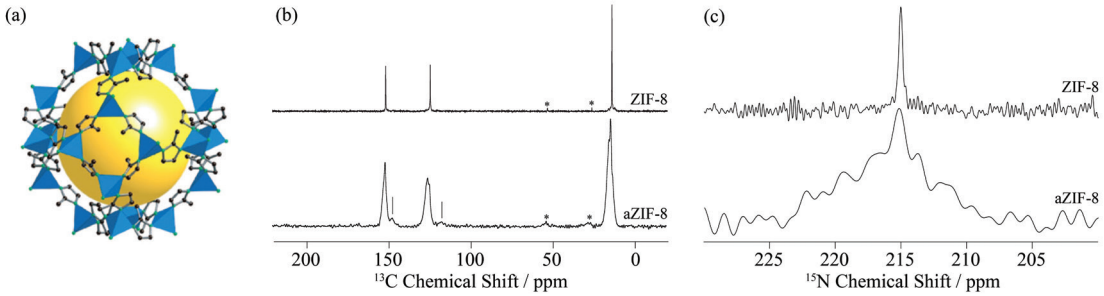

Figure 2. (a) Crystal structure of ZIF-8.[1] Blue: ZnN_4 tetrahedra, black: C, green: N. Hydrogen atoms are omitted for clarity. The yellow sphere of diameter 11.60 Å represents the largest space available in the framework. (b) ^{13}C and (c) ^{15}N (20.0 T, 21 kHz MAS) CP MAS NMR spectra of ZIF-8 and aZIF-8. Asterisks (*) and small vertical lines (|) denote spinning sidebands and a second phase, respectively.

References

1. Park, K. S.; Ni, Z.; Cote, A. P.; Choi, J. Y.; Huang, R.; Uribe-Romo, F. J.; Chae, H. K.; O'Keeffe, M.; Yaghi, O. M. *Proc. Natl. Acad. Sci. U. S. A.* **2006**, *103*, 10186.
2. Bennett, T. D.; Goodwin, A. L.; Dove, M. T.; Keen, D. A.; Tucker, M. G.; Barney, E. R.; Soper, A. K.; Bithell, E. G.; Tan, J.-C.; Cheetham, A. K. *Phys. Rev. Lett.* **2010**, *104*, 115503.
3. Bennett, T. D.; Cao, S.; Tan, J. C.; Keen, D. A.; Bithell, E. G.; Beldon, P. J.; Friscic, T.; Cheetham, A. K. *J. Am. Chem. Soc.* **2011**, *133*, 14546.
4. Bennett, T. D.; Simoncic, P.; Moggach, S. A.; Gozzo, F.; Macchi, P.; Keen, D. A.; Tan, J.-C.; Cheetham, A. K. *Chem. Commun.* **2011**, *47*, 7983.

Probing Supramolecular Self-Assembly at Natural Isotopic Abundance by ^{1}H Double-Quantum and ^{14}N-^{1}H MAS NMR

Manjunatha Reddy G. N.,[1] Lucia Gramigna,[2] Stefano Masiero[2] and Steven P. Brown[1]

[1]*Department of Physics, University of Warwick*

[2]*Department of Organic Chemistry "A. Mangini", University of Bologna, Italy*

Overview

The combination of high magnetic field (20 Tesla) and fast magic-angle spinning (MAS), here at 75 kHz using the 850 MHz Facility's Jeol 1 mm probe, yields high-resolution ^{1}H spectra for moderately-sized organic molecules. Such ^{1}H solid-state NMR spectra can be obtained at natural isotopic abundance and provide valuable insight into intermolecular interactions, e.g., hydrogen bonding and CH-π and π-π interactions, that drive self assembly.[1] Specifically, we present here ^{1}H double-quantum (DQ) and ^{14}N-^{1}H HMQC spectra for a guanosine derivative analogous to a vinylbenzene derivatized guanosine that was demonstrated[2] to undergo light-activated switching between ribbon and quartet self-assembly. ^{14}N-^{1}H solid-state NMR experiments[3-5] are particularly valuable for probing N-H…X and X-H…N hydrogen-bonding arrangements, as, for example, recently demonstrated for a different guanosine derivative.[6]

^{1}H DQ and ^{14}N-^{1}H Spectra

Figures 1 and 2 present ^{1}H DQ MAS and ^{14}N-^{1}H HMQC spectra of 2',3'-*O*-isopropylidine-5'-azoguanosine, respectively. Specifically, the spectra correspond to two separate preparations (left and right parts of Figure 1 and top and bottom of Figure 2) and show that polymorphism is exhibited. For the ^{14}N-^{1}H experiments, the left-hand spectra correspond to a short recoupling time ($\tau_{RCPL} = 8\tau_R = 107$ μs), such that only one-bond NH correlation peaks are observed for the NH and NH_2 moieties. At longer recoupling times, correlations to non-protonated nitrogen resonances are observed: e.g., from a ^{14}N-^{1}H spectrum of $dG(C3)_2$ presented in Ref. [6], the N7 ^{14}N resonance is expected at ~ +60 ppm. By comparison to the ^{1}H DQ MAS and ^{14}N-^{1}H spectra presented in Ref. [6] for $dG(C3)_2$, the obtained spectra seem to indicate ribbon-like self-assembly, with the highest-ppm NH ^{1}H resonances being observed at ~14 and ~12 ppm for the two distinct polymorphs. This research was supported by EPSRC grant EP/K003674/1.

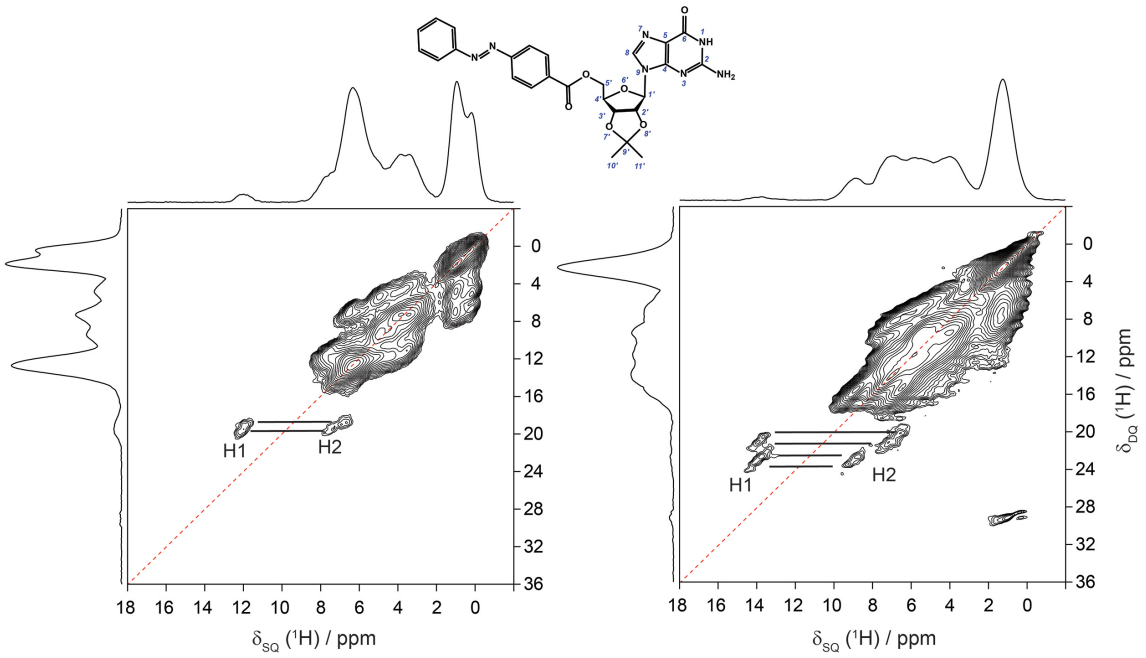

Figure 1. ^{1}H DQ MAS (850 MHz, 60 kHz MAS) spectra of two preparations (left and right) 2',3'-O-isopropylidine-5'-azoguanosine, recorded with one rotor period of BABA recoupling.

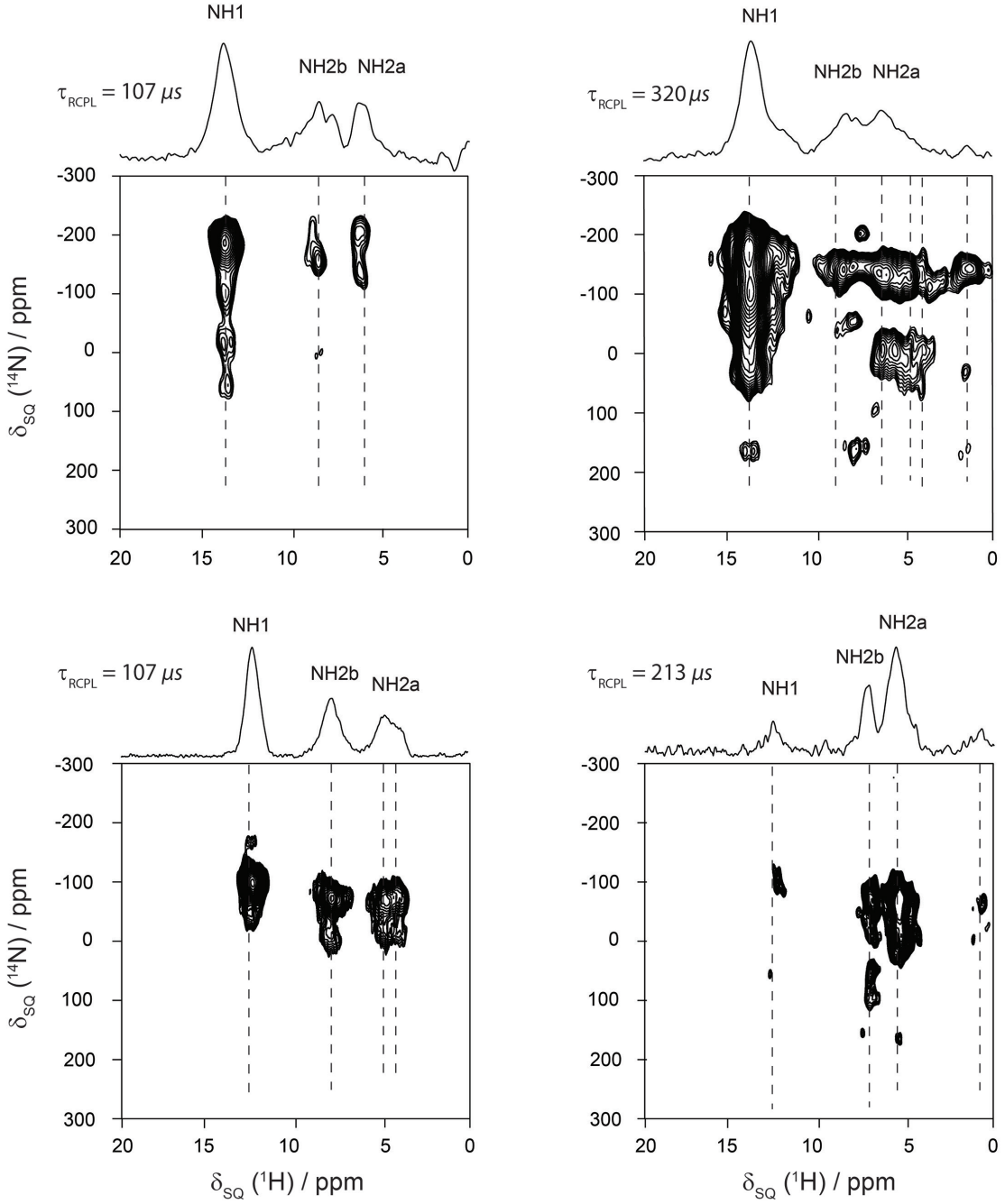

Figure 2. ^{14}N-^{1}H HMQC (850 MHz, 75 kHz MAS) spectra of two preparations (top and bottom) of 2',3'-O-isopropylidine-5'-azoguanosine, recorded using n = 2 R^3 durations of (left) $\tau_{RCPL} = 8\tau_R = 107$ μs and (right) $\tau_{RCPL} = 16\tau_R = 213$ μs or $\tau_{RCPL} = 24\tau_R = 320$ μs.

References

1. Brown, S. P. *Solid State Nucl. Magn. Reson.* **2012**, *41*, 1.
2. Lena, S.; Neviani, P.; Masiero, S.; Pieraccini, S.; Spada, G. P. *Angew. Chem., Int. Ed. Engl.* **2010**, *49*, 3657.
3. Gan, Z. H.; Amoureux, J. P.; Trebosc, J. *Chem. Phys. Lett.* **2007**, *435*, 163.
4. Cavadini, S.; Abraham, A.; Bodenhausen, G. *Chem. Phys. Lett.* **2007**, *445*, 1.
5. Tatton, A. S.; Bradley, J. P.; Iuga, D.; Brown, S. P. *Z. Phys. Chem.* **2012**, *226*, 1187.
6. Webber, A. L.; Masiero, S.; Pieraccini, S.; Burley, J. C.; Tatton, A. S.; Iuga, D.; Pham, T. N.; Spada, G. P.; Brown, S. P. *J. Am. Chem. Soc.* **2011**, *133*, 19777.

Enhancement of ^{14}N Overtone Polarization Using Symmetry Based Recoupling Sequences

Ibraheem M. Haies,[1,2] James A. Jarvis,[3] Philip T.F. Williamson[3] and Marina Carravetta[2]

[1]*College of Science, University of Mosul, Iraq*

[2]*Department of Chemistry, University of Southampton*

[3]*Centre for Biological Sciences, University of Southampton*

Overview

The application of magic-angle spinning (MAS) ^{14}N overtone spectroscopy is a promising method for the characterization of structure and dynamics at ^{14}N sites in organic and biological molecules.[1] A current limitation of the technique, however, lies in the absence of efficient polarization techniques, which would enable both signal enhancement and the possibility of performing correlation spectroscopy. Our previous studies had suggested that despite theoretical considerations that predict a drop in overtone excitation at higher magnetic fields, significant signal enhancements are observed at higher magnetic fields due to a reduction in the second-order quadrupolar interaction. We describe here the evaluation of ^{14}N overtone signal enhancements achieved at high magnetic field at the UK 850 MHz Solid-State NMR Facility, and ascertain whether the R-symmetry based polarization transfer technique, PRESTO,[2] developed at lower magnetic fields, gives improved ^{14}N overtone signal enhancements at higher magnetic fields. Experiments were performed to measure the ^{14}N overtone signal by direct acquisition, and by enhancement with PRESTO, on samples of glycine (C_Q = 1.18 MHz) and N-acetyl-valine (NAV) (C_Q = 3.18 MHz), which has a quadrupolar coupling of a similar magnitude as that found in proteins.

Results

Direct excitation ^{14}N overtone spectra were acquired on glycine in order to assess the sensitivity of the ^{14}N overtone transition at 20.0 Tesla on a sample with a moderate quadrupolar interaction. A representative spectrum is shown in Figure 1. With the appropriate choice of resonance offset, excellent quality spectra were obtained for 1024 coadded transients with a signal to noise greater than that observed at magnetic field strengths corresponding to ^{1}H Larmor frequencies of 400 and 600 MHz, suggesting that the efficiency of excitation of the ^{14}N overtone does increase with field strength.

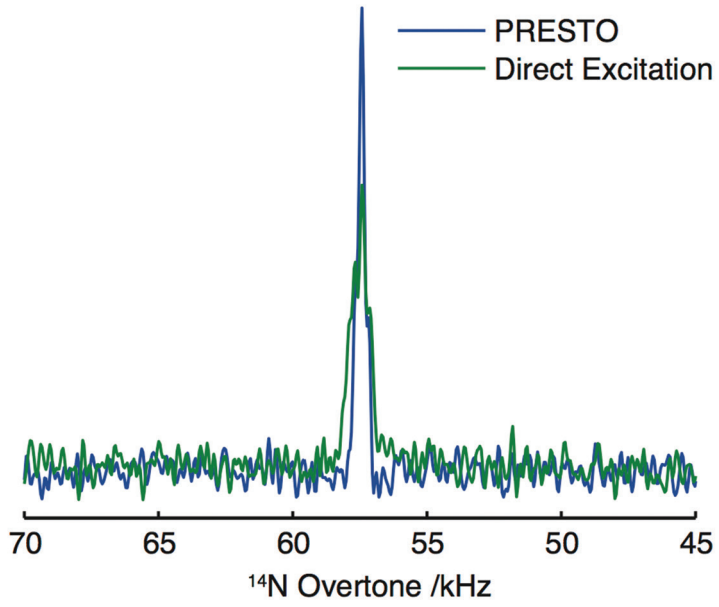

Figure 1. Direct excitation (green) and PRESTO-enhanced (blue) ^{14}N overtone spectra acquired at the 850 MHz Facility on a 33 mg sample of glycine at natural isotopic abundance in a 3.2 mm MAS rotor spinning at 20 kHz. In both experiments, a 275 μs 90° pulse with a corresponding ^{14}N nutation frequency of 70 kHz was used for ^{14}N overtone pulses, and SPINAL-64 decoupling at a ^{1}H nutation frequency of 100 kHz was applied during acquisition. An $R18_2^5$ sequence was used for PRESTO polarization transfer; with 21 R/R^{-} pairs and a ^{1}H nutation frequency of 89 kHz. 1024 transients were coadded in each experiment.

To further enhance the sensitivity, magnetization was transferred from protons within the sample to the ^{14}N overtone transition using the PRESTO pulse sequence. This symmetry based R-sequence, unlike cross polarization, permits the transfer of polarization from ^{1}H to ^{14}N using minimal manipulation of the ^{14}N overtone transition. Furthermore, the symmetry elements within the sequence can be optimized for available rf and spinning performance. Using a $R18_2^5$ sequence, enhancements of ~50% were observed in signal intensity, when compared with data obtained by direct acquisition. The PRESTO enhanced spectrum is also shown in Figure 1.

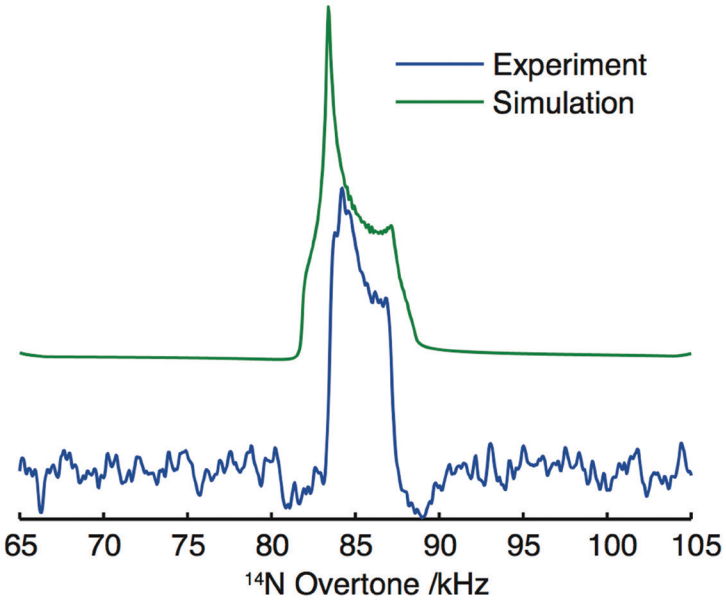

Figure 2. Experimental (blue) and simulated (green) direct excitation ^{14}N overtone spectra of NAV at 20.0 Tesla. The experimental spectrum was acquired on a 31 mg sample of NAV spinning at 20 kHz. A 275 μs 90° pulse with a corresponding ^{14}N nutation frequency of 70 kHz was used for ^{14}N overtone pulses, and SPINAL-64 decoupling at a ^{1}H nutation frequency of 100 kHz was applied during acquisition. 40,000 transients were coadded. The simulated spectrum was obtained using Spinach.[3]

To assess the possibility of using ^{14}N overtone spectroscopy to study molecules with spin interactions that mimic those found in biological solids, spectra were recorded on *N*-Acetyl-Valine (NAV). The asymmetric amide ^{14}N site in NAV has a quadrupolar coupling constant of 3.18 MHz; a similar magnitude to that commonly found in proteins. The direct acquisition spectrum of NAV is shown in Figure 2. Comparison of the experimental spectrum with that simulated reveals good agreement between the lineshapes, and the experiment was more sensitive than when performed at magnetic field strengths corresponding to ^{1}H Larmor frequencies of 400 or 600 MHz. This highlights that even in the presence of larger quadrupolar interactions, at higher fields it is possible to efficiently excite the ^{14}N overtone transition and that the resulting lineshapes are of sufficient quality to quantitatively study the properties of the ^{14}N quadrupolar interaction.

References

1. O'Dell, L. A.; Brinkmann, A. *J. Chem. Phys.* **2013,** *138*, 064201.
2. Zhao, X.; Hoffbauer, W.; Schmedt auf der Günne, J.; Levitt, M. H. *Solid State Nucl. Magn. Reson.* **2004**, *26*, 57.
3. Hogben, H. J.; Krzystyniak, M.; Charnock, G. T. P.; Hore, P. J.; Kuprov, I. *J. Magn. Reson.* **2011,** *208*, 179.

2D and 3D ^{13}C NMR Studies of Whole Plant Stems

Paul Dupree,[1] Jennifer C. Mortimer,[1] Dharmesh Patel,[2] Thomas J. Simmons,[1] Steven P. Brown[2] and Ray Dupree[2]

[1]*Department of Biochemistry, University of Cambridge*

[2]*Department of Physics, University of Warwick*

Overview

A major technological challenge in using plant biomass for renewable energy is to release the sugars from cellulose and other polysaccharides effectively and cheaply. Pilot biofuel production processes involve the use of energy-intensive harsh biomass pretreatments, and also require the addition of high quantities of enzymes to break down the biomass. Progress in improving these steps is restrained by the limited understanding of the molecular basis of plant cell wall 'recalcitrance' – the difficulty in deconstructing lignocellulose into fermentable sugars. The main carbohydrate components in the cell walls are xylan, a polymer of 5-carbon xylose, and cellulose, a polymer of 6-carbon glucose. The molecular arrangement of these in secondary plant cell walls (woody materials) is poorly understood. Whilst ^{13}C NMR should be a good probe of the local environment, almost all NMR experiments on plants have necessarily been 1D so that there is considerable overlap of signals from the different components which makes it very difficult to fully interpret the spectrum. Recently Dick-Perez et al.[1] used enriched ^{13}C to study the *primary* cell walls of plants germinated and grown in the dark in a liquid culture with uniformly ^{13}C labelled glucose as the carbon source. Whole seedlings including roots were powdered and had extensive chemical treatment before NMR. Our aim is to study the *secondary* cell walls important for bioenergy and we have used *Arabidopsis* plants grown in air enriched with $^{13}CO_2$ as the carbon source achieving ~97% ^{13}C incorporation. The stems of these plants were inserted into MAS rotors with minimal pre-treatment and no chemical treatment or ball milling. Experiments at 500 MHz, although allowing resolution and assignment of major components, suffered from considerable overlap, and time was requested for 2D and 3D ^{13}C-^{13}C-^{13}C experiments at the 850 MHz Facility to improve the resolution.

Results

A ^{13}C refocused INADEQUATE spectrum was acquired to probe connectivities via one-bond C-C *J* couplings. The polysaccharide region of the spectrum, shown in Figures 1a and 1b, reveals clear cross-peaks within each of two cellulose environments, e.g. $C^1$4-$C^1$5, $C^2$4-$C^2$5. In the literature, environment C^1 has been assigned to internal cellulose chains, and C^2 to surface or amorphous chains. Additional polysaccharide cross-peaks that are not yet assigned are also visible. A 3D ^{13}C-^{13}C-^{13}C DARR experiment was run to further aid resolution, and to probe spatial relationships between components in the cell wall. In this experiment two mixing times t_{m1} and t_{m2} are used, where t_{m1} is short (~10ms) and t_{m2} can be either short or long.[2] A long t_{m2} allows the observation of both intramolecular and intermolecular correlations, whilst for a short t_{m2} only intramolecular connections should be visible. An example is shown in Figure 1c for an F_2, F_3 plane at 88.8 ppm corresponding to the cellulose $C^1$4 for mixing times t_{m1} of 10 ms and t_{m2} of 300 ms. In the F_2 (y) direction, the intramolecular sites (except for C2 and $C^1$5 which have almost identical shifts) are well resolved. The longer distance correlations for this $C^1$4 site are visible in the *x* direction at F_2 = 88.8 ppm, where proximities to the second cellulose environment $C^2$4 and $C^2$6 are clearly visible, as are peaks at ~ 53 and 56 ppm in the methoxy/lignin region. Connections are also visible in the 1D slice at 88.8 ppm to syringyl and guaicyl lignin units. Note the lignin peaks are not observed in the Dick-Perez et al. studies of *primary* cell walls. A ^{13}C DARR plane at 84.2 ppm corresponding to the second cellulose environment $C^2$4 is shown in Figure 1d. Once again, the intramolecular connectivities are clear, except for C3 and $C^2$5 which have almost identical shifts. The longer distance correlations for this $C^2$4 site to the first cellulose environment $C^1$4 and $C^1$6 are clearly visible. This second cellulose environment also shows proximity to the lignin methoxy region. The suggested proximity of both glucose environments to lignin raises interesting questions about the identity and arrangement of the respective cellulose chains in the cell walls. Mutant plants with differing cellulose crystallinities and cell wall compositions are now being grown to further aid assignment.

References

1. Dick-Perez, M.; Zhang, Y.; Hayes, J.; Salazar, A.; Zabotina, O. A.; Hong, M. *Biochemistry* **2011,** *50,* 989.
2. Li, S.; Zhang, Y.; Hong, M. *J. Magn. Reson.* **2010**, *202*, 203.

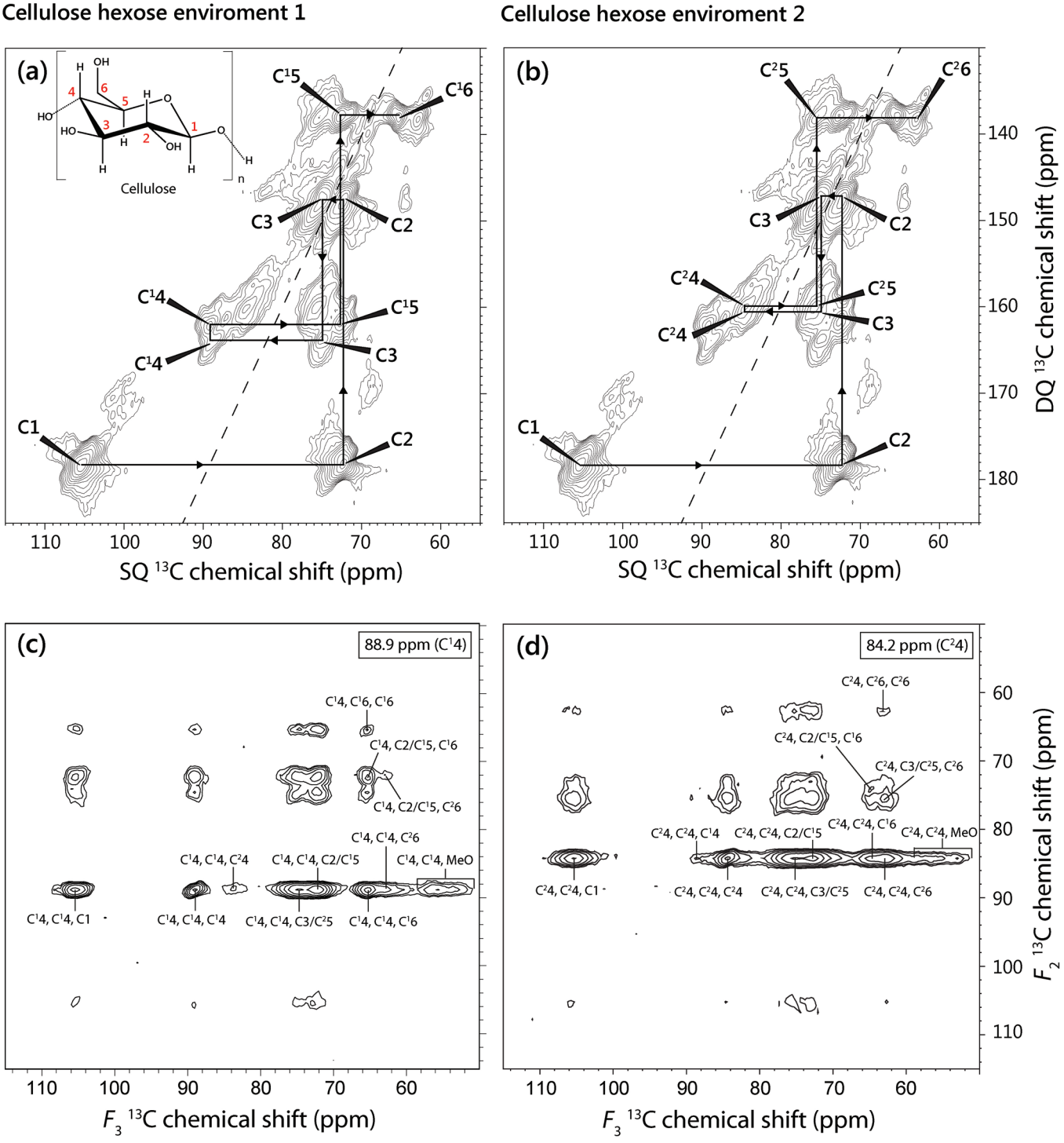

Figure 1. Spectra acquired from ^{13}C-labelled wild type Arabidopsis stems. (a, b) The sugar region of a 2D ^{13}C INADEQUATE spectrum. Two glucose environments in cellulose are annotated. (c, d) A 3D ^{13}C-^{13}C-^{13}C DARR spectrum with spin diffusion mixing times of 10 ms and 300 ms. Selected planes for C4 of the two glucose environments are shown. MeO- denotes the methoxyl group of lignin or pectin.

Zinc Substitution Sites in β-Tricalcium Phosphate for Waste Immobilisation

Ray Dupree, Andy T Grigg and Diane Holland

Department of Physics, University of Warwick

Overview

We have a long established interest in materials which are used for the immobilisation of nuclear waste from the domestic power industry and legacy waste from various defence programmes. We are currently using a range of techniques to investigate the site substitution preferences for various surrogate waste cations in β-tricalcium phosphate (β-TCP) in order to understand the limits on the loading of nuclear waste in this host. Zinc is present in significant concentrations in some legacy wastes and therefore of major interest to this programme. In the case of Zn^{2+} substitution, the evidence from X-ray and neutron diffraction is that the Zn^{2+} cations cause a contraction of the unit cell; however the exact nature of the substitution is unknown due to conflicting evidence from various sources. We have performed natural abundance ^{43}Ca NMR experiments with the aim of improving our understanding of the mechanism of Zn^{2+} substitution.

Background

β-tricalcium phosphate ($Ca_3(PO_4)_2$ contains 5 Ca sites[1] of different oxygen coordination, and therefore different dimensions, which are capable of accommodating the different size ranges of the cations found in radioactive waste. Ca(1), Ca(2) and Ca(3) sites are 7 or 8 coordinated and can potentially exchange with ions such as Sm^{3+} (a surrogate for Am^{3+}, Pu^{3+}) whilst the Ca(5) site is 6 coordinated and can accommodate smaller cations such as Ga^{3+}, Mg^{2+} and Zn^{2+}. The Ca(4) site is only 50% occupied (with a bond-valence sum of only 0.7).

Characterisation of substituted β-TCP systems has relied on X-ray and neutron diffraction to date, though site occupancies are difficult to quantify accurately for this very large unit cell. Figure 1 shows cell parameters which we have obtained by Rietveld analysis of diffraction data from the $Ca_{3-x}Zn_x(PO_4)_2$ system. Whilst there is an almost linear shrinkage along the a-axis on replacing Ca^{2+} by the smaller Zn^{2+}, there are dramatic changes in slope for both the c-axis and cell volume at x = 0.3 as hinted at previously.[2] This suggests a change in substitution mechanism at this composition, possibly from Ca(5) replacement (fully substituted at x = 0.286) to Ca(4) replacement (complete at x = 0.429).

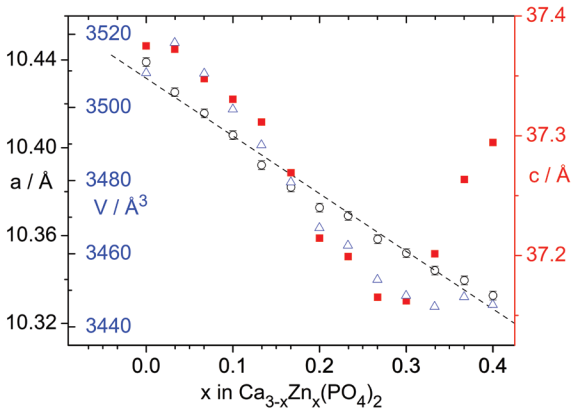

Figure 1: Cell parameters and cell volumes obtained for $Ca_{3-x}Zn_x(PO_4)_2$ as a function of x. The dashed line has been drawn to show the near linear decrease in the a-axis parameter, ○, whilst both the c-axis parameter, ■, and cell volume, △, has been drawn to show a dramatic change at about x = 0.3.

^{31}P NMR is remarkably sensitive to changes on the next-nearest neighbour calcium sites and a 500 MHz NMR spectrometer at Warwick was used first to address the substitution problem by studying the changes to ^{31}P spectra with increasing exchange of Zn^{2+} for Ca^{2+}. The ^{31}P data can be successfully simulated using a model which assumes that Zn^{2+} substitutes *initially* onto the Ca(5) site. There are only three crystallographically distinct P sites in β-TCP, but the local environments are determined by the occupancy of the next-nearest neighbour Ca sites (i.e. Ca^{2+}, Zn^{2+} or vacancy). This leads to eight possible NMR peaks. If substitution onto the Ca(4) site also occurs, the number of peaks rises to 11.[3] A model of this complexity is difficult to fit *uniquely*, and as such cannot be relied upon. Figure 2 shows a simulation of a ^{31}P spectrum obtained from a sample with x = 0.267 to illustrate this complexity. Therefore ^{43}Ca NMR has been used to observe the calcium environment directly with the aim of hopefully eliminating any ambiguity.

^{43}Ca Solid-State NMR Experiments

Spectra were obtained for $Ca_{3-x}Zn_x(PO_4)_2$ samples with x = 0.167 and 0.367, as these are compositions which have similar c-axis parameters but different cell-volumes and a-axis parameters. They also straddle the composition at which the model predicts a change from Ca(5) to Ca(4) substitution. Each spectrum took 2 days to acquire using a 7 mm MAS probe. Figure 3a shows the natural abundance ^{43}Ca spectrum for pure β-TCP obtained previously at the 850 MHz Facility together with a simulated spectrum. This can be compared with the spectra from the x = 0.167 and 0.367 samples (Figure 3b). The fit to the β-TCP spectrum is in agreement with the expected site occupancies for the pure material and also with the relation between ^{43}Ca shift and mean Ca-O distance identified by Gervais *et al.*[4] The changes which we observe for the x = 0.167 and 0.367 Zn substituted samples are as follows:

a) the peak assigned to Ca(5) is missing from the substituted spectra indicating that substitution initially occurs on the Ca(5) site;

b) there is an upfield shift of peaks from Ca(1), Ca(2) and Ca(3), which is usually due to lengthening of Ca-O bonds, but coincides here with a shrinking unit cell. It is however accompanied by a correlation between the Ca(4)-P(1) torsion angle and Zn concentration;

c) there is always intensity in the region currently associated with the Ca(4) site, which could indicate that:

   i. Ca(4) is not substituted;

   ii. Ca(3) has shifted and broadened into this region;

   iii. Ca(4) has been misassigned.

^{43}Ca spectra from samples with different substitution levels are needed to clarify this.

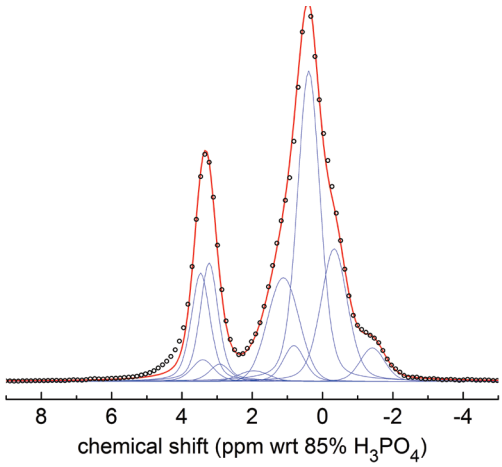

Figure 2. A ^{31}P (11.7 Tesla) spectrum of $Ca_{3-x}Zn_x(PO_4)_2$ (x = 0.267) together with a simulation based on Zn^{2+} substitution onto the Ca(5) site .

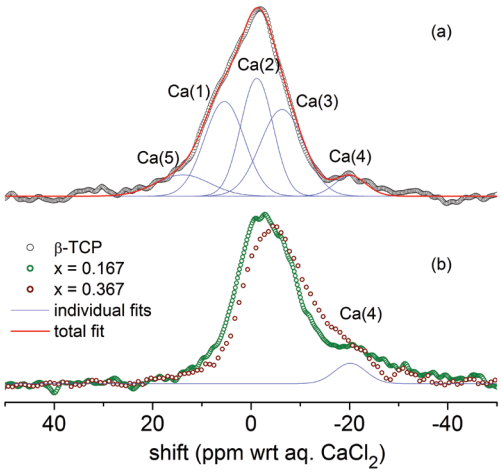

Figure 3. Natural abundance ^{43}Ca spectra recorded at 20.0 Tesla for (a) β-TCP and (b) $Ca_{3-x}Zn_x(PO_4)_2$ (x = 0.167 and 0.367). Individual peak fits are shown in blue, with that for Ca(4) repeated in the $Ca_{3-x}Zn_x(PO_4)_2$ spectra.

References

1. Yashima, M.; Sakai, A.; Kamiyama, T.; Hoshikawa, A. *J. Solid State Chem.* **2003**, *175*, 272.
2. Bigi, A.; Foresti, E.; Gandolfi, M.; Gazzano, M.; Roveri, N. *J. Inorg. Biochem.* **1997**, *66*, 259.
3. Grigg, A. T.; Mee, M.; Mallinson, P. M.; Fong, S. K.; Gan, Z.; Dupree, R.; Holland, D. *J. Solid State Chem.* **2014**, *212*, 227.
4. Gervais, C.; Laurencin, D.; Wong, A.; Pourpoint, F.; Labram, J.; Woodward, B.; Howes, A. P.; Pike, K. J.; Dupree, R.; Mauri, F.; Bonhomme, C.; Smith, M. E. *Chem. Phys. Lett.* **2008**, *464*, 42.

Isotopic and Structural Dilution to Improve Interpretation of Spin Diffusion DOR Spectra

Ray Dupree, Diane Holland and Oliver Alderman

Department of Physics, University of Warwick

Overview

We have investigated mechanisms by which the resolution of peaks in ^{11}B DOR and spin-diffusion (SD) DOR spectra can be improved, so that the interconnectivity of the structural units in borate crystals and glasses can be established. Isotope dilution to 25% ^{11}B, combined with DOR, can yield peak widths less than 0.2 ppm which is close to the limit of the probe shimming. However, at low ^{11}B concentrations, build-up of cross-peaks in SD DOR is too weak to achieve significant intensity in the timescale available. Structural dilution, i.e. isolation of groups of boron atoms, has also been briefly explored and we show that isolated rings containing 3 B (+ 3 O) atoms have ^{11}B DOR peaks which are slightly narrower (10-20%) than similar non-isolated units, but that this will need to be combined with isotope dilution if further narrowing is to be achieved.

Background

We are interested in the structural environment of boron in glasses, from simple binary borates to the much more complex borosilicate glasses which have considerable technological importance.[1] Boron is unique in oxide glass structure due to its capacity for producing well-defined medium range order (MRO) by the formation of rings, generally 6-membered (3B + 3O), containing various combinations of 3- and 4-coordinated boron (B(III) - [BO_3] planar triangles and B(IV) - [BO_4] tetrahedra).[2] In order to obtain a better understanding of the factors which stabilise this MRO in glasses, we have been studying the ^{11}B NMR spectra of crystalline borates. In particular, ^{11}B DOR NMR and SD DOR, combined with CASTEP calculations, have been used to assign the peaks in the spectra from borate crystals to sites in the superstructural units which constitute the known crystal structures.[3] This information can then be used to identify the units present in crystals and glasses of unknown structure. The small δ_{iso} ranges of trigonal, B(III), and tetrahedral, B(IV), sites (each typically 4 ppm) combined with the quadrupolar nature of the nucleus, mean that multiple sites are rarely resolved by MAS NMR, necessitating the use of DOR to remove the second-order quadrupole broadening. However, resolution is still limited by residual homonuclear dipolar broadening and we have therefore sought to reduce this by limiting the number of ^{11}B-^{11}B interactions using isotope dilution (replacing ^{11}B by ^{10}B) or by isolating groups of ^{11}B atoms using other network groups (in this case [GeO_4] units).

^{11}B DOR and Spin-Diffusion DOR Spectra

Figure 1 shows ^{11}B spectra obtained from dipotassium tetraborate ($K_2B_4O_7$) samples in which the ^{11}B isotope concentrations are 100% and 25%. It illustrates the improvement in resolution obtained using the DOR probe at the 850 MHz Facility as compared to that obtained using conventional MAS NMR at 11.75 T. In the latter (25%) case, whilst there is marked narrowing of the B(IV) peaks close to 0 ppm, there is little improvement (other than some sharpening of the divergences) in the quadrupole broadened B(III) peaks where the field gradients associated with the planar [BO_3] units are large. This second-order quadrupole effect can be removed by the use of DOR, giving dramatic narrowing of the B(III) peaks and the use of isotope dilution gives further narrowing, yielding peaks whose width is largely controlled by crystalline perfection and probe shimming.

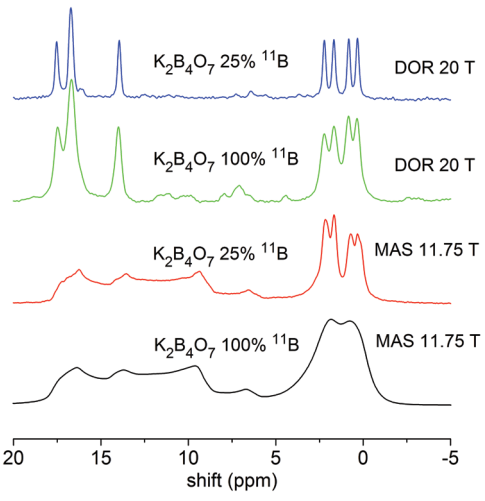

Figure 1. Comparison of line narrowing achievable by using DOR rather than MAS and by diluting to 25% ^{11}B.

Figure 2 compares the effect of isotope dilution and structural dilution. It shows ^{11}B DOR spectra from crystals of caesium triborogermanate, CsB_3GeO_7, which contains triborate [B_3O_5] units isolated from each other by [GeO_4] tetrahedra (Figure 3),[4] and caesium triborate CsB_3O_5 which contains triborate units which are linked by bonds between B(III) and B(IV) in neighbouring triborate units.[5] Spectra are shown for CsB_3O_5 with 100% and 25% ^{11}B for comparison.

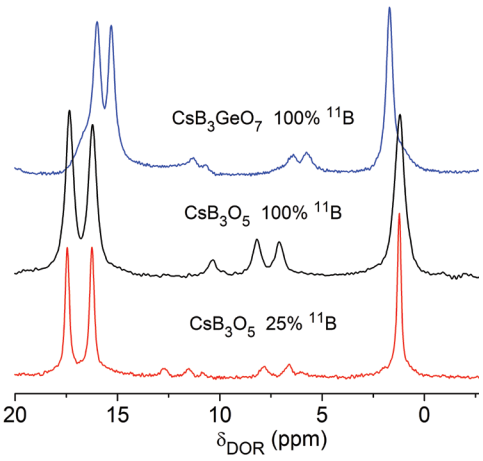

Figure 2. Comparison of DOR line narrowing achievable using isotope dilution (25% ^{11}B) and structural dilution (isolated $[B_3O_5]$ units).

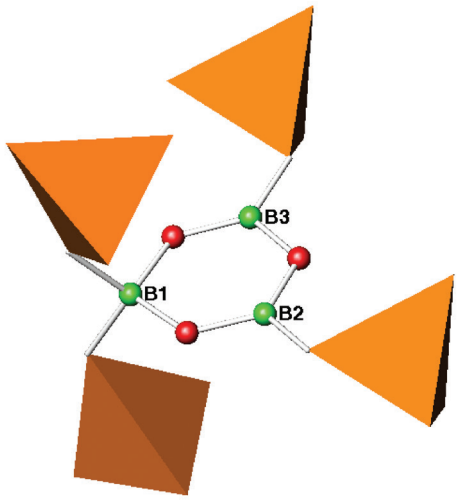

Figure 3. Fragment of the CsB_3GeO_7 structure showing how the triborate units (red – oxygen; green – boron) are separated from each other by $[GeO_4]$ tetrahedra (orange).

The line narrowing seen in the 1D ^{11}B DOR spectra of isotopically dilute samples is carried over into the ^{11}B SD DOR spectra. However, the increased resolution achieved by reducing the residual homonuclear dipolar interaction also reduces the signal as the number of neighbouring ^{11}B nuclei is much smaller, leading to drastically reduced intensity in the cross peaks, even after long mixing times. Figures 4a and 4b show the B(III) and B(IV) manifolds from a 50% ^{11}B $K_2B_4O_7$ sample (chosen for a compromise between resolution and signal intensity) for a 40 ms mixing time. The resolution is excellent but only one B(III)-B(III) cross peak is observed (Figure 4a) and possibly one B(IV)-B(IV) cross peak (Figure 4b), with no cross peaks between B(III) and B(IV) despite the B(III) separation being ~ 4.7 Å compared with ~ 2.6 Å from the non ring linking [BO3] group to a B(IV). Figure 4c shows a ^{11}B SD DOR spectrum for a 80 ms mixing time where a possible weak peak between a B(III) and B(IV) is observed. It is clear that distance is not the only factor affecting magnetisation exchange but the relative orientations between the electric field gradient tensors and dipole vector are also important.

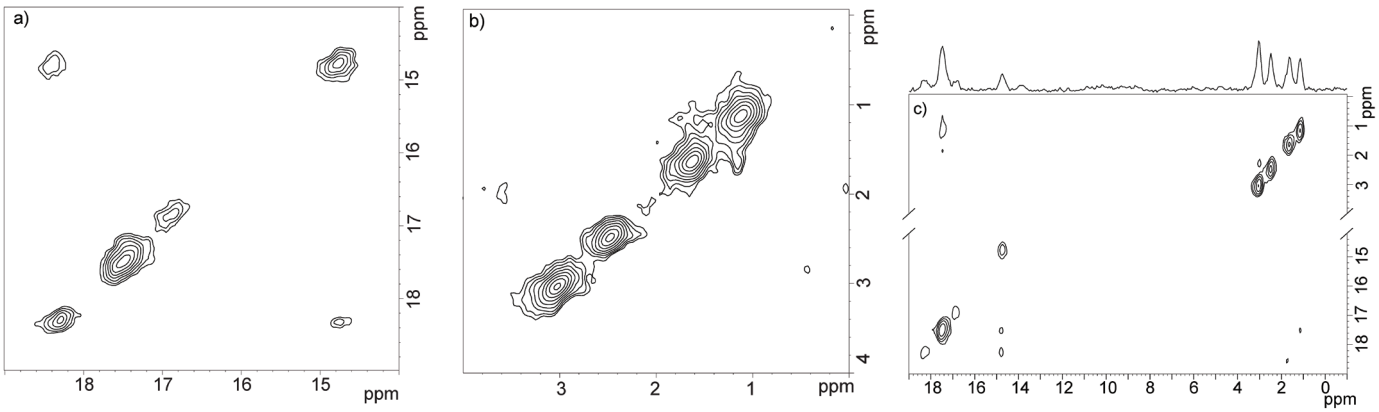

Figure 4. Regions of ^{11}B SD DOR spectra for $K_2B_4O_7$ with 50% ^{11}B. (a) B(III) manifold, mixing time of 40 ms; (b) B(IV) manifold, mixing time of 40 ms; (c) mixing time of 80 ms.

References

1. Howes, A. P.; Vedishcheva, N. M.; Samoson, A.; Hanna, J. V.; Smith, M. E.; Holland, D.; Dupree, R. *Phys. Chem. Chem. Phys.* **2011**, *13*, 11919.
2. Wright, A. C. *Phys. Chem. Glasses: Eur. J. Glass Sci. Technol. B* **2010**, *51*, 1.
3. Alderman, O. L. G.; Iuga, D.; Howes, A. P.; Pike, K. J.; Holland, D.; Dupree, R. *Phys. Chem. Chem. Phys.* **2013**, *15*, 8208.
4. Kong, F.; Jiang, H. L.; Hu, T.; Mao, J. G. *Inorg. Chem.* **2008**, *47*, 10611.
5. Krogh-Moe, J. *Acta Cryst.* **1974**, *B30*, 1178.

The Effect of Metal Catalysts and Cathode Reactivity on the Electrochemical Processes in the Lithium-Oxygen Battery

Michal Leskes, Amy J. Moore and Clare P. Grey

Department of Chemistry, University of Cambridge

Overview

The lithium-air battery is, in principle, a promising candidate for use as an energy storage system. Theoretically, it can store almost an order of magnitude more energy than a conventional lithium ion battery based on the reaction of lithium and oxygen to form lithium peroxide.[1] In practice, the development of the battery is still at early stages with challenges including the identification of stable electrolyte systems, inert and porous cathode materials and efficient catalytic species.[2] Significant improvements can only be achieved with a careful analysis of the electrochemical products formed during the operation of the cell. We have recently demonstrated, using high field measurements of ^{17}O NMR spectra, that solid-state NMR can provide a detailed description of the electrochemical products and processes taking place in the oxygen electrode.[3,4] While lithium peroxide is indeed identified as the main product in carbon electrodes, non-negligible electrolyte decomposition is occurring leading to degradation of the cell. Here we extend this approach further: Using the increased sensitivity offered by high-field measurements at the 850 MHz Facility along with very fast MAS, we can identify the influence of metal catalysts which are added to the carbon electrode. Furthermore, using ^{13}C enriched electrodes, we show that the carbon electrode itself is not inert, leading to the formation of lithium carbonate upon extended cycling.

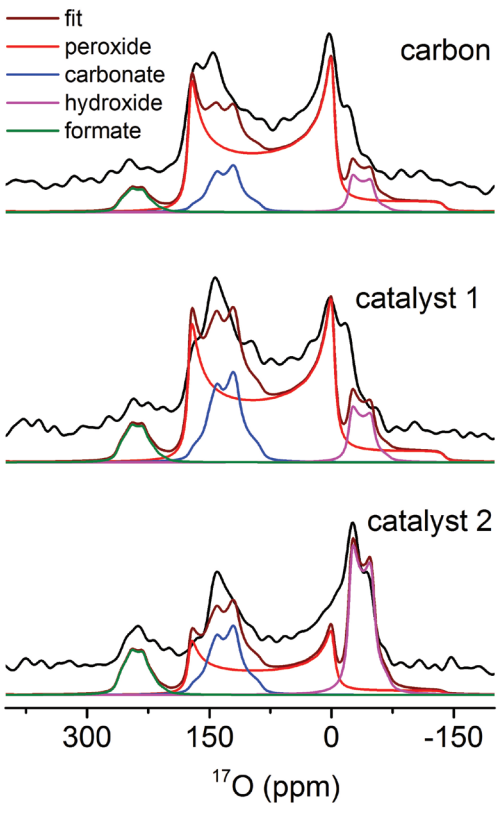

Figure 1 ^{17}O Hahn echo spectra of discharged electrodes acquired at 60 kHz MAS.

^{17}O Spectra of Products Formed in Electrodes Loaded with Metal Particles

The addition of precious metal particles to the carbon electrode has been shown to lower the over-potential of the charging process and in some cases also that of the discharge.[5] In order to test the effect of precious metals on the processes taking place in the electrode, we have cycled cells under a ^{17}O enriched atmosphere resulting in ^{17}O enrichment of the products formed in the cells. Figure 1 presents spectra acquired from three electrodes, carbon only and carbon with the addition of two types of metal particles. While in the carbon only electrode, lithium peroxide accounts for about 80% of the signal, when one type of metal is added (catalyst 2) lithium hydroxide is the major product. Catalyst 1, however, did not lead to significant changes in the ^{17}O spectrum and therefore is expected to have little or no effect on the electrochemical processes. Catalyst 2 is most likely promoting electrolyte decomposition processes instead of the formation of the desired peroxide.

^{13}C and ^{17}O Solid-State NMR Study of the Carbon Electrode Reactivity

Another source of parasitic side reactions that can affect the performance of the battery is the reactivity of the carbon electrode. ^{17}O MAS spectra acquired from ^{13}C enriched electrodes that were discharged once and three times in a ^{17}O enriched oxygen atmosphere are shown in Figure 2a and b, respectively. The spectra were fitted with the ^{17}O line shapes expected for the various discharge products and it is clear that, on the third cycle, parasitic side reactions dominate the electrochemical process, as only a very small amount of lithium peroxide is detected. Lithium carbonate is a major product on the third cycle, and a comparison of the ^{13}C spectra acquired from these two electrodes reveals the formation of ^{13}C enriched lithium carbonate on the 3rd discharge (resonating at about 170 ppm), indicating it originates from the carbon electrode itself. ^{13}C {^{17}O} Rotational Echo Adiabatic Passage Double Resonance[6] (REAPDOR) dephasing experiments were performed to evaluate the spatial proximity of the products and the carbon electrode. The dephasing curve of the carbonate signal (Figure 2d, red) was successfully simulated, confirming that the ^{17}O enrichment level was about 25% and revealing that the carbonate group is relatively immobile. Comparison of the extent of dephasing between the 1st and 3rd cycle (Figure 2d, pink and blue respectively) can indicate that wider areas of the carbon surface are covered with the ^{17}O enriched electrochemical products in the 1st cycle.

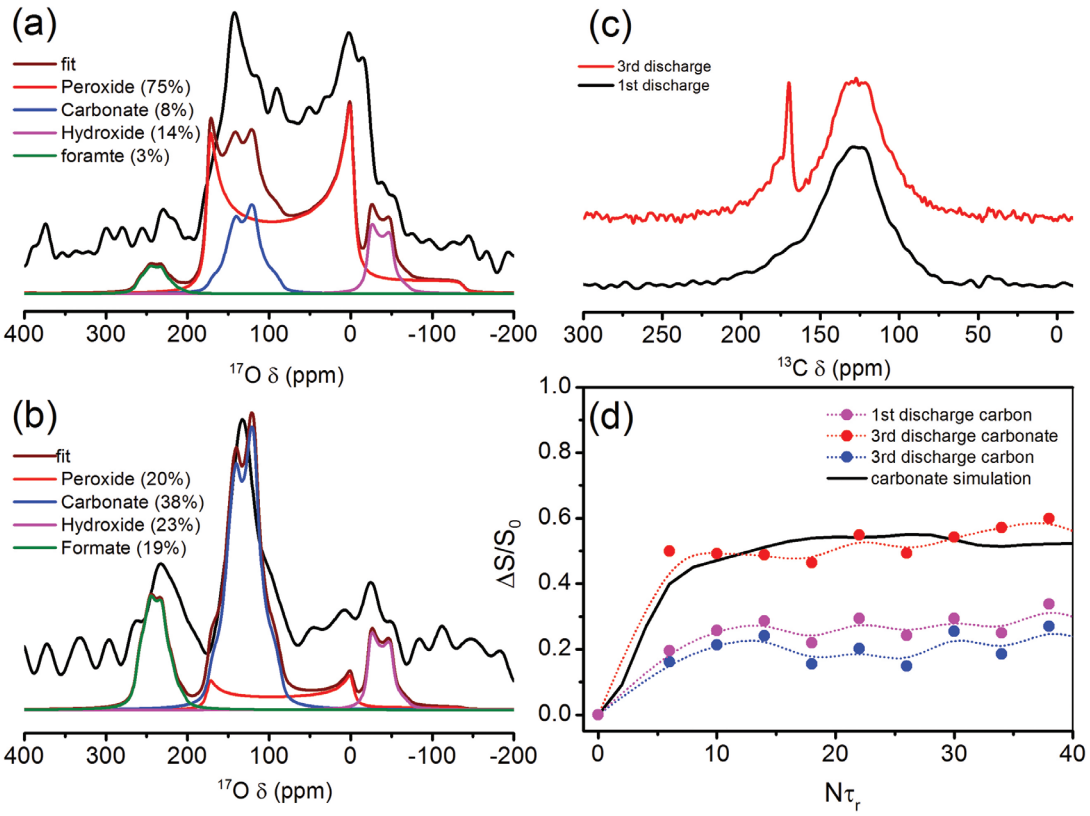

Figure 2 ^{17}O Hahn echo spectra acquired at 60 kHz MAS from ^{13}C enriched carbon electrodes after the (a) 1st and (b) 3rd discharge. Corresponding ^{13}C spectra and ^{13}C {^{17}O} REAPDOR dephasing curves are shown in (c) in (d), respectively, both acquired at 25 kHz MAS.

References

1. Bruce, P. G.; Freunberger, F. A.; Hardwick, L. J.; Tarascon, J.-M. *Nat. Mater*. **2012**, 11, 19.
2. Grishkumar, G.; McCloskey, B.; Luntz, A. C.; Swanson, S.; Wilcke, W. *J. Phys. Chem. Lett.* **2010**, 1, 2193.
3. Leskes, M.; Drewett, N. E.; Hardwick, L. J.; Bruce, P. G.; Goward, G. R.; Grey, C. P. *Angew. Chem. Int. Ed.* **2012**, 51, 8560.
4. Leskes, M.; Moore, A. J.; Goward, G. R.; Grey C. P. *J. Phys. Chem. C* **2013**, 117, 26929.
5. Lu, Y. C.; Gasteiger, H. A.; Shao-Horn, Y. *J. Am. Chem. Soc*. **2011**, 133, 19048.
6. Gullion, T. *Chem. Phys. Lett.* **1995**, 246, 325.

High-Field ^{25}Mg NMR of a Rechargeable Magnesium Ion Battery Electrode $Mg_2NaV_2(PO_4)_2F_3$

Yan-Yan Hu, Zigeng Liu, Sylvia Britto, Sian E. Dutton and Clare P. Grey

Department of Chemistry, University of Cambridge

Overview

Safer, cheaper, and more sustainable alternatives to current lithium ion batteries (LIBs) are at the forefront of energy research, and one promising strategy is to use other ions to transport charge.[1] Owing to the divalent nature of Mg^{2+}, magnesium ion batteries (MIBs) are predicted to achieve sustainably higher energy density with greater stability than state-of-the-art LIBs. Limitations of MIBs studied so far are the high energy barriers for diffusion of the divalent Mg^{2+} through the host crystal structure and through MgO layers formed on the surface of the electrode upon electrolyte decomposition, the difficulty in extracting Mg out of the structure, and low cell voltages (1 – 1.3 V as opposed to 3.0 – 4.0 V for LIBs). Various promising cathode materials capable of reversible magnesium insertion have been investigated in our group, including transition metal spinel oxides (MgM_2O_4, M = Fe, Mn) which offer scope for attaining higher cell voltages due to the high variable oxidation states of the transition metal cations and NASICON-type $Mg_2NaV_2(PO_4)_2F_3$, which facilitates Mg diffusion by providing an open structural framework. We have been able to achieve full theoretical capacity (135 mAh/g) using $Mg_2NaV_2(PO_4)_2F_3$ as the cathode in MIBs. X-ray diffraction (XRD) reveals bulk structural changes upon Mg insertion and extraction. Here, on the basis of our ^{25}Mg NMR investigation of relevant model compounds and first principles calculations, we conducted ^{25}Mg NMR studies of the electrochemically cycled electrodes at high magnetic field to achieve high resolution and good sensitivity in order to gain insights into the local structural changes and solid-electrolyte interphase formation.

Results

The electrode was prepared by first electrochemically extracting 2 Na out of the pristine structure $Na_3V_2(PO_4)_2F_3$ (Figure 1a) and then 1 Mg was inserted via cycling the electrode against Mg metal to form $MgNaV_2(PO_4)_2F_3$ at the end of discharge. ^{25}Mg NMR spectra were acquired at the 850 MHz Facility with a 4 mm HX low-gamma probe at 12 kHz MAS. Analysis of the spectrum in Figure 1b reveals a component with an isotropic shift of 53 ppm and a quadrupole coupling constant of ~3.6 MHz. The information will be compared later against parameters obtained from first principles calculations. Although a significant amount of MgO was expected to form due to electrolyte decomposition of $Mg(ClO_4)_2$ on the surface of the electrode, no obvious signature of MgO was observed in ^{25}Mg NMR (Figure 1b) nor in the XRD characterization. Two explanations are possible: First, the MgO formed on the surface is amorphous, which leads to no signal in XRD and a very broad spectrum (low sensitivity) in NMR. This possibility will be probed in future work by investigating sensitivity enhancement techniques (e.g. QCPMG). Second, the surface of the $NaV_2(PO_4)_2F_3$ is not susceptible to severe electrolyte decomposition within the voltage window (0.05 – 3.3 V) explored here.

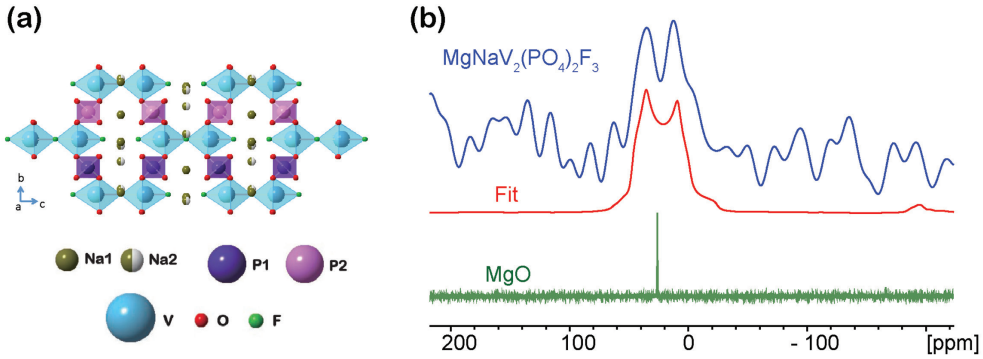

Figure 1. (a) Structure of pristine $Na_3V_2(PO_4)_2F_3$. Two of the Na were electrochemically replaced by 1 Mg to obtain $MgNaV_2(PO_4)_2F_3$. (b) ^{25}Mg NMR of the cathode at the end of discharge with a composition of $MgNaV_2(PO_4)_2F_3$, together with a best-fit spectrum, and a ^{25}Mg spectrum of MgO.

References

1. Aurbach, D.; Lu, Z.; Schechter, A.; Gofer, Y.; Gizbar, H.; Turgeman, R.; Cohen, Y.; Moshkovich, M.; Levi, E. *Nature* **2000**, *407*, 724.

Characterisation of Zinc Phosphates by ^{67}Zn NMR

Nasima Kanwal,[1,2] Isaac Abrahams,[1] Natalia Karpukhina,[2] Dinu Iuga[3] and John V. Hanna[3]

[1]*School of Biological and Chemical Sciences, Queen Mary University of London*

[2]*Barts and The London School of Medicine and Dentistry, Queen Mary University of London*

[3]*Department of Physics, University of Warwick*

Overview

The zinc cation, Zn^{2+}, is the specific component of a number of biomedical materials including bioactive glasses and cements. Zn^{2+} is important as it is often solely because of the presence of these zinc ions that certain types of the biomedical materials can be formed. A variety of zinc oxide based cements that are used widely in dentistry, e.g. zinc phosphate, zinc polycarboxylate and zinc oxide - eugenol, or zinc imidazole cements formed from zinc phosphate glasses, are based on the ability of the zinc cation to chelate and build up the planar complexes at an early reaction time which then later transform into more stable phases. The structure of these initial transient complexes is very poorly understood. ^{67}Zn NMR may give an opportunity to structurally characterise the local environment of the zinc cations in these inorganic solids and provide a better insight into the understanding of zinc-containing biomedical materials.[1-3]

Results

Figure 1 presents ^{67}Zn NMR spectra acquired for two crystalline polymorphs of zinc polyphosphate, specifically a high-temperature (top) and low-temperature (bottom) form. These results can now be compared with simulated spectra to extract further structural information on the zinc environment.

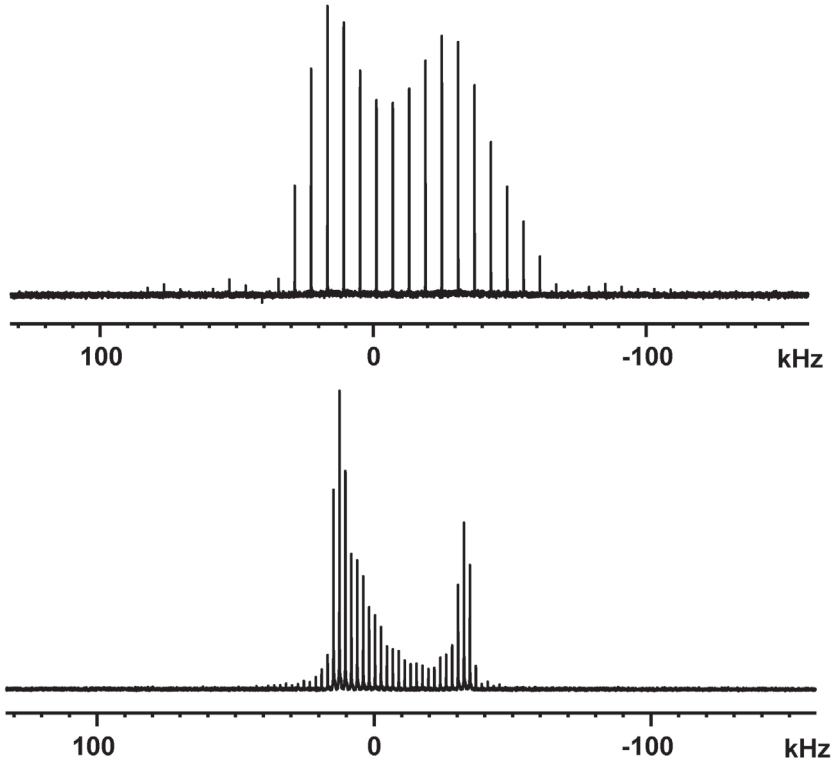

Figure 1. ^{67}Zn static NMR spectra of the low-temperature (top) and high-temperature (bottom) polymorphs of the zinc polyphosphate $Zn(PO_3)_2$ acquired using the QCPMG sequence (experimental times of 22 h and 24 h, respectively).

References

1. Sutrisno, A.; Terskikh, V. V.; Shi, Q.; Song, Z.; Dong, J.; Ding, S. Y.; Wang, W.; Provost, B. R., Daff, T. D.; Woo, T. K.; Huang, Y. *Chem., Eur. J.* **2012**, *18*, 12251.
2. Sutrisno, A.; Liu, L.; Xu, J.; Huang, Y. *Phys. Chem. Chem. Phys.* **2011**, *13*, 16606.
3. Hanna, J. V.; Smith, M. E. *Solid State Nucl. Magn. Reson.* **2010**, *38*, 1.

Solid-State NMR Studies of Immobilised Enzymes: ^{17}O NMR of Associated Water

Nicole E. Fauré,[1,2] Stephen Wimperis[2] and Peter J. Halling[1]

[1]*Department of Pure & Applied Chemistry and WestCHEM, University of Strathclyde*

[2]*School of Chemistry and WestCHEM, University of Glasgow*

Overview

Multiple-quantum ^{17}O NMR experiments give information about the correlation time and amount of water associated with immobilised enzymes.

Introduction to Immobilised Enzymes and Water Interactions

Immobilisation of enzymes by attachment to solid support materials is an important technology allowing easy recovery and reuse. The resulting biocatalysts can be applied for preparative syntheses in current and potential industrial processes, and are also useful in analysis. Despite extensive published literature on enzyme immobilisation, new methods are generally developed rather empirically. This is mainly because little is known about what happens to the enzyme molecules during immobilisation, because all that is measured is their catalytic activity. We are investigating the potential of solid-state NMR to give information about the state and interactions of the enzyme molecules in immobilised preparations. Because we seek methods that can be applied to immobilised enzymes prepared by others, including industrial catalysts, we favour approaches that do not require labelled proteins. In this context, there is no problem with the use of labelled probe reagents.

During our time at the 850 MHz Facility in 2013, we continued some MAS NMR studies looking for far-downfield ^{1}H signals associated with the active site of our model enzyme α-chymotrypsin. We also commenced MAS NMR studies of the enzyme immobilised on alumina supports, paralleling our previous work with silicas. But this report will focus on a third area: examining ^{17}O signals from enriched water associated with the protein. Interactions of water with enzymes are very important in their function, affecting the ionisation and mobility of groups at the protein surface. Water molecules are also important in the interaction of enzymes with their reactants and products, either because they must be displaced in the process, or in some cases when they make bridging interactions. Sometimes immobilised enzymes are used in mainly non-aqueous media, with the bulk phase made up of species such as organic solvents, supercritical fluids or ionic liquids. In these systems the amount of residual water bound to the enzyme is known to have important effects on function, but there is a lack of techniques to assess its state, even to reliably quantitate how much remains.

^{17}O NMR Measurements with $H_2{}^{17}O$

Relaxation measurements with the quadrupolar (spin I = 5/2) ^{17}O nucleus are complicated by the frequent observation of multiexponential behaviour. Simplification can be achieved in multiple-quantum NMR studies where, for spin I = 5/2, four- and five-quantum coherences relax exponentially. Figure 1 shows that a strong four-quantum-filtered NMR signal can be obtained from ^{17}O in the water surrounding the immobilised enzyme (added with mass approximately equal to that of the whole immobilised preparation). MAS is used because of the heterogeneity of the sample. By varying the evolution period in the multiple-quantum filter and fitting the observed signal intensity to a first-order decline, relaxation rate constants can be obtained for both the four-quantum and five-quantum experiments (Figure 2). The values obtained are shown in Table 1.

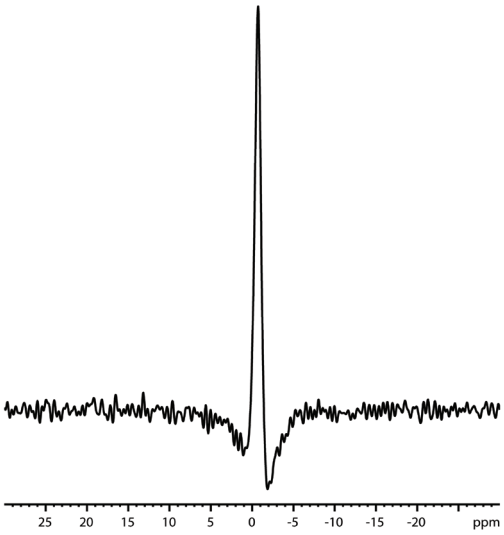

Figure 1. Four-quantum-filtered ^{17}O MAS NMR spectrum of silica-chymotrypsin-^{17}O enriched water, recorded at B_0 = 20 T. Evolution period: 4 μs; creation period: 2 ms; 12800 aquisitions.

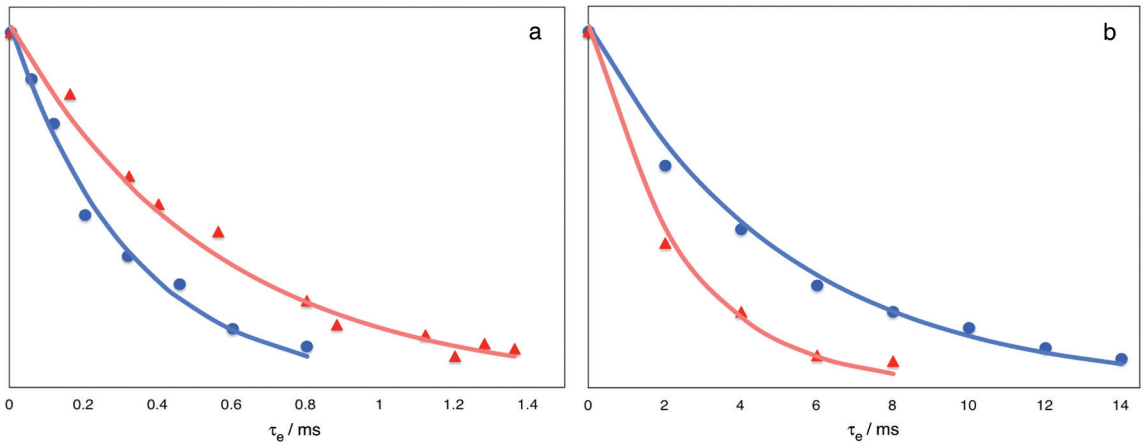

Figure 2. ^{17}O NMR peak amplitude as a function of evolution time in (a) a four-quantum NMR experiment and (b) a five-quantum NMR experiment. Data and fitted lines for immobilised chymotrypsin on silica with pore sizes 10 nm (blue circles) and 20 nm (red triangles). Note the change in τ_e scale between (a) and (b).

Pore size / nm	R_{4Q} / s^{-1}	R_{5Q} / s^{-1}	Correlation time / ns	Bound water per enzyme / (mol/mol)
10	6140	389	7.32	345
20	3610	814	3.59	425

Table 1. Relaxation rate constants from four- and five-quantum ^{17}O NMR experiments and resulting correlation times and bound water : enzyme ratios. A value of 7.6 MHz has been assumed for the ^{17}O quadrupolar coupling constant in H_2O.

By combining these two relaxation rate values, and assuming the theoretical treatment of Chung and Wimperis[1] to be valid, we can obtain estimates of the correlation times of motions associated with relaxation, and the number of water molecules perturbed by interaction with the immobilised enzyme. This leads to the further values in Table 1.

The numbers of water molecules calculated are plausible for the count of those surrounding the protein surface. For a fuller picture we would also need to consider the possibility of water molecules interacting with sites on the silica surface (ones not masked by the attached protein or silane coupling agent used as a first step in immobilisation). We also need to consider that interactions would be expected to be much stronger at some sites on the protein surface (e.g., around charged groups) than at others. It is also likely that water molecules exchange rather rapidly between sites on the protein surface and the bulk, and that there is no clear dividing line between these two states. If we extend studies to low-water media it will probably be easier to distinguish water molecules bound to the protein from those dissolved in a bulk non-aqueous phase surrounding the enzyme. The environments will be more different, exchange slower, and intermediate states will be almost non-existent.

References

1. Chung, C. W.; Wimperis, S. *Mol. Phys.* **1992**, *76*, 47.

^{71}Ga and ^{73}Ge NMR Studies of Nd Doped GeS_2-Ga_2S_3 Glasses Used in New Bright Fibre Laser Devices for Medical Applications

Stephen P. Day,[1] Emma R. Barney,[2] Angela Seddon,[2] David Furniss[2] and John V. Hanna[1]

[1] *Department of Physics, University of Warwick*

[2] *Department of Engineering, University of Nottingham*

Overview

Contemporary medical device research has led to the development of mid-IR absorption technologies to monitor the progress of diseases *in situ* on a timescale that can remove the need for lengthy biopsies. Optimising chalcogenide glass compositions so that they can host sufficient rare earth (RE) ion concentrations (e.g., Nd) in environments which are conducive to lasing is one project under this remit.[1] There is evidence in the literature suggesting that the addition of Ga to the glasses is key to ensuring a suitable RE environment. One study has used optical studies to demonstrate that the addition of Ga_2S_3 (incorporating Ga^{3+} in tetrahedral units) induces a corresponding increase in the RE fluorescence intensity,[2] while other work confirmed this result and used *ab initio* molecular dynamics (MD) to show that Ga-S-RE correlations persist in the melt significantly longer than As-S-RE bonds.[3] There is also evidence indicating that Ga incorporation may induce cluster or cage formation in which the RE ion sits, thus isolating it from other network cations.[4] Direct experimental evidence of this correlation is essential in order to confirm these modelling results. As both Ga^{3+} and Ge^{4+} cations comprise the glass network in the samples that are core to this study, the aim of this study is to thus determine how strongly associated the RE position is with respect to these cations sites by observing paramagnetic broadening associated with the study of the ^{71}Ga and ^{73}Ge nuclei. As the strength of the electron-nuclear dipolar interaction exhibits a $1/r^3$ dependence, the magnitude of the paramagnetic broadening will directly correlate to the average distance between the RE and cation, showing clearly whether Ga is preferentially bonded (via S bridges) to the RE position.

^{71}Ga MAS NMR Studies

^{71}Ga MAS NMR measurements from the chalcogenide glass series $x(Nd_2S_3)(100–x)(25Ga_2S_3\text{-}75\ GeS_2)$ (x = 0, 3, 4.5, 6) acquired at 20 T have yielded direct evidence that the RE (i.e. Nd^{3+}) cation is in reasonably close proximity to Ga positions (see Figure 1). The ^{71}Ga spectrum for the Nd-free glass sample ($25Ga_2S_3{\cdot}75GeS_2$) depicts a single lineshape (apparent shift of δ ~250-300 ppm) which is assigned to four coordinate Ga (GaS_4) in a disordered network. This disorder is due to positional displacement (i.e., distributions of bond angles and bond distances) and atomic displacement with each Ga position potentially experiencing Ga and/or Ge in the second coordination environment. Upon the addition of 3 mol% Nd to the nominal composition, the ^{71}Ga MAS NMR lineshape becomes immediately influenced by a broad anisotropy spanning ~4000 ppm, presumably from the paramagnetic electron-nuclear dipolar interaction. The subsequent addition of 4.5 and 6 mol% Nd to these glass preparations causes this anisotropic width to increase to ~7000 ppm, with a second resonance at an apparent shift of δ ~900 ppm emerging at 4.5 mol% and becoming dominant at 6 mol%. This ^{71}Ga shift is outside the conventional chemical shift range and is probably also due to the increasing proximity of the Ga^{3+} speciation to paramagnetic Nd^{3+}, thus inducing a prominent paramagnetic (downfield) shift that may be influenced by both Fermi contact and electron-nuclear dipolar interactions. These observations clearly show that paramagnetic Nd^{3+} exhibits an intimate association with the Ga speciation in these glass preparations, either by nearest neighbour or more elaborate clustering phenomena.

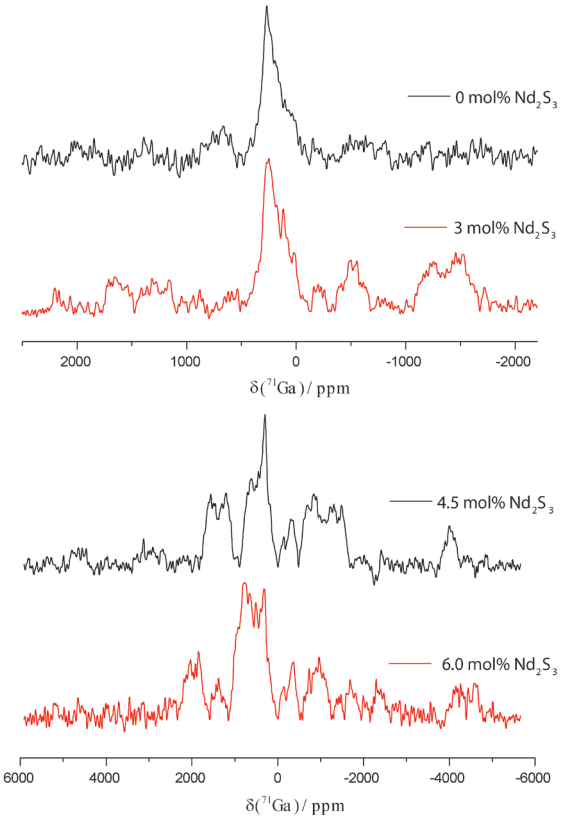

Figure 1. ^{71}Ga NMR data measured for the glass series $x(Nd_2S_3)(100\text{-}x)(25Ga_2S_3{\cdot}75\ GeS_2$ (x=0, 3, 4.5, 6).

^{73}Ge Static NMR Studies

^{73}Ge static (solid echo) NMR spectra obtained at 20 T (850 MHz) on two glasses x(Nd_2S_3)(100–x)(25Ga_2S_3-75 GeS_2) (x = 4.5 and 6) from this series are shown in Figure 2. Although a full and accurate analysis of these ^{73}Ge lineshapes is restricted by the signal to noise ratio of these very broad central and satellite transition resonances, some attempts at elucidating the isotropic chemical shift (δ_{iso}) of this resonance has been attempted by assuming quadrupole only (middle and right) and quadrupole/CSA (left) models. These analyses demonstrate that regardless of the approach taken, a δ_{iso} value of ~ –100 to –300 ppm is obtained which is well within conventional ^{73}Ge chemical shift ranges and the influence of paramagnetic effects is not immediately apparent. This infers that the addition of RE cations to this chalcogenide glass preparation has a more profound influence on the Ga^{3+} speciation through close association and/or clustering, with the Ge^{4+} speciation remaining relatively unperturbed by paramagnetic influences generated by the presence of Nd^{3+} cations.

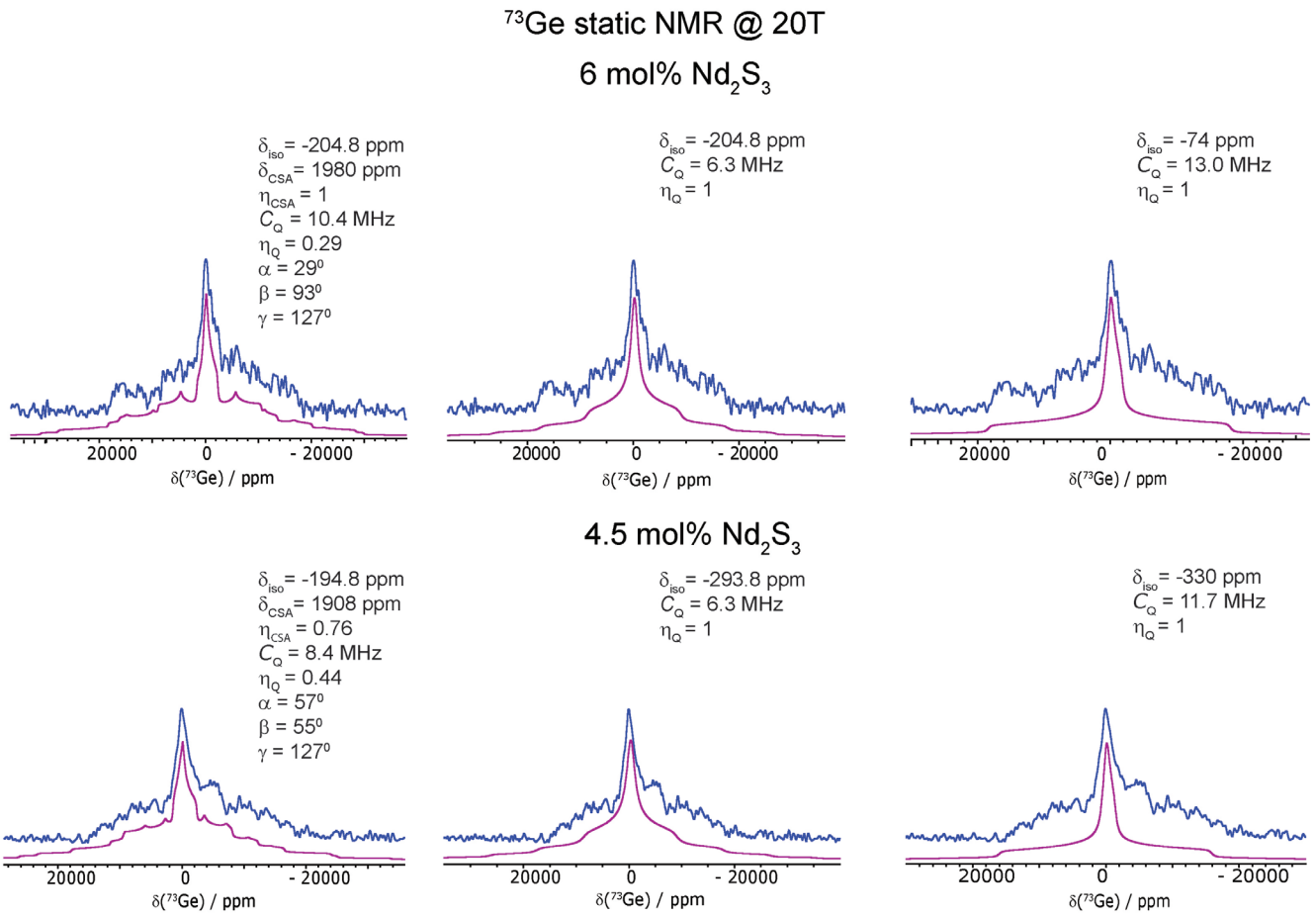

Figure 2. ^{73}Ge NMR spectra for the glasses x(Nd_2S_3)(100-x)(25Ga_2S_3·75 GeS_2 (x=4.5, 6), with three possible simulation models.

References

1. Seddon, A. B.; Tang, Z.; Furniss, D.; Sujecki S.; Benson T. M. *Opt. Express* **2010**, *18*, 26704.
2. Aitken, B. G.; Ponader, C. W.; Quimby, R. S. *C. R. Chimie* **2002**, *5*, 865.
3. Lee, T. H.; Simdyankin, S. I.; Hegedus, J.; Heo, J.; Elliot, S. R. *Phys. Rev. B* **2010**, *81*,104204.
4. Tang, Z.; Neate, N. C.; Furniss, D.; Sujecki, S.; Benson, T. M.; Seddon A. B. *J. Non-Cryst. Solids* **2011**, *357*, 2453.

^{71}Ga Fast MAS Experiments on Gallium Doped Perovskites

Stephen P. Day,[1] Peter R. Slater[2] and John V. Hanna[1]

[1]*Department of Physics, University of Warwick*

[2]*School of Chemistry, University of Birmingham*

Overview

Many perovskites and perovskites-related systems possess the structural flexibility necessary to incorporate significant amounts of oxyanion doping; a doping strategy that improves ionic conduction thus promoting their applicability for solid oxide fuel cell operation.[1,2] For the perovskite-related systems $Sr_2(Sc/Ga)_{2-x}P_xO_{5+x}$ and $Sr_2(Sc/Ga)_{2-x}S_xO_{5+(3/2)x}$, conductivity measurements suggest that high levels of Ga incorporation into the structure impedes conduction, thereby suggesting that the Ga position is acting as an oxide ion vacancy trap. Detailed structural characterisation is necessary to prove or disprove this hypothesis, but the local disorder of these systems has been shown to inhibit detailed structural refinement via diffraction techniques. Solid-state ^{71}Ga MAS NMR is used to probe the short-range Ga^{3+} environments, where the combination of high magnetic field (20 T) and fast MAS (using the Jeol 1 mm probe) have allowed the identification of four, five and six-fold coordination Ga speciation in these systems.

^{71}Ga MAS NMR Experiments

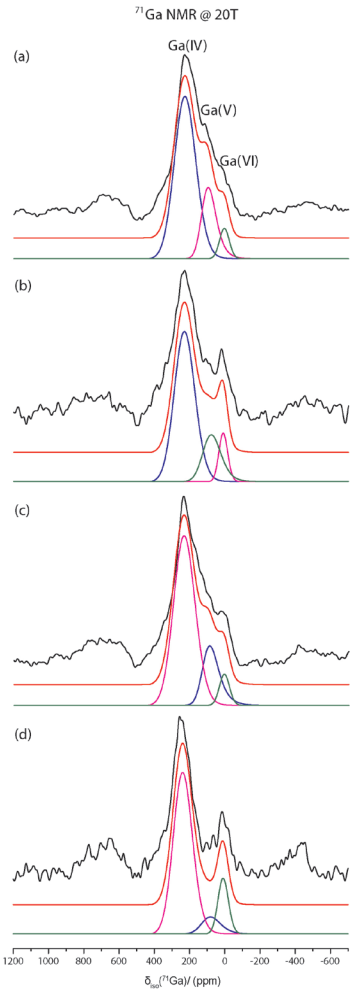

From Figure 1, marked resolution enhancement upon increasing B_0 and MAS frequency demonstrates the necessity for fast spinning and high magnetic fields in order to study the speciation of the Ga. Despite this improvement in resolution, the broadness of the ^{71}Ga lineshape makes interpretation far from trivial (see Figure 2). Its exact form is dependent on the distribution of the local environments, which is not known *a priori* and therefore the lineshapes can be difficult to model. The Czjzek model provides an analytic expression for MAS NMR spectral lineshapes that tails towards high field due to a distribution of NMR quadrupolar parameters caused by disorder.[3] This lineshape is convoluted with a Gaussian distribution of isotropic chemical shifts to fit the ^{71}Ga MAS NMR data.

The typical ^{71}Ga isotropic chemical shift range for the different coordination environments measured in gallate and oxide based systems are as follows: Ga^{VI} 41-57 ppm, Ga^{IV} 200-242 ppm, with Ga^{V} observed in the intermediate chemical shift range of ~70-200 ppm.[4] Given Ga is known to correlate with the P content, and that Ga also substitutes with six-coordinate Sc, it is expected that some distribution of four and six coordinate Ga environments must exist in these systems. Furthermore, for high quality simulations of the ^{71}Ga MAS NMR lineshapes to be achieved, significant intensity in the Ga^{V} region needs to be introduced. Hence, given that the Ga speciation is dominated by Ga^{IV} and Ga^{V} environments (i.e., not fully coordinated Ga^{VI} positions expected in a perovskite lattice), it can be inferred that the majority of Ga^{3+} positions are O deficient and they are acting as a vacancy trap where this deficiency resides permanently on the Ga^{3+} positions, thus hindering O conductivity.

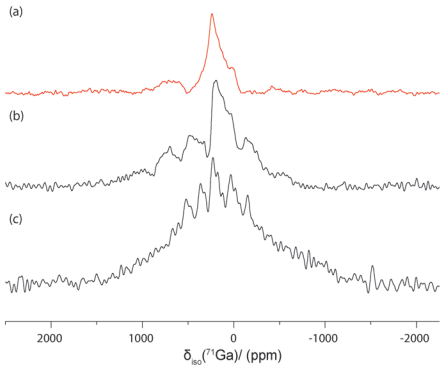

Figure. 1. ^{71}Ga MAS spectra of $Sr_2Sc_{1.0}Ga_{0.9}S_{0.1}O_{5.15}$ at a) 20.0 T, ν_r = 74 kHz, with DFS, b) 14.1 T, ν_r = 60 kHz solid echo, and c) 14.1 T, ν_r = 31.25 kHz solid echo.

Figure 2. ^{71}Ga DFS spectra (20.0 T, 74 kHz MAS, 24 hours experimental time) of a) $Sr_2Sc_{1.2}Ga_{0.7}P_{0.1}O_{5.1}$ b) $Sr_2Sc_{1.0}Ga_{0.9}P_{0.1}O_{5.1}$ c) $Sr_2Sc_{1.0}Ga_{0.9}S_{0.1}O_{5.15}$ d) $Sr_2Sc_{0.6}Ga_{1.3}S_{0.1}O_{5.15}$ with a corresponding simulation based upon the GIM Czjzek model.

^{45}Sc STMAS NMR Experiments

Kim et al. investigated the isotropic chemical shift of ^{45}Sc in a range of solid oxide materials and reported that in simple inorganic oxides (without the influence of protons or organic functional groups) the isotropic chemical shift δ_{iso} is dominated by nearest neighbour interactions.[5] Hence, there is a strong correlation between δ_{iso} and the Sc coordination number for these systems: six coordinated Sc is reported in the 108-158 ppm range, with higher coordination number environments being reported at lower chemical shifts. The ^{45}Sc STMAS NMR spectrum for $Sr_2Sc_{1.5}P_{0.5}O_{5.5}$ presented in Figure 3e clearly demonstrates that both five and six coordinate Sc is present in this structure; as the Ga incorporation is increased, the ScO_5 unit at δ ~170 ppm is observed to disappear (see Figure 3a-3d). This suggests that Ga is incorporated into the structure at O deficient (Ga^{IV} and Ga^{V}) positions, thus forcing the Sc speciation to occupy fully coordinated Sc^{VI} positions in the perovskite lattice.

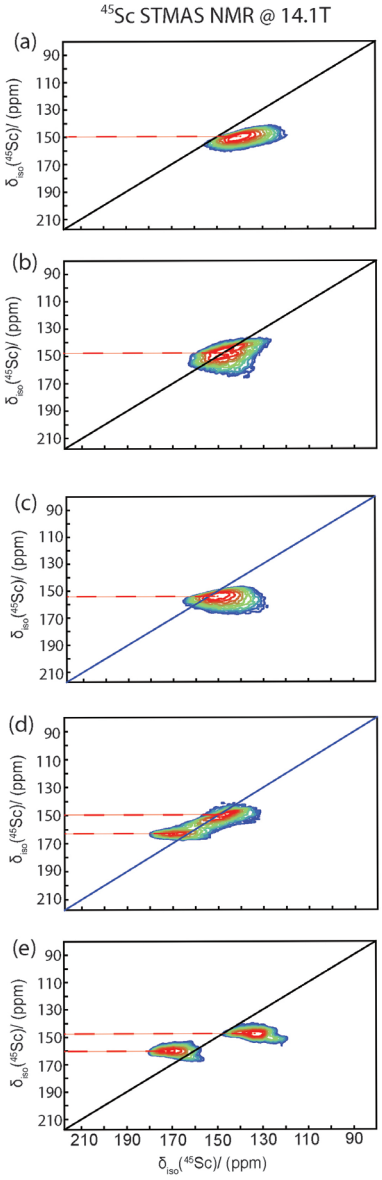

Figure. 3: ^{45}Sc STMAS data acquired at 14.1 T, ν_r = 20 kHz for
a) $Sr_2Sc_{1.2}Ga_{0.7}P_{0.1}O_{5.1}$
b) $Sr_2Sc_{1.0}Ga_{0.9}P_{0.1}O_{5.1}$
c) $Sr_2Sc_{1.0}Ga_{0.9}S_{0.1}O_{5.15}$
d) $Sr_2Sc_{0.6}Ga_{1.3}S_{0.1}O_{5.15}$
e) $Sr_2Sc_{1.5}P_{0.5}O_{5.5}$

^{31}P MAS NMR Data

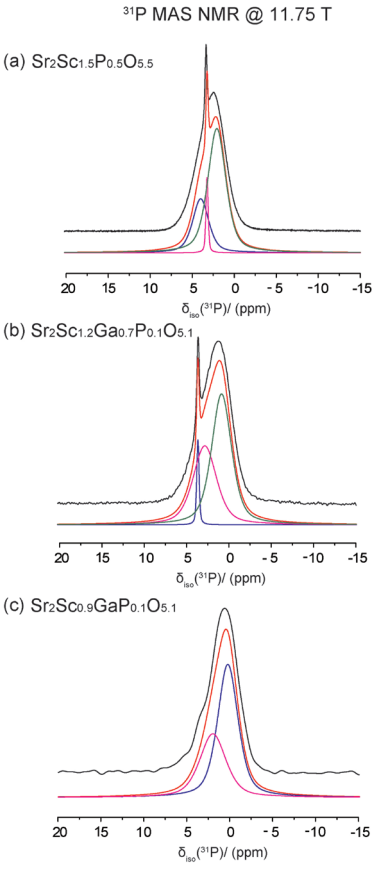

Figure. 4: ^{31}P (11.75 T) single-pulse MAS NMR data with accompanying simulations.

^{31}P MAS NMR spectra are shown in Figure 4. The shift range is consistent with ^{31}P arranged in tetrahedral units and the distribution of P species in these data is sensitive to the extent of the Ga doping. A narrow resonance can be observed at δ ~3.0-3.5 ppm for the samples with the least amounts of Ga doping. This narrow resonance has a relatively long T_1 ~ 120 s which is usually indicative of a highly crystalline environment. An impurity phase was not able to be detected in XRD studies; furthermore, the XRD data was unable to refine the perovskite atomic positions. Hence, the number of inequivalent P sites was estimated by fitting the ^{31}P NMR MAS data using half Gaussian/half Lorentzian peaks. It was determined that three resonances were optimal for the material without any Ga doping and this acted as a template to fit the other spectra. Given that the P content of the samples is relatively small, we might expect a predominance of Q^0 species with a possibility of Q^1 species where differences in tetrahedral environment due to the number of nearest neighbour ligands influences the ^{31}P isotropic chemical shift. Further, we might postulate that these three resonances correspond to no vacancies, a single vacancy and two vacancies in the Sc coordination sphere in the next nearest neighbour bonding arrangement of the P environments.

References

1. Porras-Vazquez, J. M.; Kemp, T. F.; Hanna, J. V.; Slater, P. R. *J. Mater. Chem*. **2012**, *22*, 8287.
2. Porras-Vazquez, J. M.; Slater, P. R. *J. Power Sources* **2012**, *209*, 180.
3. Le Caer, G.; Brand, R. A. *J. Phys. Condensed Matter* **1998**, *10*, 10715.
4. Middlemiss, S. D.; Blanc, F.; Pickard, C. J.; Grey, C. P. *J. Magn. Reson.* **2010**, *204*, 1.
5. Kim, N.; Hsieh, C.-H.; Stebbins, J. F. *Chem. Mater.* **2006,** *18*, 3855.

In-Situ NMR Studies of Urea Inclusion Compound Crystallization: Guest Competition and Growth Inhibition

Colan E. Hughes, Gregory R. Edwards-Gau, Vasileios G. Charalampopoulos and Kenneth D. M. Harris

School of Chemistry, Cardiff University

Overview

Our previous research has demonstrated the ability of *in-situ* NMR techniques to reveal new fundamental understanding of crystallization processes, particularly with regard to monitoring the evolution of the solid phase as a function of time.[1] Some of our latest work in this field has focused on different aspects of the crystallization of urea inclusion compounds (UICs). In these materials, the urea molecules form a tunnel "host" structure. The tunnels are densely filled with "guest" molecules (Figure 1), which are typically long-chain alkanes or α,ω-dihalogenoalkanes. In the present work, we focus on two specific features, in particular the competitive co-inclusion of two different types of guest molecule within the urea host structure and modification of the crystallization process by designed crystal-growth inhibitors.

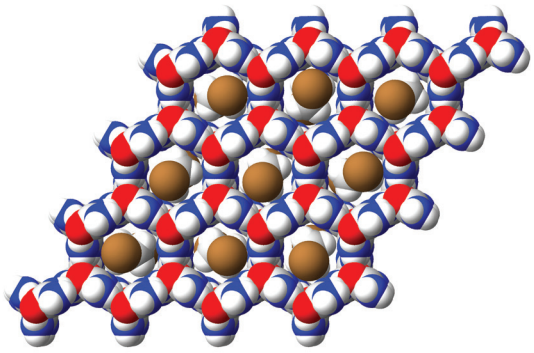

Figure 1. The crystal structure of a UIC.

Guest Competition

A topic of considerable interest in this field is the competitive co-inclusion of two types of guest molecule within the urea host structure. Whilst *ex-situ* analysis of the products from such crystallization experiments can reveal the total amounts of the two guests included within the host structure, only *in-situ* analysis can reveal the mechanism by which the crystallization proceeds, together with the time dependence and selectivity of the uptake of the two types of guest.

Figure 2 shows *in-situ* NMR results from two crystallization experiments for a solution of urea, 1,8-dibromooctane (DBO) and undecane (UD) in methanol. The two experiments differed in the rate of cooling of the solution from 50 °C to 20 °C to induce crystallization. In each experiment, the sample initially comprised the DBO/UD/urea solution plus a separate phase of liquid UD. The liquid UD phase is observed to disappear at the same time that new signals appear due to guests in the solid UIC. In the fast cooling experiment, both DBO and UD are observed as guests in the UIC whereas, under conditions of slow cooling, only UD is observed in the UIC host structure.

In the spectral region highlighted in yellow, two peaks are observed for the methyl group of UD in the case of fast cooling, indicating that two distinct local environments exist for the methyl groups. These environments are rationalized as methyl groups adjacent to the methyl end-group of another UD molecule within the one-dimensional host tunnel and methyl groups adjacent to the bromine end-group of a DBO molecule. Thus, when both UD and DBO are incorporated as guests into the UIC, they are distributed in a disordered manner within the same tunnels, rather than forming separate domains.

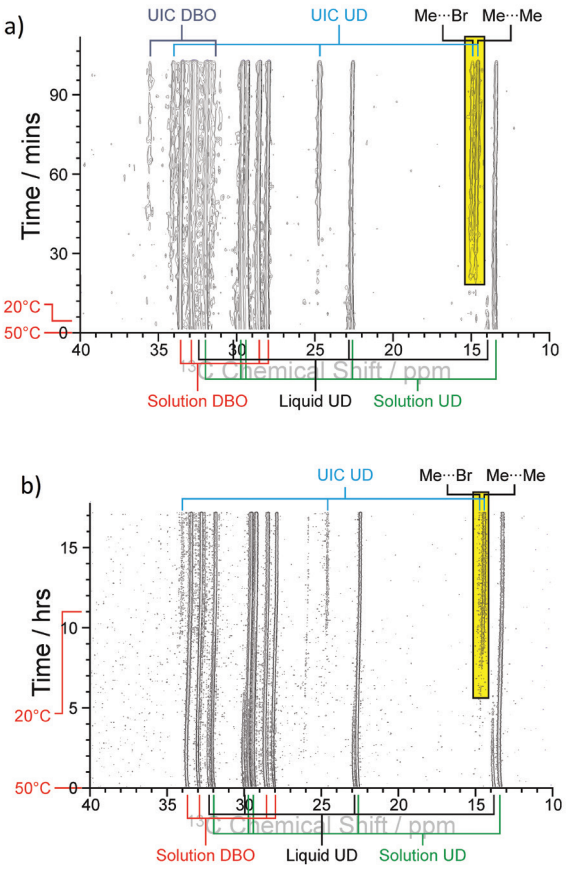

Figure 2. In-situ ^{13}C NMR spectra of urea, DBO and UD crystallizing from methanol with (a) fast cooling and (b) slow cooling from 50 °C to 20 °C.

Crystallization in the Presence of Crystal-Growth Inhibitors

Our group is currently studying the impact of inhibitor molecules on the growth of UIC crystals. Our earlier work[2,3] developed a general strategy for achieving a high degree of control over crystal morphology of UICs by introducing crystal growth inhibitors. Such inhibitors are designed to interact preferentially with certain crystal faces during crystal growth, selectively decreasing the rate of growth of these faces (while having no effect on the rate of growth of other faces) and consequently altering the crystal morphology. Using this strategy, it was shown that crystals of UICs can be prepared with any desired morphology ranging from long hexagonal needles (the natural growth morphology) to flat hexagonal plates.

For UICs, another issue of particular interest is chirality, as the urea host tunnel structure is chiral. In the absence of any chiral influence, both right- and left-handed UIC crystals are formed in crystallization experiments, but their crystal morphologies are indistinguishable (long, thin needles with hexagonal cross-section in each case). However, we have found recently that crystallization of UICs in the presence of designed chiral compounds leads to a bimodal distribution of crystal morphologies. In particular, some crystals are the normal long, thin needles whereas other crystals are shorter and wider than normal. We may hypothesize that the chiral compounds influence the usual growth behaviour selectively for one enantiomorphous form of the UIC crystals, by enantioselective interaction with the surfaces of the growing crystals.

Figure 3 shows *in-situ* solid-state ^{13}C NMR results for two crystallization experiments to prepare the UIC containing 1,8-dibromooctane (DBO) guest molecules. In one case, no crystal growth inhibitor was present; in the other case, 10% of the guest concentration was replaced by the inhibitor N-lauroyl-L-phenylalanine (NLLF). In the absence of inhibitor, crystallization occurs after about 30 mins, as seen by the disappearance of peaks due to a separate liquid phase of DBO (blue) and the appearance of peaks due to DBO in the solid UIC (red). Peaks due to DBO in the solution phase (black) are present throughout the experiment. In the presence of the inhibitor, crystallization occurs after about 60 mins, again evident from the disappearance of the separate liquid phase of DBO and the appearance of DBO in the solid UIC. However, it is clear that there are differences in the final product, as the peaks due to DBO in the UIC are much weaker (the peak at 35.5 ppm is only visible at lower contour levels than shown in the figure).

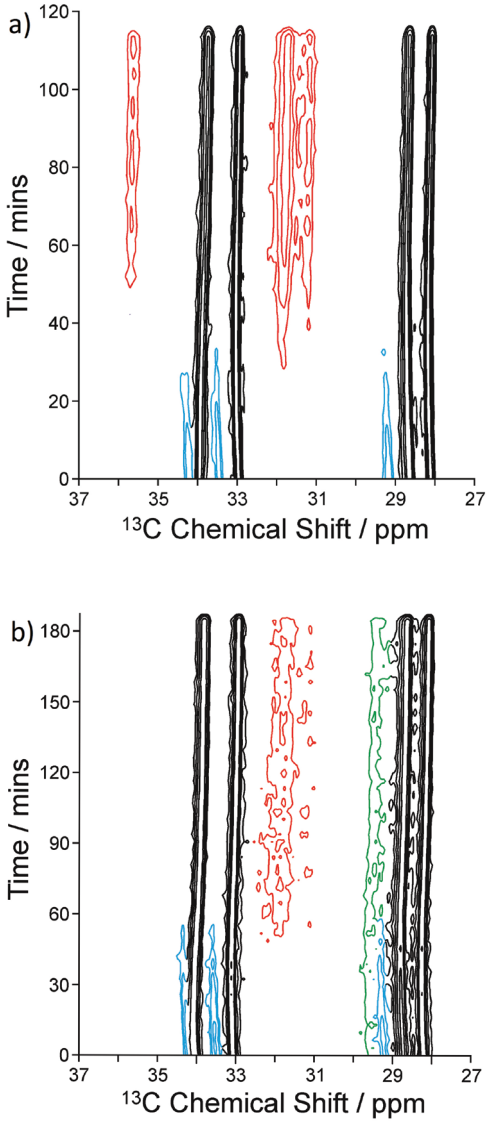

Figure 3. In-situ ^{13}C NMR spectra recorded during crystallization of DBO and urea (a) without and (b) with the NLLF inhibitor. Note the different timescales.

Concluding Remarks

The physico-chemical properties of UICs have captivated the interests of organic solid-state chemists and physicists for many years, particularly with regard to their fascinating structural and dynamic properties, and their potential applications. Our on-going research to understand the crystallization behaviour of these materials is revealing several significant observations, and it is clear that *in-situ* NMR techniques are a very powerful approach to advance our understanding of fundamental details of these processes.

References

1. Hughes, C. E.; Williams, P. A.; Peskett, T. R.; Harris, K. D. M. *J. Phys. Chem. Lett.* **2012**, *3*, 3176.
2. Lee, S.-O.; Harris, K. D. M. *Chem. Phys. Lett.* **1999**, *307*, 327.
3. Kelly, N. E.; Lee, S.-O.; Harris, K. D. M. *J. Am. Chem. Soc.* **2001**, *123*, 12682.

Exploiting Ultra-Fast MAS in the Characterization of Organic Crystals with High Z′

Colan E. Hughes,[1] P. Andrew Williams,[1] Dmytro V. Dudenko,[1,2] Steven P. Brown[2] and Kenneth D. M. Harris[1]

[1]*School of Chemistry, Cardiff University* [2]*Department of Physics, University of Warwick*

Overview

Whilst the majority of molecular crystalline materials are found to have a relatively small number (denoted Z′) of crystallographically distinct molecules in the asymmetric unit (typically with $Z' \leq 4$), some materials have surprisingly high values of Z′. We have studied two molecular crystalline materials for which the value of Z′ in the published crystal structure is particularly high. Our aim was to assess the validity of these structures by recording ^{13}C and ^{1}H-^{13}C NMR spectra with the highest possible resolution. With this aim, we exploited the resolution advantage afforded both by the high field of the 850 MHz instrument and by utilizing the high magic angle spinning frequency available with the recently installed Jeol 1 mm probe.

L-Tryptophan

The crystal structure of L-Trp has been reported recently[1] to have a huge number (Z′ = 16) of independent molecules in the asymmetric unit. A ^{1}H-^{13}C heteronuclear correlation spectrum of L-Trp was recorded (Figure 1) at 78 kHz MAS frequency. Focusing on the carboxylic acid region of the ^{13}C spectral range, two distinct groups of signals are observed, centred at 176.7 ppm and 178.3 ppm. To allow comparison with the published crystal structure, we have calculated the carboxylic acid ^{13}C chemical shifts for this structure using the GIPAW method. These calculations revealed that there are indeed two distinct groups of carboxylic acid ^{13}C chemical shifts, with eight molecules in the asymmetric unit contributing to each group. The difference between the average chemical shifts for each group is ~1.6 ppm, in close agreement with the difference observed in the experimental data. This observation provides some vindication that the published crystal structure, although having an unusually high value of Z′, may indeed be correct.

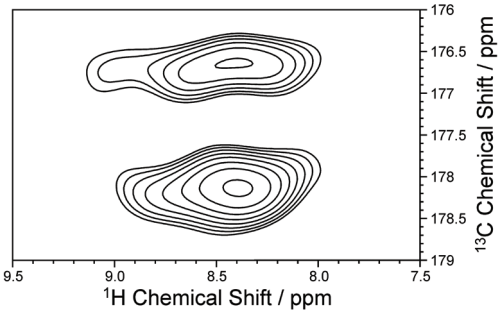

Figure 1. ^{1}H-^{13}C (78 kHz MAS) hetero-nuclear correlation spectrum of L-Trp.

Glycyl-L-Valine

The published crystal structure of glycyl-L-valine[2] has Z′ = 7. ^{1}H-^{13}C CP MAS NMR spectra, acquired at 78 kHz MAS frequency, are presented in Figure 2 for the aliphatic and carbonyl regions of glycyl-L-valine. Although not fully resolved, it is clear that there are several peaks for each resonance type, perhaps most noticeably for Vα at ~65 ppm. GIPAW calculations to determine the ^{13}C chemical shifts for the reported crystal structure are in progress and will allow the level of agreement between our NMR data and this structure to be assessed. However, it is already clear from our NMR data that Z′ is indeed relatively high.

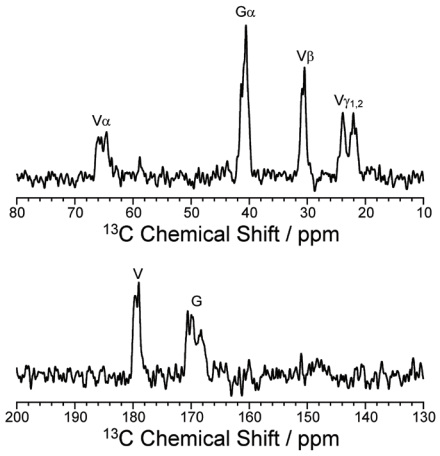

Figure 2. $^{1}H \rightarrow {}^{13}C$ CP spectra of glycyl-L-valine at 78 kHz MAS.

Concluding Remarks

Our results show that a strategy combining the measurement of experimental NMR data at high magnetic field and using very high-frequency MAS, together with CASTEP calculations of chemical shifts, can be used to assess the validity of crystal structures with unusually high values of Z′.

References

1. Görbitz, C. H.; Törnroos, K. W.; Day, G. M. *Acta Cryst. B* **2012**, *68*, 549.
2. Görbitz, C. H.; Augustdottir, S.; Bleken, F. *Acta Cryst. C* **2007**, *63*, o58.

"CLASSIC NMR": A New *In-Situ* Method to Study Crystallization

Colan E. Hughes, P. Andrew Williams and Kenneth D. M. Harris

School of Chemistry, Cardiff University

Overview

We have developed a new *in-situ* NMR strategy for mapping the time evolution of crystallization processes, involving simultaneous measurement of *both* liquid- *and* solid-state NMR spectra (manuscript in preparation). This new strategy is termed CLASSIC NMR (**C**ombined **L**iquid- and **S**olid-**S**tate ***I**n-situ* **C**rystallization NMR) and allows complementary information to be obtained on the evolution of the solid phase during the crystallization process as well as the corresponding changes in the solution phase. In particular, as crystallization proceeds (monitored by solid-state NMR), the solution state becomes more dilute, leading to changes in the speciation and the modes of molecular aggregation in solution, which are monitored by liquid-state NMR. We report the application of the CLASSIC NMR strategy to two crystallization systems.

Benzoic Acid

Benzoic acid (BA) forms stable hydrogen-bonded dimers at equilibrium in chloroform but not in acetone. However, it exhibits no polymorphism upon crystallization from these solvents. We studied this system to explore the possible formation of (i) transient polymorphs during crystallization (focusing on the solid-state component of the CLASSIC NMR data) and (ii) dimers in the super-saturated solution prior to crystallization in acetone (using the liquid-state data). Solid-state NMR did not reveal any intermediate phases, indicating that crystallization leads directly to the known solid form from both solvents. Liquid-state NMR spectra (Figure 1), recorded during crystallization, showed key differences. The ^{1}H resonances move due to the concentration change associated with crystallization. However, while the aromatic peaks (red) move to higher chemical shifts in both solvents, the carboxylic acid peak (green) moves to a higher shift in chloroform but to a lower shift in acetone. Given that the carboxylic acid ^{1}H chemical shift is higher for BA molecules in hydrogen-bonded dimers, we conclude that, at the higher, metastable concentration present during crystallization, BA *does* form dimers in acetone.

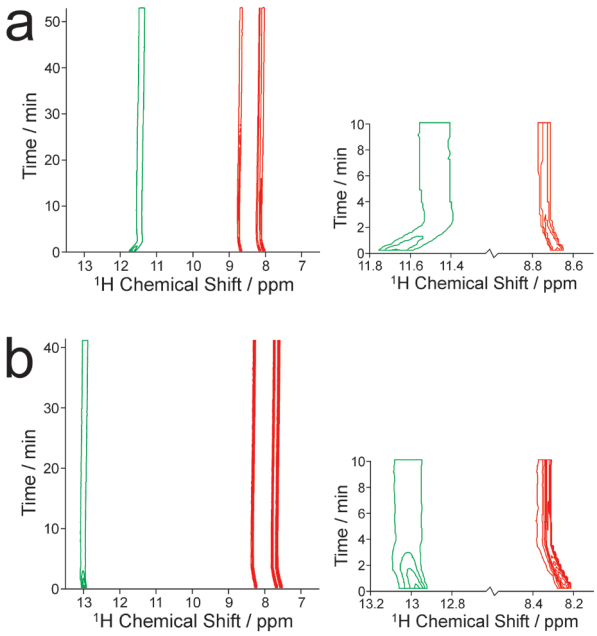

Figure 1. Liquid-state ^{1}H NMR spectra of BA crystallizing from (a) chloroform and (b) acetone.

Benzoic and Pentafluorobenzoic Acids

We have applied CLASSIC NMR to the co-crystallization of BA and pentafluorobenzoic acid (PFBA). The well established affinity for aryl and perfluoroaryl rings to form alternating π-stacking gives rise to a number of highly stable co-crystals. Our aim was to determine the point at which this affinity is manifested in the creation of alternating π-π stacks during crystallization. Figure 2 shows the liquid-state ^{1}H NMR spectra of a 1:1 BA/PFBA mixture crystallizing from CD_2Cl_2. After *ca*. 40 mins, there is a sudden change in the chemical shifts, corresponding to a rapid co-crystallization. Further experiments in other solvents are underway to characterize the pre-nucleation solutions in this system.

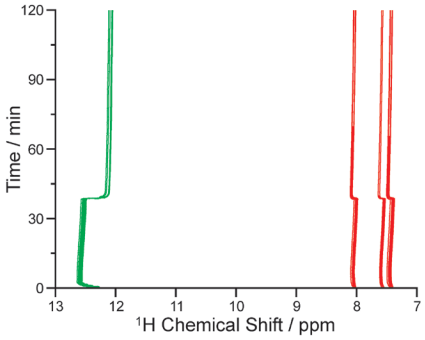

Figure 2. Liquid-state ^{1}H NMR spectra recorded in situ during co-crystallization of BA and PFBA from CD_2Cl_2.

Concluding Remarks

We now aim to apply the CLASSIC NMR methodology to gain new insights on a wide range of crystallization processes of both fundamental interest and significant biological importance.

Nanomole-Scale Quantitative Studies of Large Protein Complexes at 60-100 kHz Spinning Frequencies

Jonathan M. Lamley,[1] Dinu Iuga,[2] Hans J. Sass,[3] Andreas Oss,[4] Stephan Grzesiek,[3] Ago Samoson[4] and Józef R. Lewandowski[1]

[1]*Department of Chemistry, University of Warwick*

[2]*Department of Physics, University of Warwick*

[3]*Biozentrum, University of Basel, Switzerland*

[4]*Technical University of Tallinn, Estonia*

Overview

Proteins rarely work in isolation. Most of the time they interact with other molecules: other proteins, nucleic acids, small ligands, etc.[1] Consequently, in order to understand biological processes at atomic resolution it is often indispensible to consider proteins in molecular complexes. However, atomic resolution measurements on protein complexes pose a series of serious challenges for techniques such as NMR. In particular, protein-protein complexes are often comprised of very large molecular assemblies, for which achieving the sensitivity and spectral resolution required for quantitative studies becomes extremely difficult. For example, in solution slow tumbling of large systems induces strong transverse relaxation that leads to severe line broadening and an associated decrease in resolution and sensitivity. This challenge can be partially overcome by using TROSY-type techniques, which rely on the interference of relaxation mechanisms in order to reduce the line widths for large biomolecules.[2] Another alternative to TROSY spectroscopy in solution is provided by solid-state NMR. In the solid state in the absence of molecular tumbling resonance, line widths are independent of the size of the studied system. Consequently, if one overcomes solid state specific challenges for resolution and sensitivity, solid-state NMR could be potentially used to study structure and dynamics of proteins in even very large protein complexes. This report outlines briefly combined results of two different projects at the 850 MHz Facility that aimed at addressing the issue of sensitivity and resolution in quantitative solid-state NMR spectroscopy of large biomolecular complexes. First, we demonstrate that ^{1}H detection at fast spinning frequencies addresses the challenge of sensitivity allowing fast acquisition of high quality multidimensional NMR spectra on a few nanomoles of material (manuscript in preparation). We also demonstrate some results of protein spectroscopy at 100 kHz spinning frequencies, which renders ^{1}H-detected spectroscopy of fully protonated proteins practical. This work sets out new records for detectability in protein MAS NMR, where quantitative studies can be undertaken on samples containing as little as 3 nanomoles of labeled protein.

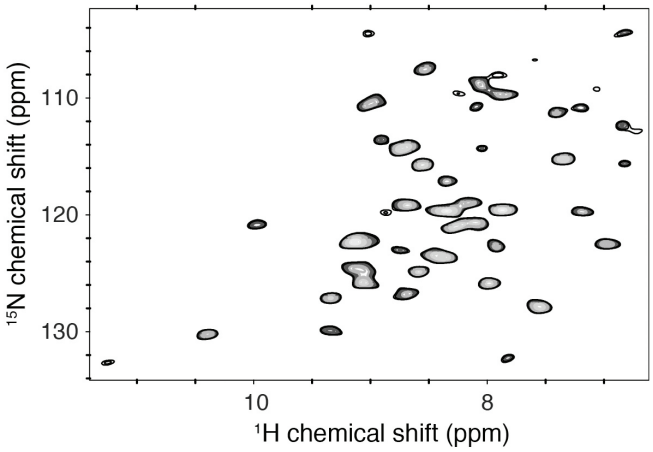

Figure 1. 2D ^{15}N-^{1}H correlation spectrum of a precipitated 300 kDa complex of 100% H_2O [U-^{13}C,^{15}N]GB1 and human immunoglobulin. The spectrum was obtained in 10 minutes at ν_r = 60 kHz and ν_{0H} = 850 MHz using ~6 nanomoles (2 mg) of the complex. A recycle interval of 0.4 s was used, with the sample containing 50 mM copper(II) EDTA.

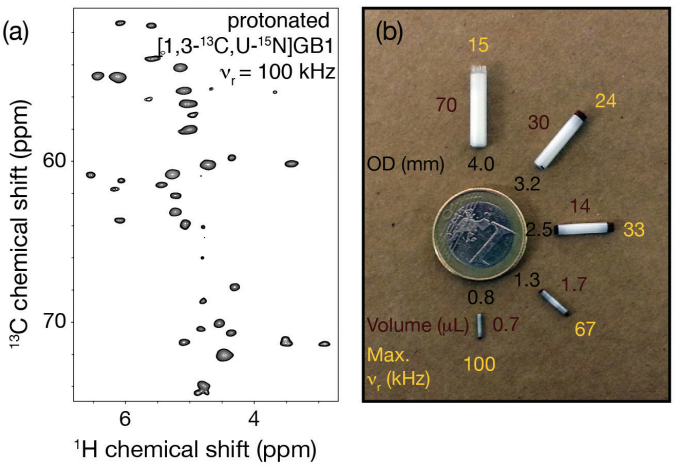

Figure 2. (a) A 2D ^{13}C-^{1}H correlation spectrum of ~46 nanomoles of crystalline protonated [1,3-^{13}C,^{15}N]GB1 obtained at ν_r = 100 kHz and ν_{0H} = 850 MHz. The observed ^{1}H line widths are as narrow as 100 Hz (0.11 ppm). (b) Comparison of outer diameter, maximum spinning frequency and volume of MAS rotors used for biomolecular NMR.

Optimizing Sensitivity for Large Protein Complexes

One of the main challenges for quantitative studies of large protein complexes is sensitivity. In this study we demonstrate that the sensitivity required for quantitative studies of large protein complexes in the solid state can be achieved by employing ^{1}H-detected experiments at 50-100 kHz spinning frequencies. For structural applications the sensitivity per unit time can be further improved by fast recycling of experiments enabled by addition of paramagnetic relaxation enhancing agents that reduce ^{1}H T_1 without inducing significant line broadening.[3] Such an approach enables the obtaining of high quality 2D-3D spectra on small quantities of protein complexes in a matter of minutes to hours. For example, Figure 1 shows a 2D ^{1}H-^{15}N correlation spectrum obtained in 10 minutes on ~12 nanomoles of GB1 in a ~300 kDa precipitated complex with natural abundance full length human immunoglobulin (IgG). The sensitivity achieved in this way enabled us to perform quantitative measurements of relaxation of GB1 in the complex as well as a series of 3D experiments to obtain distance restraints. The proposed approach should be widely applicable to quantitative studies of large biomolecular complexes, especially in combination with sedimentation by ultracentrifugation as a preparative method to produce high quality samples.[4] In particular, it will benefit application to systems that are difficult to be produced in large quantities.

Protein Studies at 100 kHz Spinning Frequency

Effective use of ^{1}H detection to improve the sensitivity of NMR experiments requires conditions leading to narrow ^{1}H line widths. At 60 kHz spinning frequency the best compromise between ^{1}H resolution and sensitivity is obtained for deuterated proteins that are fully reprotonated at exchangeable sites.[5] In order to take a full benefit of samples with a higher concentration of protons, and in particular fully protonated systems, faster spinning frequencies are required in order to improve the removal of strong ^{1}H-^{1}H dipolar couplings that lead to broadening of ^{1}H resonances. Recently, Samoson and coworkers developed a new 0.8 mm MAS probe that allows the reaching of 100 kHz spinning frequency. This new MAS regime enables effective use of ^{1}H detection in samples with high concentration of protons including fully protonated systems. For example, Figure 2 shows a 2D ^{13}C-^{1}H correlation spectrum obtained at 100 kHz on a fully protonated crystalline [1,3-^{13}C,U-^{15}N]GB1. The superior averaging of ^{1}H-^{1}H couplings afforded with this spinning frequency yields spectra with ^{1}H line widths as narrow as 90 Hz. Note that this is similar to a typical line width obtained on a 100% H_2O deuterated sample of GB1 in complex with IgG obtained at 60 kHz spinning. Even though deuteration is not strictly required at 100 kHz, it still benefits experiments performed under such conditions by improving the observed coherence lifetimes, which is crucial for multidimensional experiments. Combination of ^{1}H detection and 100 kHz spinning allows us to establish new limits for detectability in protein NMR. In Figure 3 we demonstrate that by using this approach we are able to record high quality spectra in a matter of hours on samples containing as little as 3 nanomoles of labeled protein (which corresponds to ~20 μg of GB1).

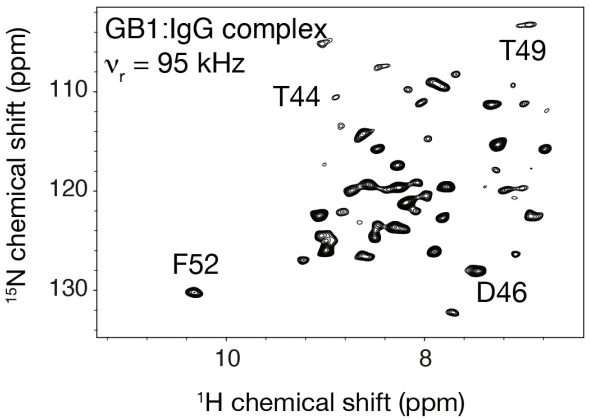

Figure 3. A 2D ^{15}N-^{1}H correlation spectrum of ~3.5 nanomoles of 100% H_2O deuterated [U-^{13}C,^{15}N]GB1 in a precipitated 300 kDa complex with human IgG obtained at ν_r = 95 kHz and ν_{0H} = 850 MHz. The experimental time was ~12 h.

References

1. Jones, S.; Thornton, J. *Proc. Natl. Acad. Sci.* **1996**, *93*, 13.
2. Fernandez, C.; Wider, G. *Curr. Opin. Struct. Biol.* **2003**, *13*, 570.
3. Parthasarathy, S.; Nishiyama, Y.; Ishii, Y. *Acc. Chem. Res.* **2013**, *46*, 2127.
4. Bertini, I.; Luchinat, C.; Parigi, G.; Ravera, E. *Acc. Chem. Res.* **2013**, *46*, 2059.
5. Lewandowski, J. R.; Dumez, J.-N.; Akbey, Ü.; Lange, S.; Emsley, L.; Oschkinat, H. *J. Phys. Chem. Lett.* **2011**, *2*, 2205.

Structural Analysis of Amyloid-Beta Oligomers and their Interactions with Polysaccharides using High-Field ^{13}C Solid-State NMR Spectroscopy

Jillian Madine,[1] Maya Pandya,[2] Edwin A. Yates,[1] Sheena Radford[2] and David A. Middleton[3]

[1]*Institute of Integrative Biology, University of Liverpool*

[2]*Astbury Centre for Structural Molecular Biology, University of Leeds*

[3]*Department of Chemistry, Lancaster University*

Overview

Between 30 and 40 proteins and peptides are currently known to assemble via small soluble oligomers into insoluble fibrillar deposits that are the pathological hallmark of human diseases and disorders, including Alzheimer's disease (AD), type II diabetes and Parkinson's disease. The relationship between the structural and toxicological properties of these amyloid, or amyloid-like, fibrils is poorly defined, yet is a question that is central to our understanding of these diseases.

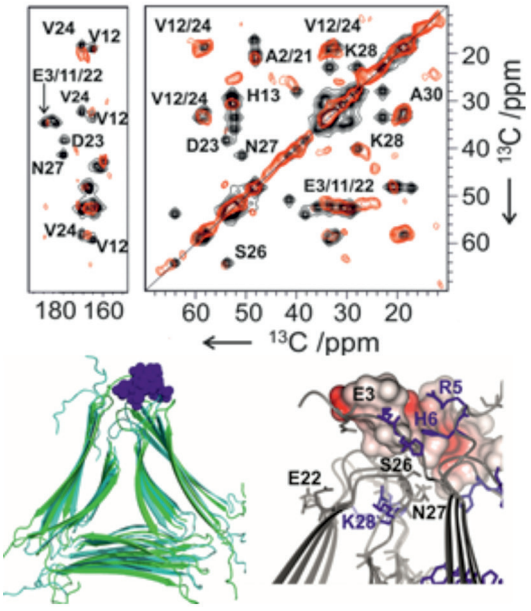

Figure 1. Top: A ^{13}C solid-state NMR PDSD spectrum of an $A\beta_{1\text{-}40}$ fibril-heparin complex (red) and simulated fit to the spectrum (black). Bottom left: a structural model of the GAG (blue)-fibril (green) complex. Bottom right: Space filling model of heparin bound to $A\beta_{1\text{–}40}$ fibrils.

Amyloid plaques of the amyloid-beta (Aβ) peptides that accumulate in AD brains also contain glycosaminoglycans (GAGs), the linear, highly sulfated polysaccharides associated with the extracellular matrix. It is now known that proteoglycans and GAGs such as heparan sulfate (HS) and dermatan sulfate (DS) co-localise widely *in vivo* with amyloid fibrils and plaques that are the pathological hallmark of human amyloidosis, stabilising fibrils and, in some cases, altering the course of amyloid assembly and the toxicity of the protein precursors of these disorders.

We used high-field solid-state NMR combined with uniform ^{13}C/^{15}N labelling and biochemical assays to unveil the first site-specific details of how the GAG heparin interacts with fibrils of the 40-amino acid AD peptide $A\beta_{1\text{-}40}$.[1] $A\beta_{1\text{-}40}$ fibrils with three-fold molecular symmetry bind 5 kDa heparin at a site flanked by the peptide's unstructured N-terminal region and the turn at the apices of the triangular geometry (Figure 1). This level of detail was gained from residue-specific ^{13}C chemical shift perturbations for the fibrils in the presence of heparin, together with a ^{13}C proton-driven spin diffusion (PDSD) experiment to reveal a complex stabilised by charged/polar amino acid side groups around the heparin molecule (Figure 1).

We have now turned our attention to the soluble oligomers that precede the deposition of insoluble fibrils and how heparin influences their molecular structure and morphology. It is well established that GAGs can profoundly influence the growth rate, fibril morphology and oligomer size, but how these effects relate to the underlying molecular structure of the oligomeric fibrillar precursors, and how these species interact with GAGs, is unknown. Such information is valuable for understanding AD and other amyloid disorders because protein oligomers are widely believed to be the pathogenic species.

Results

We prepared $A\beta_{1\text{-}40}$ oligomers and confirmed their presence by transmission electron microscopy (TEM) as shown in Figure 2. The oligomers appear as spherical aggregates over 100 nm in diameter, consistent with the on-pathway, cytotoxic species reported extensively elsewhere. In the presence of heparin the aggregates are substantially larger, being over 200 nm in diameter, suggesting that the polysaccharide has a fusogenic effect on the smaller structures.

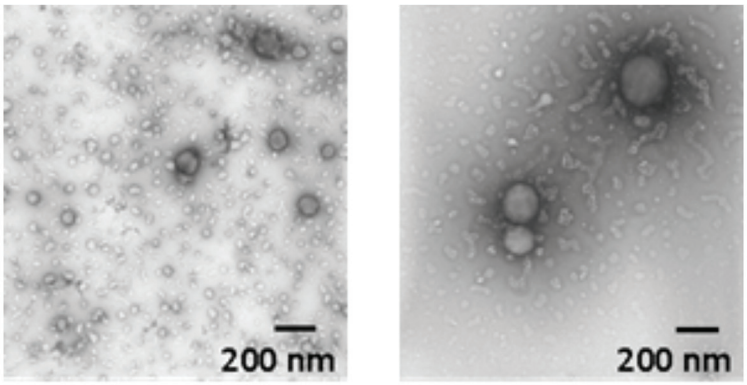

Figure 2. TEM images of $^{15}N/^{13}C$ $A\beta_{1\text{-}40}$ oligomers in the presence (right) or absence (left) of 5 kDa heparin.

High-field ^{13}C dipolar assisted rotational resonance (DARR) solid-state NMR measurements were conducted on uniformly ^{13}C and ^{15}N labelled $A\beta_{1\text{-}40}$ oligomers in the absence of heparin and in the presence of a 5-fold molar excess of heparin. Freshly prepared samples were freeze-quenched and lyophilized prior to analysis. The spectrum of oligomers alone was reminiscent of the spectrum of Aβ fibrils observed previously, with similar chemical shifts observed for most if not all residues (Figure 3a). The spectrum is thus consistent with the oligomers adopting a predominantly β-sheet structure similar to the final fibrillar architecture, although possibly with different tertiary and quaternary contacts. In the presence of heparin the spectrum was remarkably different from the spectrum for the oligomers alone. A comparison with simulated spectra indicated that the oligomer sample was almost entirely α-helical (Figure 3b). It is known that monomeric Aβ assembles into oligomers via transitory helical species, and it is possible that heparin stabilises this helical state. One concern was that the method of preparation involved the use of 10 % hexafluoroisopropanol (HFIP) in aqueous solution. HFIP is well known to induce α-helical structures in proteins and peptides. We therefore obtained spectra for oligomers prepared in NaOH in the absence of HFIP. The spectra of oligomers alone were consistent with a mixture of α-helical and β-sheet structures (Figure 3c), but in the presence of heparin the sample consisted of virtually entirely α-helical structures (Figure 3d). Hence heparin modulated the structure of Aβ oligomers prepared in two different ways.

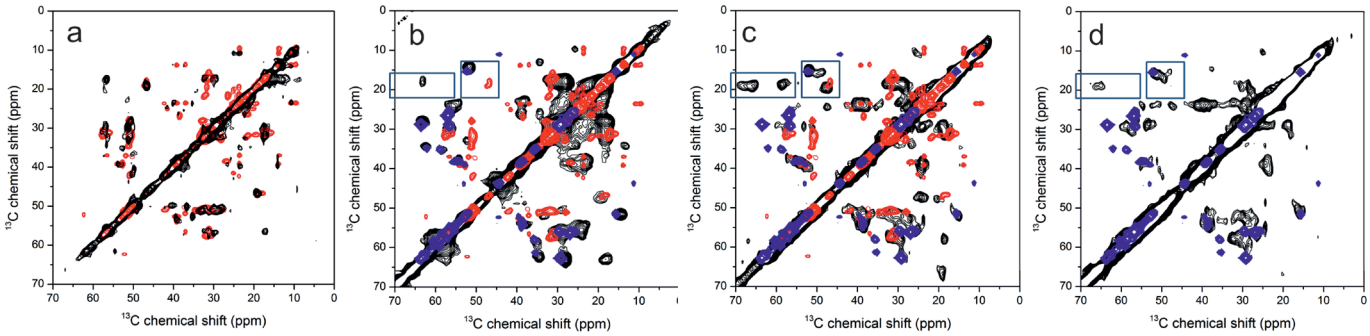

Figure 3. High-field ^{13}C DARR spectrum (at 850 MHz) of $A\beta_{1\text{-}40}$ oligomers prepared in (a) HFIP alone or (b) with heparin and prepared in (c) NaOH alone or (d) with heparin. Experimental spectra of oligomers are shown in black; an experimental spectrum of Aβ fibrils is shown in red; a simulated spectrum of α-helical Aβ is shown in blue. Rectangles indicate regions of the spectra that are diagnostic of β-sheet and α-helical structures.

In summary, high-field solid-state NMR measurements have provided compelling evidence that GAGs interact with soluble Aβ oligomers and stabilise the transitory α-helical structures that form early in the assembly pathway. These results will inform future studies of the structure-toxicity relationship of Aβ self-assembly. This work was supported by the Wellcome Trust (grant number WT088563MA).

References

1. Madine, J.; Pandya, M. J.; Hicks, M. R.; Rodger, A.; Yates, E. A.; Radford, S. E.; Middleton, D. A. *Angew. Chem. Int. Ed.* **2012**, *51*, 13140.

Multinuclear Characterisation of Magnesium-Based Cements for Specialised Applications

Laura J. Gardner, Sam A. Walling, Susan A. Bernal, John L. Provis

Immobilisation Science Laboratory, Department of Materials Science and Engineering, University of Sheffield

Overview

Magnesium-based cements are produced via an acid-base reaction of magnesia (MgO) with potassium phosphates to form magnesium potassium phosphate cements (MKPC), also known as chemically bonded phosphate ceramics or acid-base cements,[1] or with amorphous silica sources to form magnesium silicate hydrate (M-S-H) binders. Both of these types of binder have been proposed as possible cements for the immobilisation of different types of wastes arising from the nuclear fuel cycle, among other applications in rapid concrete repair (MKPC) or as a potential low-carbon cement (M-S-H). The main phase formed in MKPC is struvite-K ($MgKPO_4.6H_2O$), a potassium analogue of struvite ($NH_4MgPO_4.H_2O$), which is naturally cementitious and presents a partially amorphous structure as a consequence of its rapid setting.[2,3,4] However, this material has never before been studied by NMR. For binders in the system $MgO\text{-}SiO_2\text{-}H_2O$ (M-S-H), the sole identified reaction product is a poorly crystalline magnesium silicate compound with a highly disordered structure,[5] and whose chemistry is strongly dependent on the Mg/Si ratio. This structure also requires the application of high-resolution NMR techniques to provide detailed information regarding the local environments of magnesium, as this information has not previously been known.

High-Resolution ^{25}Mg and ^{39}K MAS NMR Spectroscopy of Struvite-K

Natural struvite-K was identified and classified as a new mineral less than a decade ago,[6] and it has been reported that its crystalline form presents a similar structure to struvite (Figure 1), as K^+ can replace NH_4^+ in the lattice of struvite due to the similar radii of these cations.[7] High resolution ^{25}Mg and ^{39}K MAS NMR spectra (Figure 2) provided for the first time information about the chemical shift and quadrupolar coupling parameters of the crystalline and amorphous components present in synthetic struvite-K, and in struvite-K blended with granulated blast furnace slag.

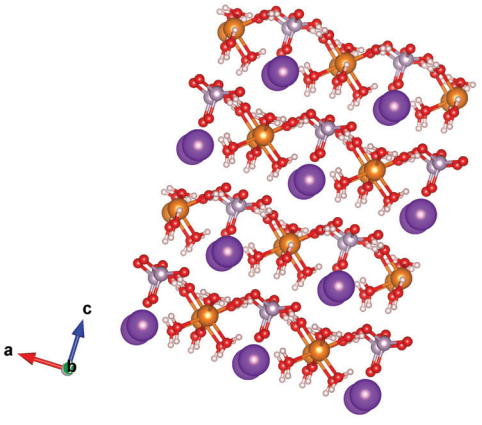

Figure 1. Crystal structure of struvite-K.

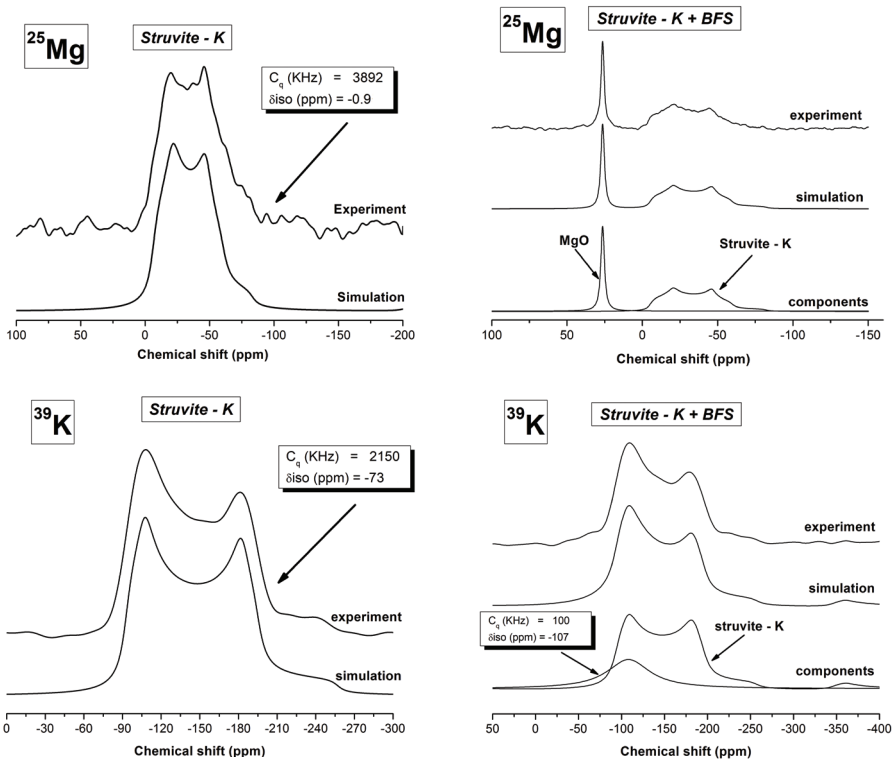

Figure 2. ^{25}Mg MAS and ^{39}K MAS NMR spectra of struvite-K with and without blast furnace slag (BFS).

^{25}Mg MAS NMR Spectroscopy of Magnesium Silicate Hydrate Cements

The UK has accumulated significant quantities of radioactive $Mg(OH)_2$ sludges from its Magnox nuclear programme which are classed as intermediate level waste (ILW) streams. The search for safe alternatives for disposal of these ILWs has motivated the development of magnesium silicate hydrate (M-S-H) binders. The microstructure of these materials is difficult to determine using conventional analytical techniques due to their highly amorphous nature, and consequently the long-term performance of these materials cannot yet be predicted. The high-resolution ^{25}Mg MAS NMR spectra of M-S-H products with different ages demonstrate at early age these cements have a talc-type structure (see Figures 3 and 4); however, under extended ageing periods, these materials show a significant change in their structure, which may have important implications for their use in waste immobilisation or construction.

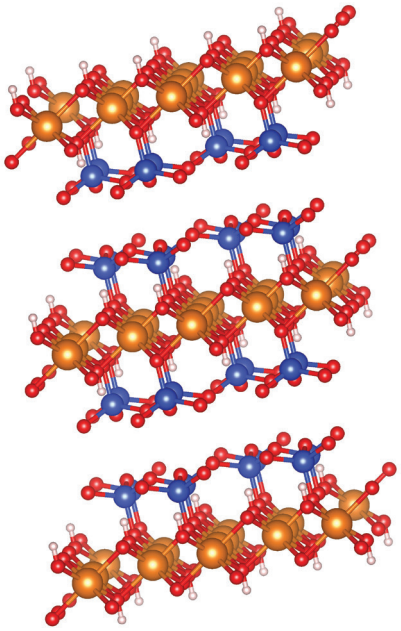

Figure 3. Crystal structure of talc.

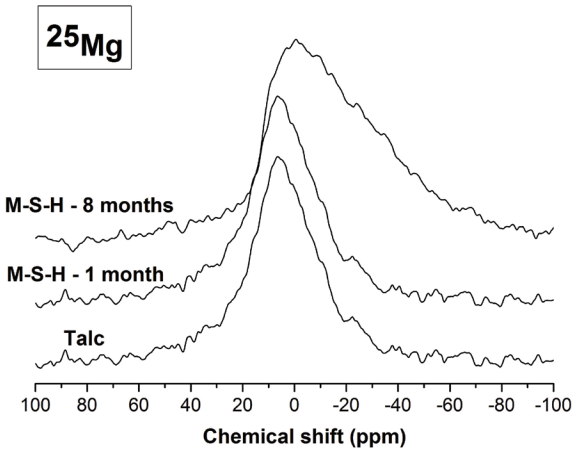

Figure 4. ^{25}Mg MAS NMR spectra of talc, and of M-S-H type cements with different ages.

References

1. Nicholson, J. W.; Wilson, A. D. *Acid-Base Cements-Their Biomedical and Industrial Applications.* (Chemistry of Solid State Materials Vol. 3) Cambridge University Press, UK, 1993.
2. Xing, F.; Ding, Z.; Li, Z.-J. *Adv. Cement Res.* **2011**, *23*, 81.
3. Ding, Z.; Li, Z. *Cement and Concrete Composites* **2005**, *27*, 11.
4. Wilson, A. D. *Chem. Soc. Rev.* **1978**, *7*, 265.
5. Brew, D.; Glasser, F. *Cement and Concrete Res.* **2005**, *35*, 85.
6. Graeser, S.; Postl, W.; Bojar, H.-P.; Berlepsch, P.; Armbruster, T.; Raber, T.; Ettinger, K.; Walter, F. *Eur. J. .Mineralogy* **2008**, *20*, 629.

7. Chauhan, C.; Vyas, P.; Joshi, M. *Cryst. Res. Technol.* **2011**, *46*, 187.

Ultra-High Magnetic Field NMR Studies of Tin-Derived Nano-Building Blocks and Hybrid Materials Including by BRAIN CP

Christian Bonhomme,[1] François Ribot,[1] Christel Gervais,[1] Danielle Laurencin[2] and Mark E. Smith[3,4]

[1]*LCMCP University Paris 06, France*

[2]*Institut Charles Gerhardt de Montpellier, France*

[3]*Vice-Chancellor's Office, Lancaster University*

[4]*Department of Physics, University of Warwick*

Overview

As a result of recent NMR developments, the characterisation of materials of increasing complexity is now possible, allowing detailed insight into their structure to be obtained. For example, the studies of Schurko and co-workers[1] have rendered the acquisition of ultra-wide line NMR spectra from solids more accessible using novel cross-polarisation (CP) approaches. Furthermore, much progress has been made in the use of NMR characterisation of low-γ quadrupolar nuclei with low natural abundance, such as ^{25}Mg.[2] Here two examples of applications of such recent NMR developments are provided. First, it is shown that tin oxo-clusters can be characterised using static ^{119}Sn NMR experiments, including ^{1}H-^{119}Sn and ^{19}F-^{119}Sn BRAIN-CP excitation schemes. Second, it is shown that intercalated Mg/Al layered double hydroxides can be easily studied by natural abundance ^{25}Mg NMR. In particular it is demonstrated that the Mg environment is sensitive to the presence of the molecules intercalated between the layers.

^{119}Sn NMR Spectroscopy of Tin Oxo-Clusters

Tin oxo-clusters are an important class of materials in the field of catalysis, and can be used as building-blocks for the synthesis of advanced organic inorganic hybrids. In their crystalline form, tin oxo-clusters are characterised by the association of definite polynuclear entities through H-bonding, and can exhibit a variety of local tin environments. To further refine the characterisation of these compounds in the solid state, and notably distinguish the different tin environments, a variety of crystalline tin oxo-clusters were synthesised exhibiting 5- and 6-fold coordinated Sn sites with variable Sn-H distances: $[(BuSn)_{12}O_{14}(OH)_6](X)_z$ (with X : OH^-, z = 2; and X : SO_4^{2-}, $SO_3CF_3^{2-}$, z = 1).

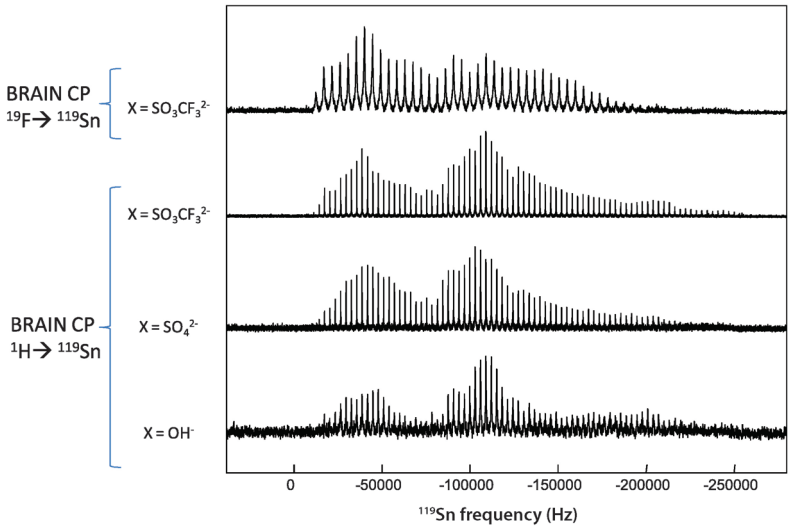

Figure 1. ^{1}H→ ^{119}Sn and ^{19}F→ ^{119}Sn BRAIN-CP experiments, showing the different 5- and 6-coordinate environments in the $[(BuSn)_{12}O_{14}(OH)_6](X)_z$ crystalline phases.

The ^{119}Sn spectra (Figure 1) obtained showed clearly that the different 5- and 6-fold Sn environments are visible in all materials, attesting to the common "$(BuSn)_{12}$" core. In the $^{1}H \rightarrow ^{119}Sn$ BRAIN CP experiments, the main differences observed were ^{119}Sn transverse relaxation properties: the materials with fewer protons in the vicinity of Sn (X = SO_4^{2-}, $SO_3CF_3^{2-}$) led to longer T_2 values thereby allowing more echoes in the CPMG acquisition and hence a better signal-to-noise. More importantly, it was demonstrated that the "BRAIN-CP" experiment can use a nucleus other than ^{1}H, i.e. ^{19}F as the polarisation source. These extensions of the BRAIN-CP experiment may be useful in the future for the characterisation of other complex phases.

^{25}Mg NMR Spectroscopy of Intercalated Layered Double Hydroxides

Layered double hydroxides (LDHs) are a family of lamellar materials which have found many applications, in fields such as catalysis, drug delivery and water treatment. Indeed, a variety of anions (both organic and inorganic) can be intercalated between the positively charged layers of cations. For example, in the case of Mg-Al layered double hydroxides ($Mg_{0.67}Al_{0.33}(OH)_2(NO_3)_{0.33}\cdot 0.5H_2O$), the nitrate anions initially present between the layers can easily be exchanged by other organic anions such as citrate. With the aim of increasing the ways of characterising such intercalated phases, it was decided to examine how local magnesium environments are affected by the presence of "organic" anions between the layers, using ^{25}Mg solid-state NMR. Figure 2 shows a comparison of ^{25}Mg natural abundance MAS NMR spectra of two LDH phases, before and after intercalation of organoboron anions. The differences between the two spectra are clear, with an increase in the range of Mg local environments after intercalation. Further experiments and modelling studies will be needed to determine the structural origin of this increased range of local magnesium environments.

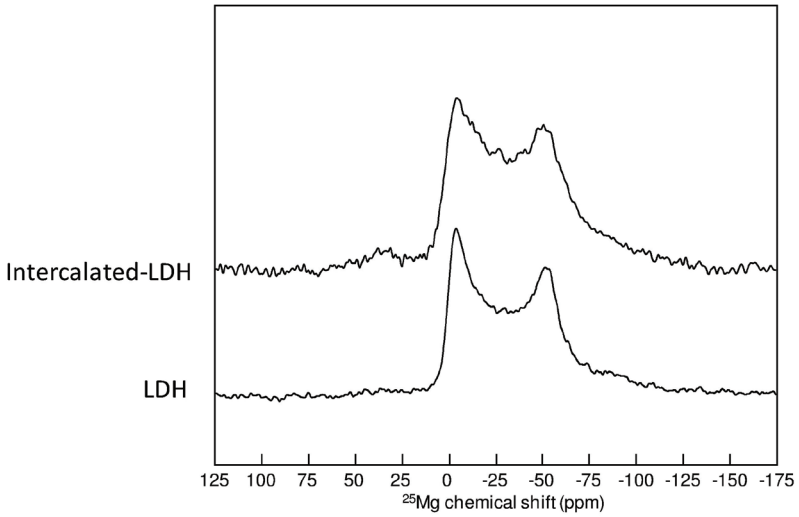

Figure 2. Nature abundance ^{25}Mg MAS NMR spectra of a layered double hydroxide, before and after intercalation of an organoboron anion. The DFS (double frequency sweep) enhancement scheme was used.

References

1. Schurko, R. W. *Acc. Chem. Res*. **2013**, *46*, 1985.
2. Freitas, J, C. C.; Smith, M. E. *Ann. Rep. NMR Spectrosc*. **2012**, *75*, 25.

Measurements of ^{1}H and ^{19}F CSAs with Ultrafast MAS: Self Assembly in Zirconium Phosphonates

Habeeba K. Miah,[1] Lyndsey Knight,[1] Francesca Martini,[1,2] Marco Geppi[2] and Jeremy J. Titman[1]

[1]*School of Chemistry, University of Nottingham*

[2]*Department of Chemistry and Industrial Chemistry, University of Pisa, Italy*

Overview

Zirconium phosphonates can be assembled to give a wide range of structures with different dimensionalities and connectivities, making them useful materials for a wide range of applications, including proton conductors, heterogeneous catalysts and fillers for polymeric composites. Recently, two novel phosphono-carboxylate ligands have been synthesized from the reaction of diethyl 2-bromoethylphosphonate with 3-carboxypyridine (nicotinic acid) and 4-carboxypyridine (isonicotinic acid).[1] Reactions of these ligands with zirconium in hydrofluoric acid result in two zirconium phosphonate compounds. Compound **1** (Figure 1a) has a chain structure with an inorganic backbone of ZrO_3F_3 octahedra and PO_3C tetrahedra. Each carboxylate group of the isonicotinate points toward an adjacent chain with one oxygen only 2.67 Å away from an equatorial F of a neighbouring ZrO_3F_3 group, suggesting a O-H…F hydrogen bond. Compound **2** (Figure 1b) has a layered structure in which the layers contain chains of ZrO_4F_2 octahedra and PO_3C tetrahedra covalently linked via the carboxylate groups of the nicotinic species. These compounds exhibit previously unobserved zirconium phosphonate structures and connectivities between chains.

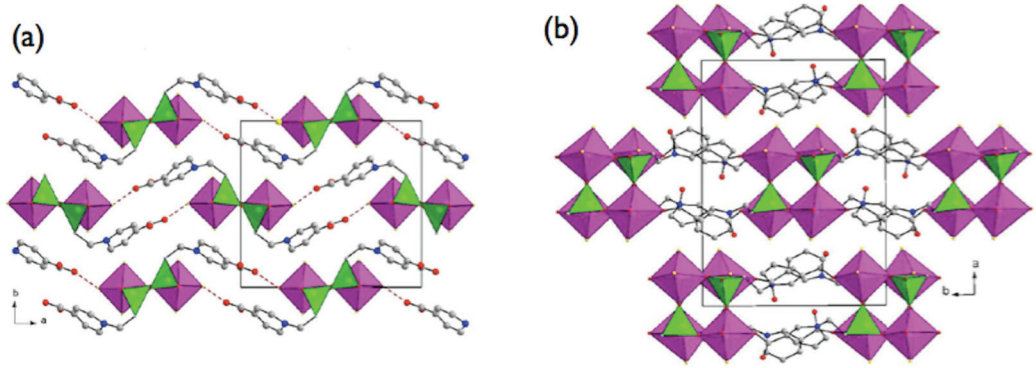

*Figure 1. Structures of zirconium phosphonates (a) **1** and (b) **2** viewed down the c axis. ZrO_3F_3 octahedra are purple, and PO_3C tetrahedra are green. Red dashed lines show the short O…F distance.*

Solid-state NMR spectroscopy provides a means to study hydrogen-bonded structures, since the ^{1}H CSA depends on the hydrogen bond length. We recently implemented a new ^{1}H anisotropic-isotropic shift correlation experiment optimized for use with ultrafast MAS (ν_r > 60 kHz).[2] In this experiment the ^{1}H CSA is measured in the indirect dimension using a symmetry-based recoupling sequence, while different ^{1}H sites are resolved via their isotropic shifts in ν_2. The use of ultrafast MAS at the high B_0 field available at the Facility optimizes the resolution of ^{1}H sites in ν_2 without the need for homonuclear decoupling. The recoupling sequences used in t_1 consist of N inversion pulses R, timed to occupy n rotor periods, where each R element of the overall sequence has duration $n\tau_r/N$ and alternate elements have phases $\pm\pi n\nu/N$. The symmetry numbers N, n and ν determine which interactions are retained in the first-order effective Hamiltonian for the sequence. Recoupling sequences suitable for measuring the ^{1}H shift parameters recouple a single-quantum Hamiltonian which takes the form

$$\bar{H}^{(1)} = \sum_j \left(\omega_j T^j_{1-1} - \omega^*_j T^j_{1+1}\right)$$

to first order, where the index j runs over all the ^{1}H shift interactions. The coefficient ω_j depends on the CSA and determines the appearance of the recoupled powder pattern observed in the evolution dimension. Suitable symmetries must also avoid inadvertently recoupling the strong ^{1}H dipolar interactions, as well as isotropic ^{1}H shifts. However, since the pulse sequence is synchronized with the spinning, the required rf amplitude increases with ν_r. Hence, many sequences become impractical at ultrafast MAS rates, and a careful choice of symmetry numbers is required to ensure operation with acceptable rf amplitudes.

Results

A number of new CSA recoupling sequences which operate even at MAS rates up to 80 kHz were demonstrated using the state-of-the-art Jeol 1 mm MAS probe available at the 850 MHz Facility. For example, Figure 2a shows an experimental ^{1}H anisotropic-isotropic correlation spectrum of ascorbic acid obtained using a $R16^{2}_{3}$ sequence with a MAS rate of 78.1 kHz. A similar spectrum recorded for **1** at 62.5 kHz is shown in Figure 2b. The resonance at δ_2 = 12.5 ppm shows a recoupled lineshape in ν_1 which corresponds to a large ^{1}H CSA of 12 ppm consistent with a strong hydrogen bond. In this case the lineshape depends additionally on the ^{1}H-^{19}F heteronuclear dipolar coupling which is also recoupled by the $R16^{2}_{3}$ sequence. The value of the coupling measured from this lineshape is consistent with a short H…F distance confirming the presence of a hydrogen bond.

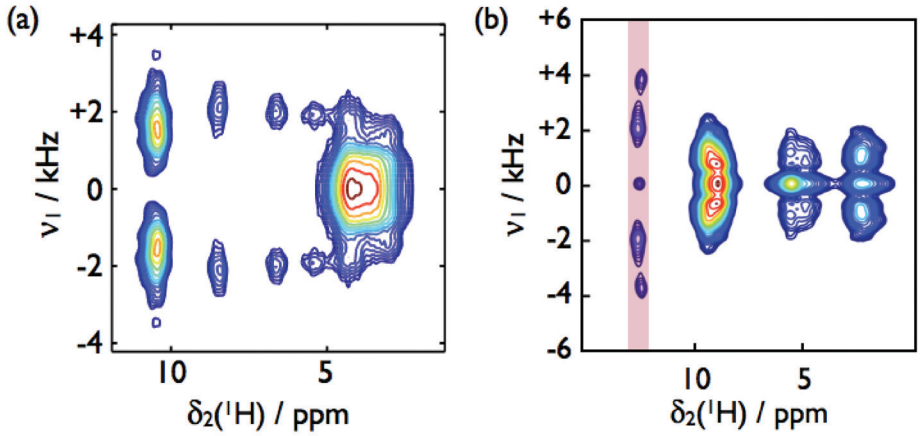

*Figure 2. Experimental ^{1}H anisotropic-isotropic correlation spectra of (a) ascorbic acid and (b) **1** recorded at a Larmor frequency of 850 MHz with a $R16^{2}_{3}$ sequence to recouple the ^{1}H CSA in ν_1. The red bar in (b) indicates the recoupled lineshape for the hydrogen-bonded proton resonance at δ_2 = 12.5 ppm.*

In addition to ^{1}H studies, ^{19}F shift parameters provide further information about the zirconium phosphonate materials. For example, with the improved resolution obtained at high field the {^{1}H}-decoupled ^{19}F spectrum (Figure 3) recorded with a MAS rate of 25 kHz shows three ^{19}F resonances for **1** with the most shielded resonance corresponding to the hydrogen bonded equatorial fluorine atoms in the ZrO_3F_3 octahedra. Resonances corresponding to the remaining axial fluorine atoms can be resolved using ^{1}H decoupling at the high B_0 field available at the 850 MHz Facility. The isotropic shift difference of 3 ppm is evidence of a small distortion from perfect octahedral geometry. However, the effect of this distortion on the ^{19}F CSA is more significant with a measured difference between the two axial fluorine atoms of 21 ppm.

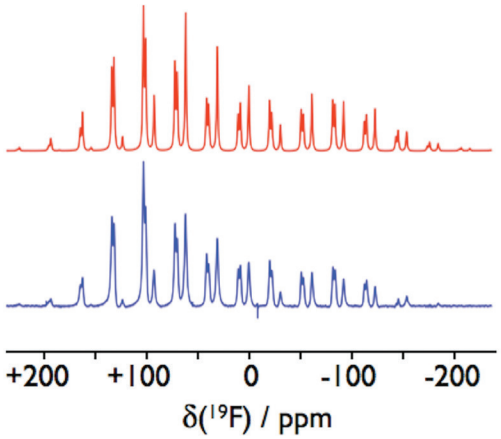

*Figure 3. {^{1}H}-decoupled ^{19}F spectrum of **1** recorded at a ^{19}F Larmor frequency of 800 MHz and a MAS rate of 25 kHz (blue) with a simulation used to extract CSA parameters (red).*

References

1. Constantino, U.; Sassi, P.; Geppi, M.; Taddei, M. *Cryst. Growth Des.*, **2012**, *12*, 5462.
2. Miah, H. K.; Bennett, D. A.; Iuga, D.; Titman, J. J. *J. Magn. Reson.* **2013**, *235*, 1.

Natural Abundance ^{33}S STMAS NMR of Ettringite

Akiko Sasaki and Stephen Wimperis

School of Chemistry, University of Glasgow

Overview

Quadrupolar nuclei account for about 70% of NMR-active nuclides. The inverse dependence of the second-order quadrupolar interaction upon magnetic field strength makes the use of B_0 = 20.0 T highly advantageous for quadrupolar nuclei with half-integer spin quantum numbers. There have been very few ^{33}S (spin I = 3/2) solid-state NMR studies in the literature, owing to the low natural abundance (0.76%) and low gyromagnetic ratio of ^{33}S, and the high expense of ^{33}S enrichment. Recently, very high field NMR has been used to advantage to overcome some of the limitations associated with low-γ quadrupolar nuclei, such as ^{33}S (ν_0 = 30.7 MHz at 9.4 T). ^{33}S solid-state NMR studies have begun to attract interest owing to the prevalence of sulphur in nature and materials science. Natural abundance ^{33}S solid-state NMR, therefore, has great potential for future applications. The aim of this project is to demonstrate the feasibility of high-resolution natural abundance ^{33}S NMR at the high B_0 fields now available. The MQMAS and STMAS NMR experiments yield high-resolution NMR spectra of half-integer spin nuclei, such as ^{33}S. STMAS is the more difficult technique to implement but shows increased sensitivity owing to effective excitation of the single-quantum satellite transitions, making it advantageous for the study of low-γ nuclei.[1]

Ettringite ($Ca_6Al_2(SO_4)_3(OH)_{12}\cdot 26H_2O$) is a cementitious mineral that is central to the chemistry of concrete and cement. The crystal structure is known[2] (Figure 1a) and there has been an early ^{27}Al MAS NMR study.[3] There have been two ^{33}S MAS NMR studies of ettringite at high field.[4,5] These two studies disagree, with one simulating the ^{33}S MAS NMR spectrum with a single S site[4] and the other simulating it with three S sites[5] (in accordance with the XRD structure), leaving uncertainty in the number of crystallographically different S sites observed by ^{33}S NMR (Figures 1b and 1c). Figures 1d and 1e show our simulated ^{33}S STMAS NMR spectra of ettringite at 20.0 T using parameters suggested in References 4 and 5. Here, we hope to characterise the distinct S sites in ettringite using ^{33}S STMAS and resolve the ambiguity present in the current literature. In addition, we expect to be able to address questions relating to disorder and dynamics of the intercolumn SO_4^{2-} species.

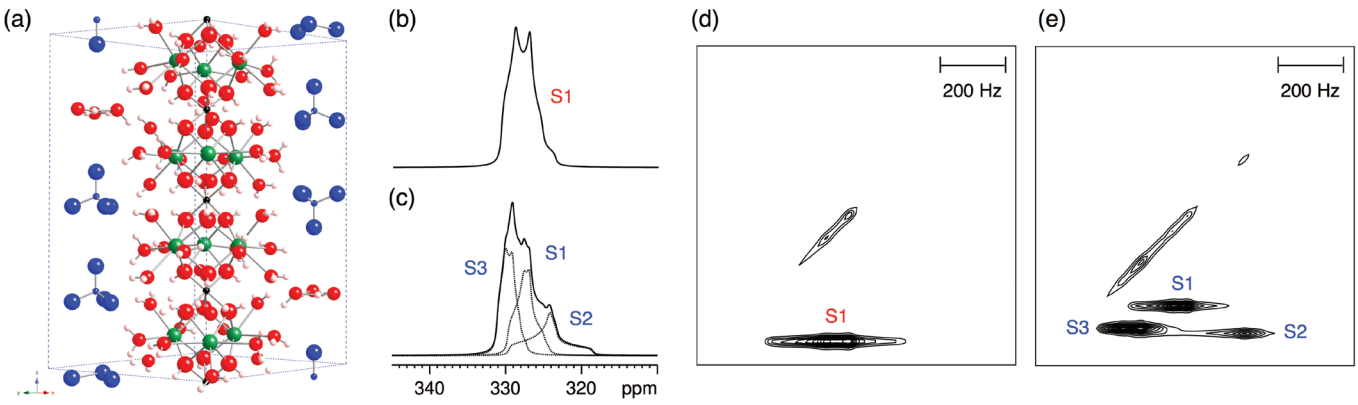

Figure 1. (a) Ettringite unit cell with a column of Al^{3+} (black) and Ca^{2+} (green) ions linked through O (red) atoms of OH^- ions and H_2O groups. The vertical column of SO_4^{2-} tetrahedra (blue) contains further H_2O molecules located between SO_4^{2-} groups. (b, c) Simulated ^{33}S MAS NMR spectra of ettringite at 20.0 T using parameters suggested in References 4 and 5. (d, e) Simulated ^{33}S STMAS NMR spectra of ettringite at 20.0 T using parameters suggested in References 4 and 5. The sets of parameters were (b, d) δ = 330 ppm, C_Q = 700 kHz and η = 0.45 and (c, e) δ = 329.8, 329.6, 331.3 ppm, C_Q = 591, 810, 516 kHz and η = 0.72, 0.97, 0.50 with the relative intensity 1:1:1.

Natural Abundance ^{33}S STMAS of a Model System

The first stage of this project was the technical implementation of ^{33}S STMAS experiments. We have established a protocol for accurate spinning angle setting using ^{85}Rb STMAS spectra of $RbNO_3$ and confirmed that a 4-mm MAS probe is suitable for our STMAS experiments. We also demonstrated how to extrapolate optimum pulse lengths for ^{33}S STMAS experiments,[1] where the sensitivity is too low to optimise the pulse length on the sample of interest. To demonstrate the feasibility of natural abundance ^{33}S STMAS experiments, we then chose a model system of 1:1 molar mixture of sodium sulphate (Na_2SO_4) and sodium sulphate (K_2SO_4) and recorded a ^{33}S spin-echo MAS spectrum (Figure 2a). The fitting parameters agreed with the reported values in the literature.[6] Figure 2b shows our natural abundance ^{33}S STMAS spectrum of the 1:1 molar mixture of Na_2SO_4 and K_2SO_4. Although the resolution in the F_1 dimension could be improved, the signal-to-noise ratio was sufficient to yield the NMR parameters δ_{CS} = 340.7, 336.3 ppm and P_Q = 646, 966 kHz in good agreement with the ^{33}S MAS spectrum in Figure 1a.

Natural Abundance ^{33}S STMAS of Ettringite

Our ettringite sample was obtained from a mineralogical collection and its identity was confirmed by powder X-ray diffraction (XRD). In Figure 2c, we have fitted our ^{33}S spin-echo MAS spectrum with two ^{33}S sites, employing δ = 332.0, 331.1 ppm, C_Q = 600, 812 kHz and η = 0.29, 0.34 with the relative intensity 1:1. Since we expected the isotropic ^{33}S peaks in ettringite to have more similar frequencies than those in the sulphate mixture, the value of t_1^{max} was increased in the STMAS experiment for better resolution. We then successfully obtained the natural abundance ^{33}S STMAS spectrum of ettringite shown in Figure 2d. This spectrum indicates the presence of at least one or, possibly, two ^{33}S sites, the latter assumption yielding the NMR parameters δ_{CS} = 332.2, 330.9 ppm, and P_Q = 610, 820 kHz in good agreement with the ^{33}S MAS spectrum in Figure 2c.

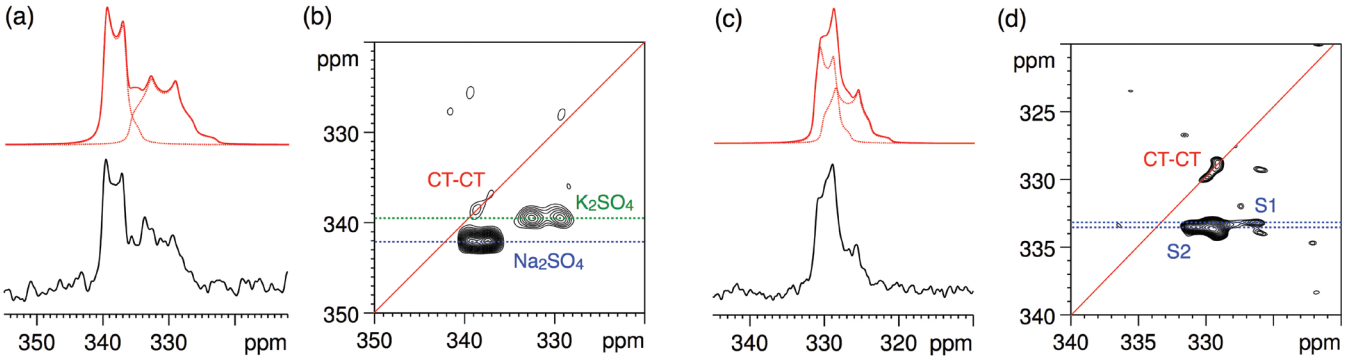

Figure 2. (a) Natural abundance ^{33}S spin-echo MAS NMR spectrum of 1:1 molar mixture of sodium sulphate (Na_2SO_4) and potassium sulphate (K_2SO_4) and corresponding lineshape fit (red). 4928 transients were averaged with a relaxation interval of 30 s. Total experiment time of 41 hours. The fitting parameters were δ = 340.8, 336.8 ppm, C_Q = 655, 959 kHz and η = 0.13, 0.41 with the relative intensity 1:1. (b) Natural abundance ^{33}S STMAS NMR spectrum of 1:1 molar mixture of sodium sulphate (Na_2SO_4) and potassium sulphate (K_2SO_4). 192 transients were averaged for each of 67 t_1 increments, with a relaxation interval of 20 s. Total experiment time of 71.5 hours. (c) Natural abundance ^{33}S spin-echo MAS NMR spectrum of ettringite and corresponding lineshape fit (red). 60000 transients were averaged with a relaxation interval of 1 s. Total experiment time of 16.7 hours. The fitting parameters are given in the text. (d) Natural abundance ^{33}S STMAS NMR spectrum of ettringite. 1952 transients were averaged for each of 160 t_1 increments, with a relaxation interval of 1 s. Total experiment time of 87 hours.

References

1. Dowell, N. G.; Ashbrook, S. E.; Wimperis, S. *J. Phys. Chem.* B **2004**, *108*, 13292.
2. Goetz-Neunhoeffer, F.; Neubauer, J. *Powder Diffr.* **2006**, *21*, 4.
3. Skibsted, J.; Henderson, E.; Jakobsen, H. J. *Inorg. Chem.* **1993**, *32*, 1013.
4. d'Espinose de Lacaillerie, J.-B.; Barberon, F.; Bresson, B.; Fonollosa, P.; Zanni, H.; Fedorov, V. E.; Naumov, N. G.; Gan, Z. *Cem. Concr. Res.* **2006**, *36*, 1781.
5. Hansen, M. R.; Brorson, M.; Bildsøe, H.; Skibsted, J.; Jakobsen, H. J. *J. Magn. Reson.* **2008**, *190*, 316.
6. Wagler, T. A.; Daunch, W. A.; Panzner, M.; Youngs, W. J.; Rinaldi, P. L. *J. Magn. Reson.* **2004**, *170*, 336.

Distribution of Octahedral and Tetrahedral Ga in γ-Ga_2O_3

Daniel M. Dawson,[1] Sharon E. Ashbrook,[1] Helen Y. Playford[2] and Richard I. Walton[2]

[1]*School of Chemistry and EaStCHEM, University of St Andrews*

[2]*Department of Chemistry, University of Warwick*

Overview

Gallium oxide, Ga_2O_3, is of potential importance to electronics and catalysis. However, despite its apparent relationship to widely studied Al_2O_3, its polymorphism is complicated and poorly understood. We recently prepared and structurally characterised various forms of Ga_2O_3.[1] In addition to the known α and β polymorphs, we confirmed the identity of three disordered polymorphs, γ, ε and κ, using total neutron scattering to examine short- and long-range structure. Here, we focus on a more detailed study of the structure of the γ polymorph. γ-Ga_2O_3 is essentially a metal-deficient spinel containing Ga^{3+} distributed over partially-occupied octahedral, Ga(VI), and tetrahedral, Ga(IV), sites. Our neutron diffraction experiments indicate the presence of two crystallographic Ga(VI) and two Ga(IV), with the local symmetry of the Ga(VI) lowered from the perfect spinel symmetry (*Fd*-3*m*) such that the Ga-O bond lengths are not all equal.[1] We have completed a reverse Monte Carlo (RMC) simulation of a crystalline sample of γ-Ga_2O_3, and have shown that the structural model agrees well with the experimental data. For γ-Ga_2O_3 with smaller particle size, the neutron Bragg scattering suggests that the distribution of Ga(IV) and Ga(VI) is different than in the highly crystalline sample. In the present work, we used high-field ^{71}Ga MAS NMR experiments to probe the distributions of Ga(VI) and Ga(IV) within three samples of γ-Ga_2O_3 with different particle sizes.

Results

Three samples of γ-Ga_2O_3 were prepared with different particle sizes; ~30, 15 and 5 nm, and characterised crystallographically by Bragg diffraction and pair distribution function (PDF) analysis (manuscript in preparation). The intensities of the peaks in the Bragg diffraction patterns indicated that there was greater occupation of the Ga(IV) sites with decreasing particle size, whereas the PDF analysis indicated that the average Ga-O bond length was the same in all samples (*i.e.*, the average coordination environment of Ga did not change). Integration of the ^{71}Ga MAS NMR spectra of the three samples, shown in Figure 1, revealed an essentially constant Ga(IV) : Ga(VI) ratio. We believe that there is increased occupancy of the Ga(IV) sites in the bulk of the particles, as observed by Bragg diffraction, but the surface of the particles undergoes reconstruction to give a higher proportion of Ga(VI). The increased surface area : volume ratio of the smaller particles offsets the increased occupancy of Ga(IV) in the bulk of the particles, giving rise to almost constant overall Ga(IV) : Ga(VI) ratios for all particle sizes. It is interesting to note that, with such small particles, the "bulk" technique of Bragg diffraction is more sensitive to the nanoparticle structure, while the "local" technique of NMR is more sensitive to the bulk structure, which includes the disordered surface as well as the ordered core in such nanocrystalline oxides.

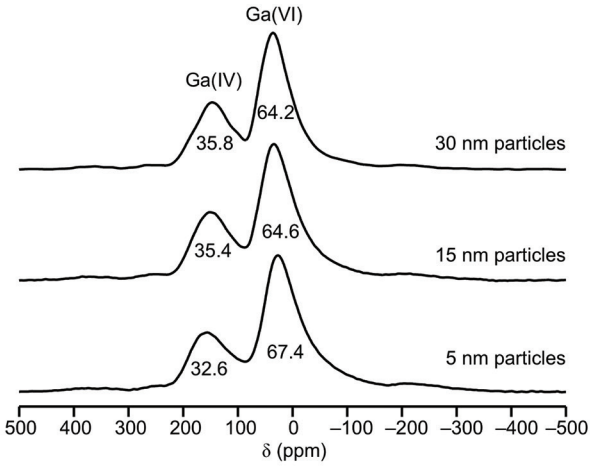

Figure 1. ^{71}Ga (20.0 T, 62.5 kHz MAS) spin-echo spectra of γ-Ga_2O_3 with the given average particle diameters. The relative integrated intensities of the resonances are indicated.

References

1. Playford, H. Y.; Hannon, A. C.; Barney, E. R; Walton, R. I. *Chem. Eur. J.* **2013**, *19,* 2803.

User Comments

"A variety of unique probes, in particular with options of triple-resonance experiments at extra-high MAS and in combination with a high magnetic field, all provide a solid basis for obtaining unique structural information on biologically-important samples."

Oleg Antzutkin, University of Warwick

"NMR experiments carried out at the 850 MHz Facility permit a gain in sensitivity and resolution not available in our in-house instruments and from which very detailed structural features on crystalline and amorphous porous frameworks could be readily obtained. The unique availability of a very fast magic-angle spinning probe (78 kHz) offers a powerful approach to investigate quadrupolar nuclei, such as ^{93}Nb, and to obtain unprecedented resolution."

Frédéric Blanc, University of Liverpool

"It is too early to assess the impact, but we believe, and are testing, the view that the resolution is better at 850 MHz, which may allow us to distinguish different polysaccharides in the plant cell walls."

Paul Dupree, University of Cambridge

"The range of nuclei (^{25}Mg, ^{43}Ca, ^{87}Sr, ^{93}Nb) that we looked at and the quadrupolar interactions would have been very difficult at lower field, and in a number of cases impossible."

Mark E. Smith, Lancaster University

"The spectral resolution obtained for protons at 850 MHz using 80 kHz MAS has allowed us to develop efficient new methods for measuring proton chemical shift parameters. In combination with first-principles calculations these provide a simple way of establishing hydrogen atom positions and hydrogen bond parameters in organic crystals."

Jeremy J. Titman, University of Nottingham

Ultra pure deuterated detergents and lipids for membrane protein NMR studies

- 20 to 25 % of human proteome consists of membrane proteins.
- 40 % of available drugs are targeting membrane proteins.
- Less than 100 membrane protein structures have been solved by NMR

Improved signal to noise ratio. Solubilizing a membrane protein in detergents and lipids that are deuterated at the fatty acid chains can dramatically improve the NMR spectra of the protein.

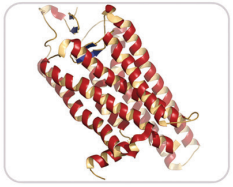

The highest purity. Detergents and lipids are purified meticulously to suit the most rigorous requirements of membrane protein work. We guarantee that our deuterated product will perform as well as or better than any commercially available compound – deuterated or natural abundance.

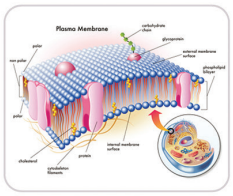

Only available from Cortecnet

Cortecnet is pleased to propose the widest range of deuterated detergents and lipids, including diacyl phosphatidylcholines and glycerols and lyso-lipids. Best-selling compounds include:

d27- LMPG

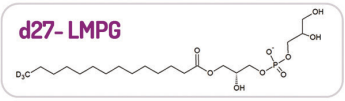

d31- LDAO

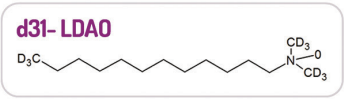

d26- DH7PC

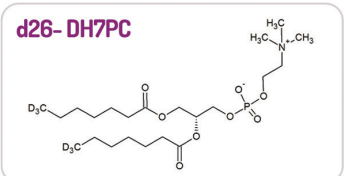

Since more than 15 years, Cortecnet is known as one of the most reliable supplier of NMR consumables and stable isotope enriched products. Cortecnet is composed of a team of analytical engineers capable to understand and fulfill all your needs. Over the years, Cortecnet has developed a strong professional network including thousands of academic labs and industrial companies all around the world.

CortecNet S.A.S
15/17, rue des Tilleuls
78960 Voisins-Le-Bretonneux, France
Tél : 33 (0)1 30 12 11 31 - 33 (0)1 30 43 86 54
Email : pcorcos@cortecnet.com
www.cortecnet.com

cortecnet
INNOVATION ACCELERATOR IN LIFE SCIENCE

CortecNet Corp.
411 Ash Street, Mill Valley
CA 94941, USA
Tel: (415) 380-8700 - Fax: (415) 230-5796
Email : pcorcos@cortecnet.com
www.cortecnet.com/us

JEOL-NMR Probes

Advanced Technology and Performance

The SuperCOOL probe

Low cost nitrogen cooled probe
400MHz 5mm tunable type
^{13}C : x3 higher sensitivity
^{1}H: > x3 higher sensitivity

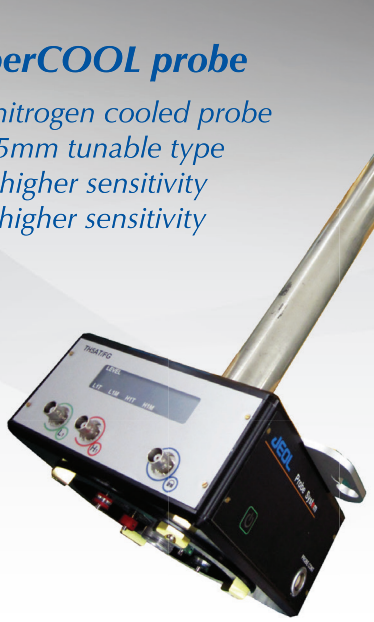

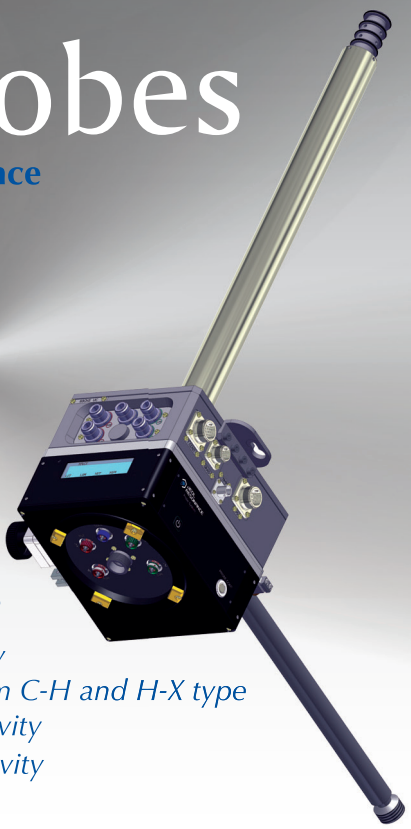

UltraCOOL Probe

For maximum sensitivity
800 and 600MHz 5mm C-H and H-X type
^{13}C : > x5 higher sensitivity
^{1}H: > x4 higher sensitivity

+44 (0)1707 377117

JEOL

www.jeol.com

sales@jeoluk.com

BRUKER

All Industries Rely on Scientific Analysis

Discover our portfolio of innovative push-button solutions and high performance systems based on:

- **Magnetic Resonance**
- **Mass Spectrometry**
- **Infrared Spectroscopy**
- **X-Ray Analysis**

www.bruker.com info@bruker.co.uk

Innovation with Integrity

Design by Mustard: www.mustardhot.com

Advantage West Midlands
www.advantagewm.co.uk

BBSRC
bioscience for the future

EPSRC
Engineering and Physical Sciences Research Council

investing in your future
European Regional Development Fund
European Union

Dr Dinu Iuga (Facility Manager)
Department of Physics
University of Warwick
Coventry CV4 7AL
T +44 (0) 24 761 50814
F +44 (0) 24 761 50897
E D.Iuga@warwick.ac.uk
W http://go.warwick.ac.uk/850mhz/

UNIVERSITY OF CAMBRIDGE
Durham University
University of Glasgow
The University of Nottingham
UNITED KINGDOM · CHINA · MALAYSIA
University of St Andrews
THE UNIVERSITY OF WARWICK